

Innovative Bracing System for Earthquake Resistant Concentrically Braced Frame
Structures

Liang Chen

A Thesis
in
The Department
of
Building, Civil & Environmental Engineering

Presented in Partial Fulfillment of the Requirements
for the Degree of Master of Applied Science (Civil Engineering) at
Concordia University
Montreal, Quebec, Canada

April 2011

© Liang Chen, 2011

CONCORDIA UNIVERSITY
School of Graduate Studies

This is to certify that the thesis prepared

By: Liang Chen

Entitled: Innovative Bracing System for Earthquake Resistant Concentrically Braced Frame Structures

and submitted in partial fulfillment of the requirements for the degree of

Master of Applied Science (Civil Engineering)

complies with the regulations of the University and meets the accepted standards with respect to originality and quality.

Signed by the final examining committee:

Ashotush Bagchi Chair

Oscar A. Pekau Examiner

Ramin Sedaghati Examiner

Lucia Tirca Supervisor

Approved by _____
Chair of Department or Graduate Program Director

Dean of Faculty

Date April 6, 2011

ABSTRACT

Innovative Bracing System for Earthquake Resistant Concentrically Braced Frame

Structures

Liang Chen

The chevron braced frame is a widely used seismic force resistant system in North America in areas subjected to moderate-to-severe earthquakes. However, the chevron braced frame system is limited in term of lateral loads redistribution over the building height.

Khatib et al (1988) proposed to add zipper columns to link together all brace-to-beam intersecting points with the aim to drive all compression braces to buckle simultaneously and as a result to enlarge the energy dissipation capacity of the system. Although the Commentary of AISC Seismic Provisions for Structural Steel Building (AISC 2002) contains recommendations regarding this innovative zipper steel frame systems, no design provisions are included yet.

The scope of this thesis is to refine the design method for the Zipper Braced Frame System which was initially proposed by Tremblay and Tirca (2003) and to study the system's behaviour under seismic loads by means of accurate inelastic time-history analysis.

The main objective of this research project is three-fold:

- To develop accurate computer brace models by using Drain2DX and OpenSees and to validate the accuracy of computations with experimental test results for slender, intermediate and stocky braces;
- To refine the existing design method for CBFs with strong zipper columns;
- To validate the refined design method by studying the performance of CBF systems with strong zipper columns in Drain2DX and OpenSees environment for low-, middle- and high-rise buildings.

Through this research, the overall understanding of the CBF system with strong zipper columns is improved by means of accurate numerical predictions. The outcome of this study will be further used as input data for experimental tests.

The design procedure has been divided into two phases: design of braces, columns and beams according to NBC 2005 and CSA-S16-09 and design of zipper columns. A spreadsheet was developed for a 4-, 8- and 12-storey buildings and six different pattern loads related to the distribution of internal brace forces over the structure height were proposed. Based on this study, the best suited pattern load distribution is selected and considered for zipper column design.

In order to evaluate the accuracy of modeling assumption in OpenSees, parametric studies were carried out. Comparisons between analytical and available test results have validated the accuracy of the computer models and analysis results. Three ground motion ensembles such as: regular, near-field and Cascadia were scaled to match the design spectrum for Victoria, B.C., have been considered in these analyses.

In conclusion, good seismic performance was found for all studied buildings. The forces in the zippers were equal to or lower than predicted in the design method. All zipper columns performed in elastic range while buckling of braces propagated upward or downward within seconds. It was clearly demonstrated that by using CBF's with zipper columns the storey mechanism was mitigated and in almost all cases the interstorey drift was uniformly distributed over the structure height. In addition the median estimations of the interstorey drifts were below than 2.5% h_s limit prescribed in the NBC-05 code for buildings of normal importance.

The outcomes of this research project will be further used as input data for a future experimental test planned to be conducted on an 8-storey braced frame with zipper columns sample.

ACKNOWLEDGE

It is difficult to overstate my gratitude to my supervisor, Dr. Lucia Tirca. This thesis would not be even slightly possible without her encouragement, guidance and support every step of the way. I have totally lost count of how many late evenings and weekends she has extended her working hours to help me undertake this research project during the last two years. Her enthusiasm, her inspiration, her immense knowledge as well as her great efforts toward accomplishing my dream will never be forgotten.

I am also deeply grateful to Dr. Oscar A. Pekau, Dr. Kinh H. Ha from Concordia University, Prof. Suresh Shrivastava from McGill University, Prof. Robert Tremblay and Dr. Sanda Koboevic from *École Polytechnique de Montréal* for their enlightening lectures, heartfelt advice and patient instructions. Their courses gave me tools that turned out to be essential in my research. Their ideals and concepts have had a remarkable influence on my entire career.

It was a pleasure to share this part of my life time with my colleagues and friends I met in Concordia, like Zhi Chen, Juan David Morales Ramirez, Cristina Caprarelli, Nicolae Ionel Danila, Geli Guo, Evan Irvine, Gurinderbir Singh Sooch, and all my office colleagues.

Special thanks go to Dr. Robert Tremblay for providing experimental data and to his master student Carmen Izvernari for her advice regarding the computer model.

Last but not least, I want to thank my dear parents. Every little achievement I get in my life is because of their selfless love, and I love them back.

TABLE OF CONTENTS

LIST OF FIGURES	X
LIST OF TABLES	XVII
LIST OF EQUATIONS	XVIII
CHAPTER ONE: INTRODUCTION.....	1
1.1 GENERAL	1
1.2 OBJECTIVES AND SCOPE	3
1.3 DESCRIPTION OF METHODOLOGY	4
1.4 THESIS ORGANISATION.....	5
CHAPTER TWO: LITERATURE REVIEW	7
2.1 PAST STUDIES ON THE DESIGN OF CONCENTRICALLY BRACED FRAMES WITH ZIPPER COLUMNS	7
2.1.1 <i>General</i>	7
2.1.2 <i>Tension Zipper strut approach</i>	9
2.1.3 <i>Weak Zipper strut approach</i>	10
2.1.4 <i>Strong Zipper strut approach</i>	11
2.1.5 <i>Suspended Zipper strut approach</i>	15
2.2 STUDYING THE ZIPPER BRACED FRAME BEHAVIOUR WITH DRAIN2DX	16
2.3 STUDYING THE ZIPPER BRACED FRAME BEHAVIOUR WITH OPENSEES	17
2.4 PAST STUDIES ON BRACED STEEL FRAMES BEHAVIOUR USING OPENSEES	19
CHAPTER THREE: MODELING OF TUBULAR BRACING MEMBERS UNDER QUASI- STATIC LOADING.....	24
3.1 GENERAL CHARACTERISTICS OF THE REFINED BRACE MODEL IMPLEMENTED IN DRAIN2DX	24
3.2 GENERAL CHARACTERISTICS OF THE BRACE MODEL IN OPENSEES.....	27
3.3 SELECTED EXPERIMENTAL TESTS FROM LITERATURE.....	29

3.4 COMPARISON OF ANALYTICAL INELASTIC BRACES RESPONSE IN DRAIN2DX AND OPENSEES VERSUS EXPERIMENTAL	33
3.4.1 Empirical parameters calibration for Element 05 implemented in Drain2DX.....	33
3.4.2 Comparison of analytical results using Drain2DX with experimental results	36
3.4.3 The influence of parameters required in OpenSees for the brace model.....	38
3.4.4 Comparison of analytical results using OpenSees with experimental results.....	48
3.4.5 Comparative response of braces under quasi-static loading in OpenSees and Drain2DX versus experimental test results	51
CHAPTER FOUR: DESIGN METHODOLOGY OF ZIPPER BRACED FRAME STRUCTURES.	61
4.1 DESIGN PHILOSOPHY	61
4.1.1 General design steps.....	61
4.1.2 Detailed design steps	62
4.2 THE INFLUENCE OF PATTERN LOAD SELECTION ON THE PRELIMINARY DESIGN METHODOLOGY	69
4.2.1 Sequential triangular pattern load	69
4.2.2 Other load distribution patterns considered in this study.....	71
4.2.3 Preliminary design & selected design load patterns	77
CHAPTER FIVE: SEISMIC ANALYSIS AND STRUCTURAL RESPONSE OF MULTI-STOREY ZIPPER BRACED FRAMES.....	84
5.1 ZIPPER BRACED FRAME MODELING	84
5.2 GROUND MOTIONS SELECTION AND SCALING PROCEDURE	86
5.2.1 Ground motion selection.....	86
5.2.2 Scaling of ground motion.....	88
5.3 NUMERICAL ANALYSES IN DRAIN2DX	92
5.3.1 Modeling in Drain2DX.....	92
5.3.2 Drain2DX results.....	93
5.3.3 OpenSees results.....	106
5.4 DISCUSSION OF RESULTS.....	125

CHAPTER SIX: CONCLUSIONS AND FUTURE PERSPECTIVES	129
6.1 CONCLUSIONS.....	129
6.2 FUTURE PERSPECTIVES.....	133
REFERENCES.....	134
APPENDIX I: SELECTED GROUND MOTION TIME-HISTORY RECORDS.....	140
APPENDIX II: BUCKLING SEQUENCES ZIPPER BRACED FRAME UNDER GROUND MOTION EXCITATIONS.....	146

LIST OF FIGURES

Figure 2.1 Chevron braced frames configuration and its failure mechanism (Bruneau et al, 2005).....	8
Figure 2.2 Behaviour of zipper braced frame system with weak zipper column (Tirca & Tremblay, 2004): a) zipper yields in tension; b) zipper buckles in compression.	11
Figure 2.3 Behaviour of zipper braced frame system with strong zipper columns (Tirca & Tremblay, 2004): a) brace buckling initiated at the base; b) brace buckling initiated at the roof.....	12
Figure 2.4 Mechanisms and lateral load distributions adopted for design with brace buckling initiating at the: a) upper floors; b) lower floors (Tremblay and Tirca, 2004)	13
Figure 2.5 Suspended zipper column design and its push-over curves (Bruneau et al, 2005).....	16
Figure 2.6 OpenSees abstractions (Mazzoni et al, 2005).....	18
Figure 2.7 OpenSees analysis abstraction (Mazzoni et al, 2005)	19
Figure 2.8 Comparison between test and pin-ended model with length KL: a) Hysteretic response with $R_0 = 25$, $a_1 = a_3 = 0.00001$, and $a_2 = a_4 = 0.00002$; b) Hysteretic response with $R_0 = 25$ and a_1 to $a_4 = 0.0$; c) Out-of-plane response at brace mid-length with $R_0 = 20$ and a_1 to $a_4 = 0.0$ (Aguero, A., Izvernari, C. and Tremblay, R., 2005).....	20
Figure 2.9 Chevron braced assembly (Yang et al., 2009).....	21
Figure 2.10 Chevron braced subassembly model (Yang et al., 2009)	21

Figure 2.11 Experimental and Analytical response (Yang et al., 2009).....	22
Figure 2.12 OpenSees model versus experimental by considering the low-cycle fatigue (Uriz and Mahin, 2008).....	23
Figure 3.1 Refined physical theory model of brace: a) Refined physical theory brace models; b) Basic behaviour of a brace associated with each zone (Ikeda and Mahin, 1984).....	25
Figure 3.2 Linear Idealization Curves for Tangent Modulus History (Ikeda & Mahin, 1984).....	26
Figure 3.3 Menegotto-Pinto model for steel material.....	28
Figure 3.4 Experimental set-up for single and X bracing frame configuration (Tremblay et al., 2003).....	31
Figure 3.5 Experimental set-up for single brace <i>2A</i> (Shaback, B., and Brown, T., 2003)	31
Figure 3.6 Loading protocols for specimens a) <i>S1B</i> ; b) <i>S3B</i> ; c) <i>SIQB</i> ; and d) <i>2A</i>	32
Figure 3.7 Theoretical P-M interaction curves.....	35
Figure 3.8 Hysteresis loops of specimen <i>S1B</i>	37
Figure 3.9 Hysteresis loops of specimen <i>SIQB</i>	37
Figure 3.10 Hysteresis loops of specimen <i>S3B</i>	38
Figure 3.11 Hysteresis loops of specimen <i>2A</i>	38
Figure 3.12 The considered brace model in OpenSees.....	40
Figure 3.13 Effect of the out-of-straightness parameters with buckling load captured in the hysteresis loops.....	41

Figure 3.14 Layout of different fibre discretization: a) Type “A”, with 16 fibres; b) Type “B”, with $4 \times n(m+n)$ fibres	43
Figure 3.15 Hysteresis loops of specimens <i>SIB</i> with different fibre discretization	44
Figure 3.16 Effect of different numbers of nonlinear beam-column elements on the buckling and hysteresis response of specimen <i>SIQB</i> : a) Hysteresis loops; b) Energy dissipated per half-cycles; c) Yielding & buckling forces of each half-cycle; d) Accumulated energy dissipation.....	46
Figure 3.17 Effect of the number of integration points per nonlinear beam-column element to the specimen <i>2A</i>	47
Figure 3.18 Effect of N_f and N_e on specimen <i>SIB</i> : a) $N_e=2,4,8$; $N_i=4$; $N_f=16$; b) $N_e=2,4,8$; $N_i=4$; $N_f=500$;	50
Figure 3.19 Comparative results of braces hysteresis response in terms of force-displacement: a) specimen <i>2A</i> ; b) specimen <i>SIQB</i> ; c) specimen <i>SIB</i> ; d) specimen <i>S3B</i>	52
Figure 3.20 Axial force developed per half-cycle for: a) specimen <i>SIB</i> and b) specimen <i>SIQB</i>	54
Figure 3.21 Energy dissipated per half-cycle: a) specimen <i>SIB</i> ; b) specimen <i>SIQB</i>	55
Figure 3.22 Cumulative energy dissipation per half-cycle: a) specimen <i>SIB</i> ; b) specimen <i>SIQB</i>	56
Figure 3.23 Lateral forces induced in specimen <i>S3B</i>	58
Figure 3.24 Energy dissipated by specimen <i>S3B</i> per half-cycle.....	58
Figure 3.25 Cumulative Energy dissipation of specimen <i>S3B</i>	58
Figure 3.26 Axial force developed in specimen <i>2A</i> per half-cycle.....	59
Figure 3.27 Energy dissipation of specimen <i>2A</i> per half-cycle	60

Figure 3.28 Cumulative Energy dissipation of specimen 2A.....	60
Figure 4.1 Lateral seismic force distribution	63
Figure 4.2 Computed peak axial loads in zipper columns for 4,8,12 storey building (Tremblay & Tirca, 2003)	70
Figure 4.3 The variation of vertical distribution vector of lateral forces with different k	72
Figure 4.4 Lateral force distribution vectors.....	72
Figure 4.5 Zipper mechanics & load pattern LP-SΔ: a) buckling initiate at top; b) buckling initiate at bottom.....	74
Figure 4.6 Zipper mechanics & load pattern LP-SU: a) Buckling initiate at top; b) Buckling initiate at bottom	75
Figure 4.7 Zipper mechanics & load pattern LP-SU: a) Buckling initiate at the top; b) Buckling initiate at the bottom	77
Figure 4.8 Structure plan view (Tirca and Tremblay, 2003)	78
Figure 4.9 Modelized frame (Tirca and Tremblay, 2003)	79
Figure 4.10 Comparison of zipper forces obtain from various load patterns	81
Figure 5.1 Frame model.....	86
Figure 5.2 Design and scaled response spectrum of the selected accelerograms for: a) 4- storey building; b) 12-storey building; c) 12-storey building.....	90
Figure 5.3 Axial force in zipper columns obtained from nonlinear dynamic time-history analyses of: a) 4-storey building; b) 8-storey building; c) 12-storey building	94
Figure 5.4 Computed interstorey drift: a) 4-storey building; b) 8-storey building; c) 12- storey building.....	95

Figure 5.5 Time-history response of brace buckling and beam hinging for the 4-storey building under: a) R1 regular ground motion; b) N6, Near-field ground motion; c) C2, Cascadia simulated ground motion. (the first buckled brace; subsequently buckled brace and beam hinging; yielding of brace).....	97
Figure 5.6 Time-history response of brace buckling and beam hinging for 8-storey building under: a) R1 regular ground motion; b) N6 Near-field ground motion; c) C2 Cascadia simulated ground motion. . (the first buckled brace; subsequently buckled brace and beam hinging; yielding of brace).....	99
Figure 5.7 Inelastic response of the 8-storey building under the R1 ground motion: a) simulated accelerograms, R1; b) time-history of interstorey drift; c) axial forces in zipper columns.....	100
Figure 5.8 Time-history response of brace buckling and beam hinging for 8-storey building under: a) R1 regular ground motion; b) N6 Near-field ground motion; c) C2 Cascadia simulated ground motion. . (the first buckled brace; subsequently buckled brace and beam hinging; yielding of brace).....	103
Figure 5.9 Inelastic response of the 12-storey building under the R1 ground motion: a) Simulated accelerograms, R1; b) Time-history of interstorey drift; c) Axial forces in zipper columns.....	105
Figure 5.10 Axial force in zipper columns obtained from nonlinear dynamic time-history analyses in OpenSees of: a) 4-storey building; b) 8-storey building; c) 12-storey building.....	107
Figure 5.11 Computed interstorey drift: a) 4-storey building; b) 8-storey building c) 12-storey building.....	109
Figure 5.12 Hysteresis behaviour of brace elements in 4-storey zipper braced frame under ground motion excitation R1	110
Figure 5.13 Structural response of the 4-storey zipper braced frame under ground motion R1: a) Regular ground motion excitation R1; b) Interstorey time-history record under	

ground motion excitation R1; c) Axial forces in zipper columns at specified time steps; d) Shear forces distribution along the building height at specified time steps; e) Storey forces induced into structure at specified time steps..... 111

Figure 5.14 Structural response of 4-storey zipper braced frame under ground motion N3:

a) Regular ground motion excitation N3; b) Interstorey time-history record under ground motion excitation N3; c) Axial forces in zipper columns at specified times; d) Shear forces distribution along the building height at specified times; e) Storey forces induced into structure at specified times..... 113

Figure 5.15 Structural response of 8-storey zipper braced frame under ground motion R1:

a) Regular ground motion excitation R1; b) Interstorey time-history record under ground motion excitation R1; c) Axial forces in zipper columns at specified time steps; d) Shear forces distribution along the building height at specified time steps; e) Storey forces induced into structure at specified time steps..... 115

Figure 5.16 Hysteresis loops of braces of 8-storey building under ground motion R1 .. 116

Figure 5.17 Structural response of 8-storey zipper braced frame under ground motion N2:

a) Regular ground motion excitation N2; b) Interstorey time-history record under ground motion excitation N2; c) Axial forces in zipper columns at specified times; d) Shear forces distribution along the building height at specified times; e) Storey forces induced into structure at specified times..... 118

Figure 5.18 Structural response of 8-storey zipper braced frame under ground motion N3:

a) Regular ground motion excitation N3; b) Interstorey time-history record under ground motion excitation N3; c) Axial forces in zipper columns at specified times; d) Shear forces distribution along the building height at specified times; e) Storey forces induced into structure at specified times..... 119

Figure 5.19 Structural response of 12-storey zipper braced frame under ground motion

R1: a) Regular ground motion excitation R1; b) Interstorey time-history record under ground motion excitation R1; c) Axial forces in zipper columns at specified times; d)

Shear forces distribution along the building height at specified times; e) Storey forces induced into structure at specified times.....	122
Figure 5.20 Structural response of 12-storey zipper braced frame under ground motion R5: a) Regular ground motion excitation R5; b) Interstorey time-history record under ground motion excitation R5; c) Axial forces in zipper columns at specified times; d) Shear forces distribution along the building height at specified times; e) Storey forces induced into structure at specified times.....	
	123
Figure 5.21 Structural response of 12-storey zipper braced frame under ground motion R7: a) Regular ground motion excitation R7; b) Interstorey time-history record under ground motion excitation R7; c) Axial forces in zipper columns at specified times; d) Shear forces distribution along the building height at specified times; e) Storey forces induced into structure at specified times.....	
	124
Figure 5.22 Roof displacement time-history record of the 4-storey structure under ground motion excitation R1, obtained from Drain OpenSees and ETABS: a) Ground motion R1; b) Roof displacement time-history record.....	
	126
Figure 5.23 Brace hysteresis behaviour at 1% damping.....	127
Figure 5.24 Brace hysteresis behaviour at 2% damping.....	128

LIST OF TABLES

Table 3.1 Properties of selected test specimens.....	32
Table 3.2 Calculated tensile and compressive strength of test specimens.....	33
Table 3.3 Coefficients for defining the theoretical P - M interaction curve.....	34
Table 3.4 Empirical parameters for describing the tangent modulus curves for braces with tubular sections.....	35
Table 3.5 Magnification factors for braces with tubular sections.....	36
Table 4.1 Member sections of the 4-storey structure.....	80
Table 4.2 Member sections of the 8-storey structure.....	80
Table 4.3 Member sections of the 12-storey structure.....	80
Table 4.4 Member sections of the 4-, 8-, 12-storey structure.....	83
Table 5.1 Ground motions characteristics	87
Table 5.2 Scale factors applied to the selected ground motions.....	91
Table 5.3 Analytical fundamental periods of vibration of the 4-, 8- and 12-structures..	125
Table II.1 Buckling sequences of braces in the 4-storey structure under different ground motion excitations (in sec).....	146
Table II.2 Buckling sequences of braces in the 8-storey structure under different ground motion excitations (in sec).....	147
Table II.3 Buckling sequences of braces in the 12-storey structure under different ground motion excitations (in sec).....	148

LIST OF EQUATIONS

Equation 3.1	28
Equation 3.2	42
Equation 4.1	62
Equation 4.2	62
Equation 4.3	62
Equation 4.4	63
Equation 4.5	63
Equation 4.6	67
Equation 4.7	67
Equation 4.8	68
Equation 4.9	71
Equation 4.10	71
Equation 4.11	76

CHAPTER ONE: INTRODUCTION

1.1 General

Concentrically braced frames (CBF) with different brace configurations are widely used in North America to withstand moderate-to-severe earthquakes. This system is considered as being the most stiffness efficient when braces behave in elastic range. Once the inelastic response is initiated, the lateral stiffness starts degrading and an asymmetrical response is developed. The popularity of this system is attributed to the reduced cost, supervised fabrication process and speed of erection.

Past studies have shown that braced frame structures exhibit a limited redundancy due to the tendency of earthquake loads to concentrate in a specific floor where large storey forces and interstorey drifts are developed. Consequently, this specific floor becomes vulnerable and prone to storey mechanism formation (plastic hinges in CBF columns) while the structure is driven toward a dynamic sideway collapse.

In the case of concentrically braced frames with a chevron configuration, the stability of the system is enhanced when strong floor beams are employed. These beams are designed to resist the postbuckling unbalanced vertical load transferred from braces in combination with the corresponding gravity load. When the floor beams are not designed to carry the vertical unbalanced force that develops after braces buckle, the storey shear resistance diminishes and forces are redistributed into the structural system. Even if a

chevron bracing system with larger floor beams is designed, it is relatively inefficient to redistribute the lateral loads over the building height.

In light of this, the 1995 edition of the National Building Code of Canada (NBCC'95) has imposed a limitation in the number of storeys for CBF structures in function of ductility and seismicity zone. Later on, in the 2005 edition of the National Building Code (NBCC'05) the limits were changed from the number of storeys to the height of the building expressed in meters. Although these limits are considered, the CBF system is still prone to storey mechanism formation under earthquake excitations characterised by different frequency content.

In order to mitigate the formation of storey mechanism and to achieve a stable inelastic seismic response, Khatib et al (1988) proposed to add a zipper column to link together all brace-to-beam intersecting points, with the aim being to force all compression braces to buckle and tensile braces to yield, such that a large amount of energy will be dissipated.

Although in the last decade several researchers in North America have conducted analytical and experimental studies in the field of behaviour and design of zipper braced frame systems, the concept is different and can be defined as follows: i) CBF with weak zipper strut (inelastic behaviour); ii) CBF with strong zipper strut (elastic behaviour) and iii) CBF with suspended zipper strut. Precedently, experimental studies have been conducted only for the CBF system with suspended zipper struts. These structural systems are presented in the next chapter.

On the other hand, analytical studies conducted before 2006- 2007 have employed the Drain2DX computer program, while recent studies have considered the most powerful software OpenSees (The Open System for Earthquake Engineering Simulation, McKenna, F. and Fenves, G.L., 2004) to simulate the earthquake response of the structures. If in the Drain2DX framework the inelasticity of braces was captured by the implementation of the refined physical theory brace model, in OpenSees, brace members were modeled with the nonlinear beam column element composed of several fibres and integration points for which a simulated steel material was assigned.

As mentioned, the research conducted for CBF systems with zipper columns was initiated by Khatib and Mahin (1988), continued by Sabelli (2000) who envisioned the CBF system with weak zipper struts, Tremblay and Tirca (2003, 2004) who promoted CBF system with strong zipper struts and Leon and Yang (2004, 2007) who developed CBF with suspended zipper struts. Although the Commentary of AISC Seismic Provisions for Structural Steel Building (AISC 2002) has introduced the zipper steel frame system, no design provisions are available. Furthermore, AISC has recommended the braced frame in a zipper-bracing configuration as an innovative system able to improve the post-elastic seismic performance of CBF with chevron configuration.

1.2 Objectives and Scope

The aim of this research project is three-fold:

- To develop accurate computer brace models by using the inelastic time-history software Drain2DX and OpenSees and to validate the accuracy of computations with experimental test results for slender, intermediate and stocky braces;

- To refine the existing design method for CBFs with strong zipper columns;
- To validate the refined design method by studying the performance of CBF systems with strong zipper columns in Drain2DX and OpenSees computer environment for low-, middle- and high-rise buildings.

Through this research, the overall understanding of the CBF system with strong zipper columns is improved by means of accurate numerical predictions. The outcome of this study will be further used as input data for experimental tests.

1.3 Description of methodology

For attaining the aforementioned objectives the following steps will be carried out:

- Results from experimental tests were selected to emphasise the difference in behaviour of slender, intermediate and stocky tubular braces subjected to quasi-static cyclic loads. Based on these test results, analytical brace model were developed and two computer programs such as Drain2DX and OpenSees were selected for numerical simulations. To study the influence of loading type on brace response, a forth sample (intermediate brace) was selected for investigation. All selected braces are tubular, compact cross-sections belonging to class 1 of section. This selection was made to analyse the inelastic brace response which depends on the size of the brace cross-section and type of loading.
- To bring refinement to the design method of CBFs with strong zipper columns and to assure that zipper columns behave elastically, additional lateral load distribution patterns of internal brace forces are developed herein and different brace buckling

scenarios are considered. In this regard, beside the sequential triangular load distribution employed in the previous study, the added patterns are the following: triangular; parabolic; sequential parabolic; uniform; and sequential uniform. The maximum tension and compressive force developed in zippers under each one of the aforementioned scenarios was considered for design. Therefore zipper columns are designed to withstand the probable tensile and compressive force developed in braces.

- To improve the overall understanding of the CBF with strong zipper columns and to validate the design method, a 4-, 8- and 12-storey building were analysed under three ensembles of ground motions typical for Victoria, British Columbia. The first ensemble is labelled “ordinary ground motion” and is composed of eight simulated and historical accelerograms; the second ensemble is composed of four Near-field ground motions with forward directivity and the third is composed of two simulated Cascadia subduction ground motions. The selected accelerograms were scaled to match the seismic design spectrum for Victoria. OpenSees and Drain2DX models were developed for these buildings.

1.4 Thesis organisation

This thesis is organised in six chapters. The first chapter contains a brief introduction, the scope and thesis objectives, the methodology, as well as the thesis organization. The second chapter summaries the literature review related to past studies. It presents design principles and behavioural characteristics of concentrically braced frame systems with zipper columns, as well as past studies conducted with OpenSees. Chapter 3 is related to the calibration of brace model in OpenSees and Drain2DX by using results from

available experimental tests. The computer modeling of slender, intermediate, and stocky braces subjected to quasi-static loading histories is developed. The refined design method is based on five different loading distribution patterns and is depicted in Chapter four. This method was applied for the 4-, 8-, and 12-storey building and the maximum force developed in zippers is illustrated. The fifth chapter presents the ground motion envelopes selection, the scale factor calculation and the low- middle- and high-rise building response under time-history nonlinear analyses by using Drain2DX and OpenSees. The building performance is discussed in term of forces developed in zipper columns, sequences of braces buckling and lateral interstorey drift deformation. In this study, the failure mechanism, labelled the full-height zipper mechanism, is reached when all braces have buckled and beams hinged at the braces to beam intersection point. Conclusions of this study, as well as the recommendations for the future work are presented in the sixth chapter.

CHAPTER TWO: LITERATURE REVIEW

2.1 Past studies on the Design of Concentrically Braced Frames with Zipper Columns

2.1.1 General

Chevron braced frames are widely used in Canada (Tremblay and Robert, 2001) to withstand earthquake loads. This structural system provides higher stiffness and a moderate ductility through yielding and/or buckling of braces while all other structural members such as beams, columns, and connections behave in elastic range. However, under strong seismic excitation, this system is prone to storey mechanisms, especially when beams are not designed to carry the unbalanced vertical load caused by buckled braces (Figure 2.1).

Thus, either the ground floor and/or the upper floors are prone to excessive lateral deformation after braces buckle and/or yield. Consequently, the sudden formation of the weak storey or storey mechanism drives the structure to failure instead of transferring the lateral forces to adjacent stories.

To overcome the problems caused by beam failure, several studies have been conducted by researchers (Khatib et al. 1988, Remennikov and Walpole 1998, Sabelli 2001, Tremblay and Robert 2001). The concept of strong beams, designed to carry the unbalanced forces developed when the braces lose their capacity in compression, was

proposed. Despite this design strategy, the braced frame system is still prone to storey mechanism formation.

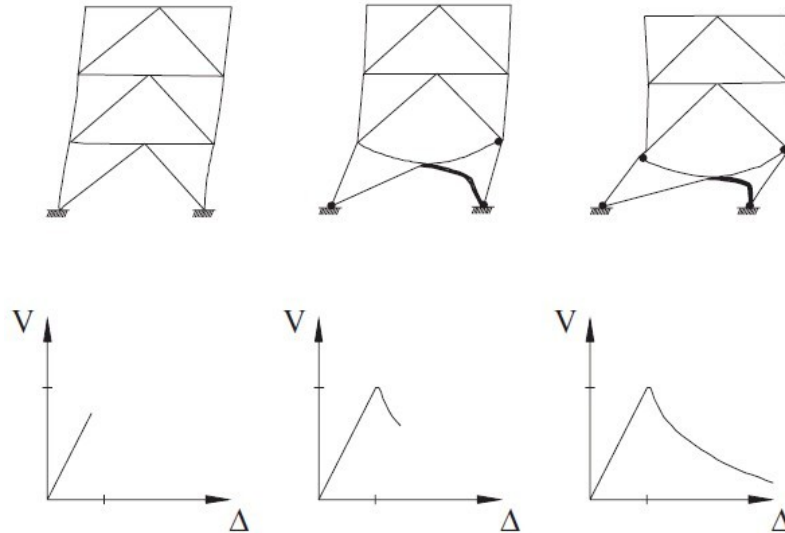


Figure 2.1 Chevron braced frame configuration and its failure mechanism (Bruneau et al. 2005)

On the other hand, Khatib has mentioned in his report (Khatib et al. 1988), “a structural configuration that achieves trilinear hysteresis loops without having to use stiff beams and slender braces, and without causing large increases in column axial forces” is in need. Further on, he proposed to add a new vertical brace, termed zipper, to attach the brace-to-beam intersection points between adjacent floors. In this respect, the zipper members act either in tension or in compression to trigger the “zipper mechanism” which forces the braces at adjacent stories to buckle simultaneously or successively.

Therefore, in “Zipper” configuration, the vertical braces transfer the unbalance force developed after the buckling of braces occurs in adjacent stories, and force the braces on these stories to buckle.

The Zipper configuration if designed properly is expected to overcome several behavioural problems and to improve the seismic response of the chevron braced system. Thus, this proposed system is able to maintain a more uniform damage distribution over the structure height and to develop stable hysteresis behaviour. Furthermore, it does not require very strong beams, and offers a relatively good performance level in terms of storey drift and energy dissipation under earthquake excitations.

In the Commentary of AISC Seismic Provisions for Structural Steel Building (AISC 2002), the Zipper steel frame system has been recommended as being a braced frame configuration able to improve the post-elastic seismic performance of chevron bracing system.

2.1.2 The tension Zipper strut approach

Following Khatib's assumption, buckling of braces initiates at the first storey and propagates upwards, which means the structure will deflect in the first vibration mode shape when the zipper effect is activated. After the first brace element buckles, tensile forces will be developed in the zipper elements to force the brace elements of the above stories to buckle subsequently. However, since only tensile force is considered in zipper elements, this theory can only apply to the cases when the first brace buckles at the first storey. This ideal behaviour mode of the zipper braced frame system requires braces on one half-span of the frame to be on the verge of buckling prior to those on the other half, such that the system will be led to deflect following the first mode deformed shape. In light of this approach, the tensile forces in the zipper members are calculated as the sum of all unbalanced vertical loads resulting from internal forces developed in the braces.

However, Khatib, in this work, formulated several questions related to the behaviour of the zipper system, which opened the door for further research.

“What happen if the buckling of braces initiates from other stories instead of the first storey? Could the zipper elements be activated in compression instead of tension? What if the structure is not in a first mode deflected shape when the zipper effect is activated? How to proportion the braces to maximize the effectiveness of zipper effect? How to choose the relative stiffness of the zipper elements and beams ?” (Khatib et al., 1988)

These questions have been addressed by the following researchers: Sabelli (2001), Tirca and Tremblay (2003, 2004) and Yang and Leon (2004, 2008).

2.1.3 The weak Zipper strut approach

In order to achieve a uniform drift distribution at each storey and to avoid the formation of the storey mechanism, R. Sabelli (2001) has proposed a design method for the zipper braced frames. For brace design, he recommended the same requirements given in the code for the concentrically braced frame system. For the zipper columns, the forces expected to be developed in tension and compression must reach the strength of braces located at the level below. In addition, zipper columns shall be designed and detailed with the expectation of inelastic demand in both tension and compression.

Based on his study which involves a 3- and a 6- storey zipper braced frames, R. Sabelli (2001) concludes that the inelastic demand on the braces is more uniformly distributed than in a chevron braced frame with strong beams. However, while the 3- storey zipper frame shows an outstanding behaviour under the ground excitations, and

deflects based on the first mode shape, several behavioural aspects have been observed in the 6-storey frame. The deformed shape of the 6-storey frame approximates the shape of the second mode of vibration instead of the first mode, while significant buckling and tension yielding have been observed in the zipper columns.

The behaviour of a chevron braced frame with weak zipper columns is shown in Figure 2.2. Both cases: zipper yielding and buckling are considered in design.

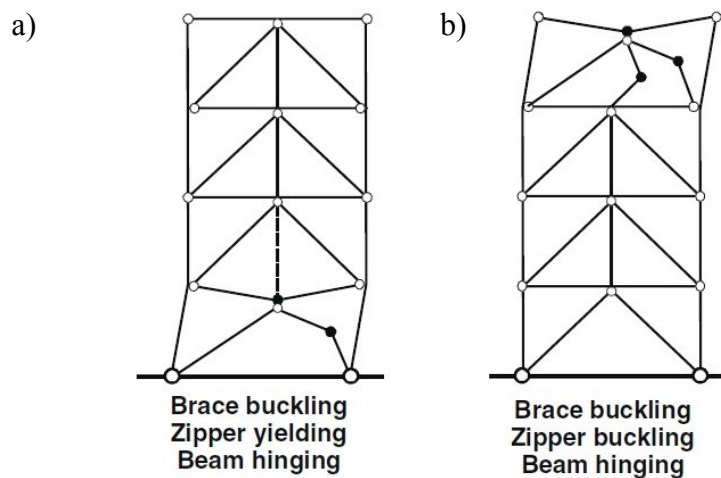


Figure 2.2 Behaviour of zipper braced frame system with weak zipper column (Tirca & Tremblay, 2004): a) zipper yields in tension; b) zipper buckles in compression.

2.1.4 Strong Zipper strut approach

With the aim of limiting the inelastic behaviour within braces, Tremblay and Tirca (2003) have proposed a design method that relies on the ability of zippers to behave elastically. Based on their proposed design methodology, three zipper braced frame buildings (4-, 8-, and 12-storey) have been designed and investigated. Close examination of the inelastic behaviour of the aforementioned braced frames has shown that both critical scenarios of zippers acting in tension and compression can be treated separately. When the brace

buckling initiates at the bottom storey and propagates upward in the frame, zipper columns are subjected to tensile forces due to the subsequent buckling of braces as shown in Figure 2.3 a). On the other hand, when the first buckled brace is located at the top floor, as the buckling of braces propagates downward, the unbalance vertical forces, projected from the braces to mid-span of the beams, are transferred as compressive forces in zipper columns (Figure 2.3 b).

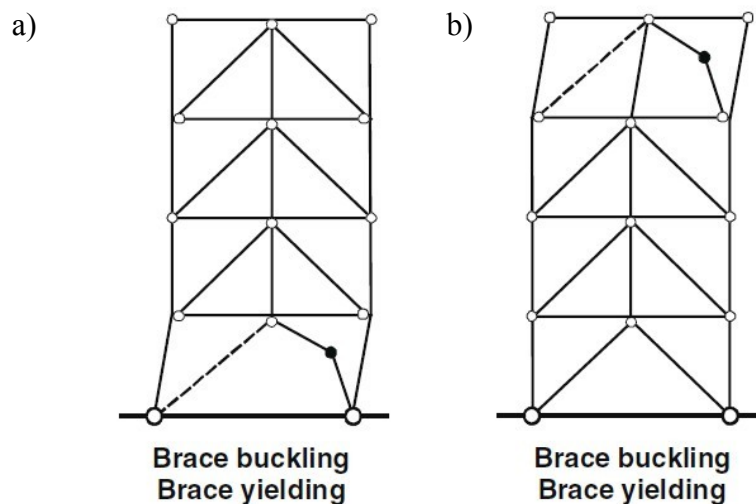


Figure 2.3 Behaviour of zipper braced frame system with strong zipper columns (Tirca & Tremblay, 2004): a) brace buckling initiated at the base; b) brace buckling initiated at the roof.

Therefore, the zipper columns are designed to carry the unbalanced load developed at the mid-span of the beams after braces buckle. To assess the force in zippers and their required compressive and tensile strength, the following two scenarios have been proposed: zippers act in tension when the first brace buckles at the base and zippers act in compression when the first brace buckles at the top of the structure. The zipper struts are designed to withstand both of the maximum compressive force and the

maximum tensile force which would be induced by the internal forces which are equal to the probable buckling/postbuckling capacity and the tensile capacity of braces.

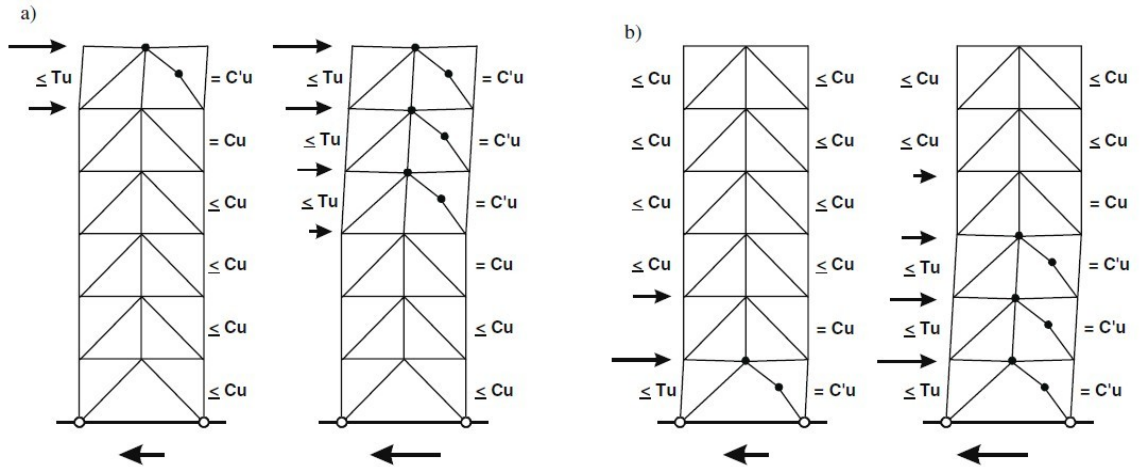


Figure 2.4 Mechanisms and lateral load distributions adopted for design with brace buckling initiating at the: a) upper floors; b) lower floors (Tremblay and Tirca, 2004)

In order to make the zipper braced frame respond as predicted, the zipper columns must remain elastic throughout the entire seismic excitations. The design methodology proposed by Tremblay and Tirca (2003) is able to predict the envelope of the maximum tension and compressive forces developed in zippers under different ground motion excitations.

In order to estimate the maximum compressive forces in zipper columns, C_z , the following assumptions have to be made:

- Lateral load distribution is assumed to vary linearly in an inverted triangular shape, from a maximum value reached at the roof level to zero at the level below the studied level.

- Plastic hinges form in beams where buckled braces are connected, which are typically the mid-points of beams.
- Braces are assumed to maintain their compressive strength, C_u , upon buckling, and their strength will drop to the postbuckling strength immediately after buckling occurs.
- The compressive forces transferred downward through zipper columns are taken by the compressive braces at the levels below the studied level. It is assumed that when the zipper at the studied level reaches the maximum compressive force, the compression acting braces at the floor below are on the verge of buckling, i.e. the compressive force in the brace reaches its compressive capacity, C_u , as shown in Figure 2.4 a).

For calculating the maximum tensile forces in the zipper columns, T_z , the following assumptions are made:

- The lateral load is assumed to vary linearly from a maximum value at the first floor (when the tensile force developed in the brace of the first floor is smaller or equal to the yielding force, T_u , or when all braces belonging to the studied tier reach the postbuckling load C_u) to zero at the floor located above the level of study.
- Plastic hinges form in the beams located above the buckled braces.
- Zipper is designed to carry at each floor the cumulative difference of the tensile force developed in the brace versus the postbuckling force C_u' (Figure 2.4 b).

In conclusion, the proposed method has been found to provide realistic estimations of the zipper column loads and a confirmation that zipper columns behave elastically. In addition, a stable inelastic response is shown for all studied structures under all regular ground motions. However, for the 12-storey building dynamic instability can occur under the Near-field and Cascadia ground motions when a full-height zipper mechanism is formed even if the zippers respond elastically. This study has underlined the requirements of future research and the validation of the proposed design method against different pattern loads beside the sequential triangular pattern load considered.

2.1.5 Suspended Zipper strut approach

Roberto T. Leon (2003) from Georgia Institute of Technology has pointed out that the formation of a full-height zipper mechanism implies a reduction on the lateral load capacity. Regarding this, Yang and Leon (2004) have proposed a modified zipper braced frame structure consisting of an increased size in top-storey braces. This concept requires the top storey braces to remain elastic and prevent the full zipper mechanism formation. This modified configuration is known as suspended zipper frames. The suspended zipper frame consists of a partial height zipper braced frame and an elastic hat truss at the top floor with the aim to prevent the overall collapse of the structure. The suspended zipper columns are able to transfer the unbalanced vertical forces developed gradually due to the brace's inelastic behaviour at the lower part of the structure to the top storey braces and support the beams at mid-span. As a result, the beams can be design to hinge, which means reduced beam sizes and a more economical design. Meanwhile, the suspended zipper frame provides a clear force path which makes the capacity design for all the structural members straightforward.

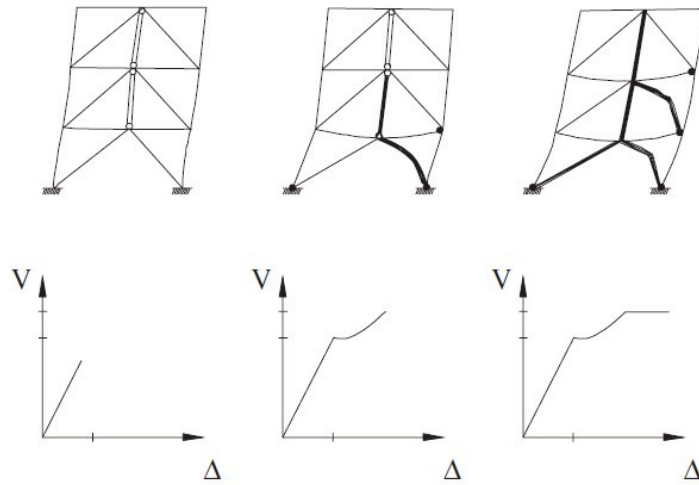


Figure 2.5 Suspended zipper column design and its push-over curves (Bruneau et al., 2005)

In their research, Leon and Yang have mainly focused on the early buckling of lower story braces which progresses upward, while having a hat truss on top of the structure as shown in Figure 2.5.

The loading path of a suspended zipper braced frame is well defined. However, since the zipper struts are designed to transfer all the unbalanced forces to the top storey, the member sizes of the elastic hat truss become too big. Thus, the main disadvantage of the suspended zipper braced frame configuration is that as the number of stories increases the strength demands of the top storey braces requires an unacceptable size of cross-section.

2.2 Studying the zipper braced frame behaviour with Drain2DX

Drain2DX is a computer program for static and dynamic analysis of plane structures developed by Department of Civil Engineering, University of California, Berkeley

(Prakash et al., 1993). It is capable of performing linear and nonlinear static and dynamic analyses.

Drain2DX has been widely used over the past three decades. The credibility of the Drain2DX output files has been examined and verified by many researchers. The studies presented in previous sections conducted by Sabelli, Tirca and Tremblay, as well as Yang and Leon, were all performed in the Drain2DX environment.

With great confidence, the Drain2DX software has been used to verify output parameters resulted from many other analysis programs, such as ETABS Non-linear.

Drain2DX uses analytical models to simulate the inelastic behaviour of structural members. Each element type implemented in Drain2DX serves a particular purpose, for instance, element type 02 is used to simulate the inelastic behaviour of beam-column members and element 05 is used for modeling inelastic bracing member behaviour. This feature made modeling in Drain2DX a straight-forward process. As will be shown in the next chapter, Drain2DX has its advantages and disadvantages in modeling.

2.3 Studying the zipper braced frame behaviour with OpenSees

The Open System for Earthquake Engineering Simulation (OpenSees) (McKenna and Fenves, 2004) is a software framework using finite element methods to develop applications to simulate the performance of structural systems subjected to earthquakes. OpenSees is capable of modeling and analyzing system response using a wide range of material models, elements, and solution algorithms. Due to its open source nature, developers, earthquake engineering researchers and users are able to dig into the source code to make their modifications for specific problems.

The OpenSees framework is built up by four main abstractions: ModelBuilder, Domain, Recorder and Analysis. The relationship between these abstractions is showed in Figure 2.6.

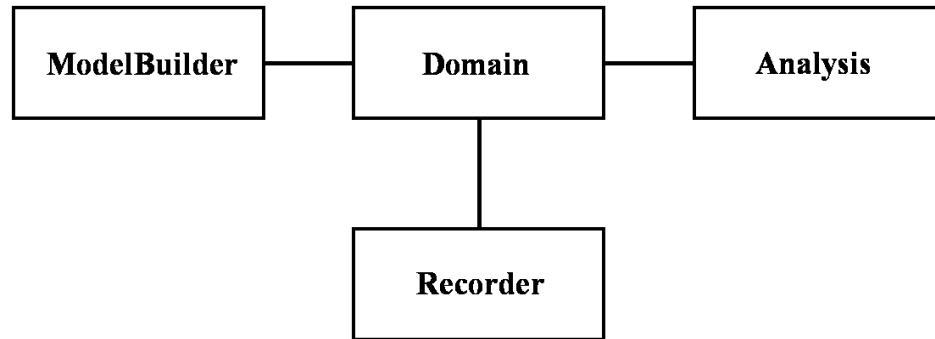


Figure 2.6 OpenSees abstractions (Mazzoni et al, 2005)

“ModelBuilder” constructs the objects in the model and adds them to the domain. The “Domain” will then hold the state of the model and send the information to “Analysis” with the aim to move the model from its state at time t to the next state at time $t+dt$. The “Recorder” monitors user defined parameters in the model during the analysis.

In a “Domain”, all details regarding the modeling have to be defined such as: Elements, Material, Nodes, Constraints, LoadPatterns and TimeSeries. Then, “Analysis” will handle the algorithm, integrator and so on as shown in Figure 2.7.

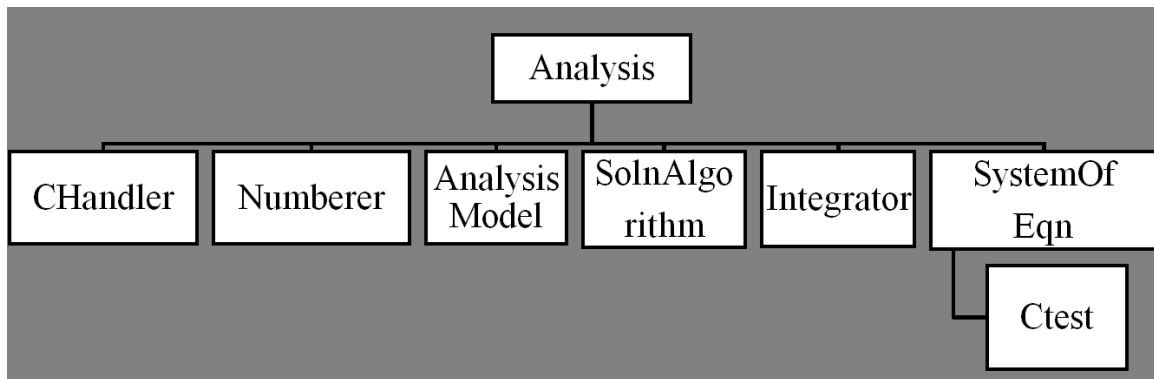


Figure 2.7 OpenSees “Analysis” abstraction (Mazzoni et al, 2005)

2.4 Past studies on Braced Steel Frames Behaviour using OpenSees

OpenSees has been developed as the computational platform for research in performance-based earthquake engineering at the Pacific Earthquake Engineering Research Center. This application has been widely adopted by researchers for nonlinear analysis of structures. Over the years, OpenSees has been refined and proven to be one of the most powerful nonlinear simulation tools providing accurate results for various analyses.

In order to validate the plastic behaviour of braces, several parameters defined in the OpenSees model have been studied and validated against the experimental test results. In general, these studies were focusing on bracing members with square or rectangular tubular cross-sections. These models were built with nonlinear beam-column elements. The Giuffre-Menegotto-Pinto hysteretic material was assigned to all the structural members. The influence of parameters such as: number of subelements, number of integration points per element as well as number of fibres were investigated by researchers (Aguero, A., Izvernari, C. and Tremblay, R., 2005, Izvernary, 2007; P. Uriz and Mahin, 2008). In addition, they considered rotational springs for modeling of the

gusset plate connections which enables braces to buckle out-of-plane. In order to calibrate the Giuffre-Menegotto-Pinto material, the variation of material parameters, such as: R_0 , a_1 , a_2 , a_3 and a_4 were investigated by Agüero et al. (2005) and validated against experimental test results, as shown in Figure 2.8.

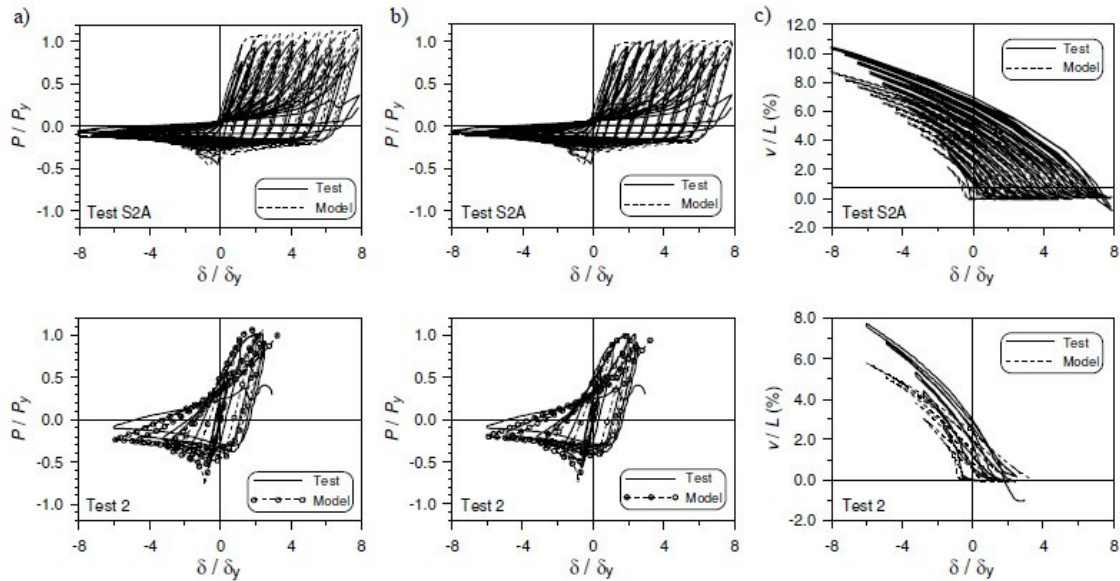


Figure 2.8 Comparison between test and pin-ended model with length KL: a) Hysteretic response with $R_0 = 25$, $a_1 = a_3 = 0.00001$, and $a_2 = a_4 = 0.00002$; b) Hysteretic response with $R_0 = 25$ and a_1 to $a_4 = 0.0$; c) Out-of-plane response at brace mid-length with $R_0 = 20$ and a_1 to $a_4 = 0.0$ (Agüero, A., Izvernari, C. and Tremblay, R., 2005).

Although there are slight differences between the model response and the experimental test, the OpenSees model offers a great accuracy in the force-deformation response and out-of-plane deformation due to its 3D analysis capability.

Chevron braced subassembly has been tested (Yang et al., 2009). The test setup is as shown in Fig. 2.9 and the subassembly is constructed with 2 HSS2x2x1/8 brace sections.

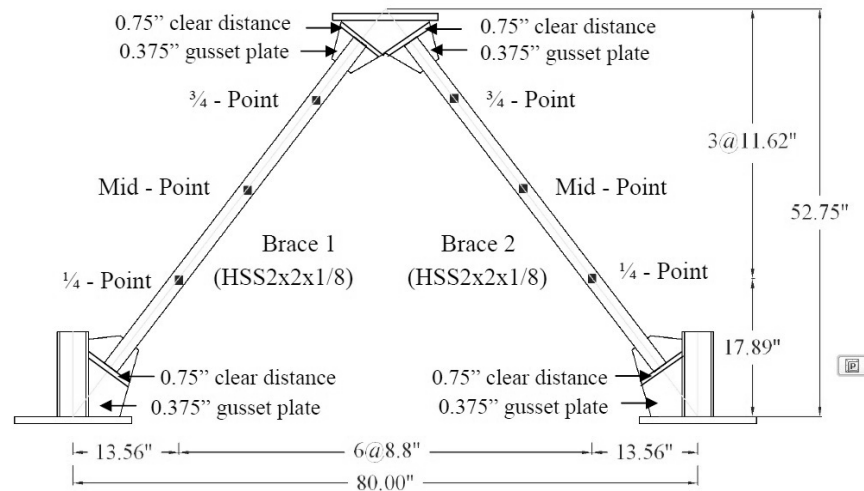


Figure 2.9 Chevron braced subassembly (Yang et al., 2009)

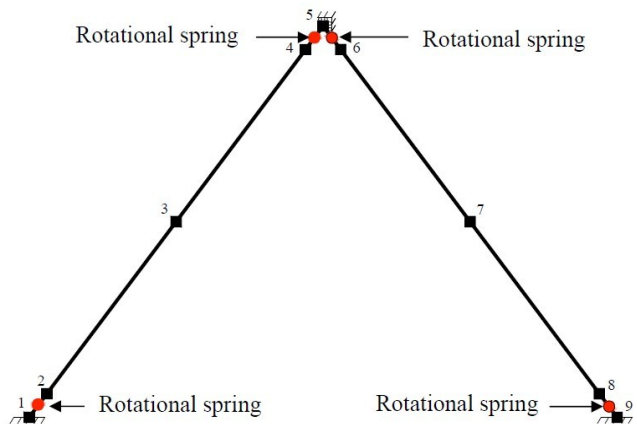


Figure 2.10 Chevron braced subassembly model (Yang et al., 2009)

The brace members were connected to beams and columns through gusset plates. All the dimensions are shown in Figure 2.9 in Imperial units. In the OpenSees model, a two-dimensional in-plane model was used. The brace members were modeled with two flexibility-formulation nonlinear beam-column elements with five fibre cross-sections along the length of each element, and a $1/100^{\text{th}}$ of the total length of braces out-of-straightness was implemented. Uniaxial Menegotto-Pinto steel material (Steel 02) was used to model the material behaviour. The gusset plates are modeled with rotational

springs with zero-length element from OpenSees Library (Figure 2.10). The properties of all the elements are modified according to the test. The force-deformation response of the chevron braced subassembly has been recorded and compared with OpenSees. It is shown that a well-defined OpenSees model is able to represent the response of the experimental test.

A comparative response of the experimental test and the OpenSees model response are shown in Fig. 2.11. A very good match is observed. However it is noted that the low-cycle fatigue is not considered in this model, which can be seen from the last cycle of experimental test data.

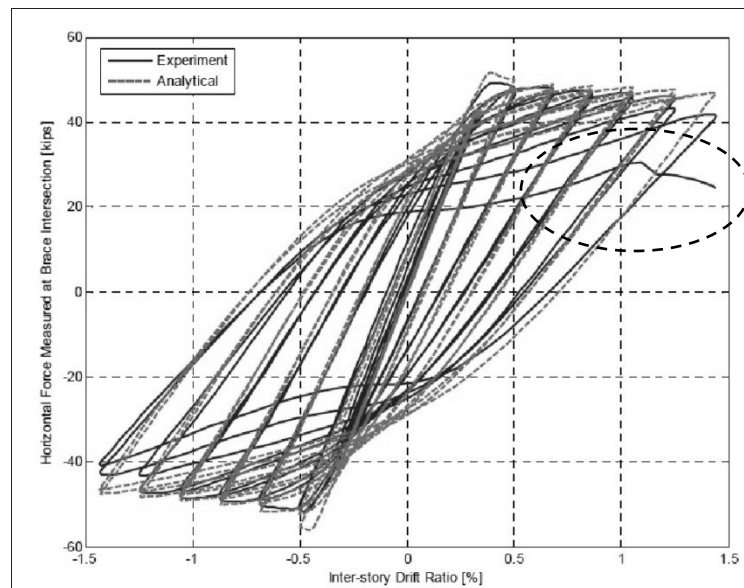


Figure 2.11 Experimental and Analytical response (Yang et al., 2009)

Furthermore, if the low-cycle fatigue and local buckling are of great concern of some particular problems, a more detailed model can be built in the OpenSees environment. This behaviour which captures the failure due to low-cycle fatigue was obtained by Uriz and Mahin and is detailed in their research report. This last study proved

again the capability of the OpenSees software to model the steel braced frame response under seismic loads as shown in Figure 2.12.

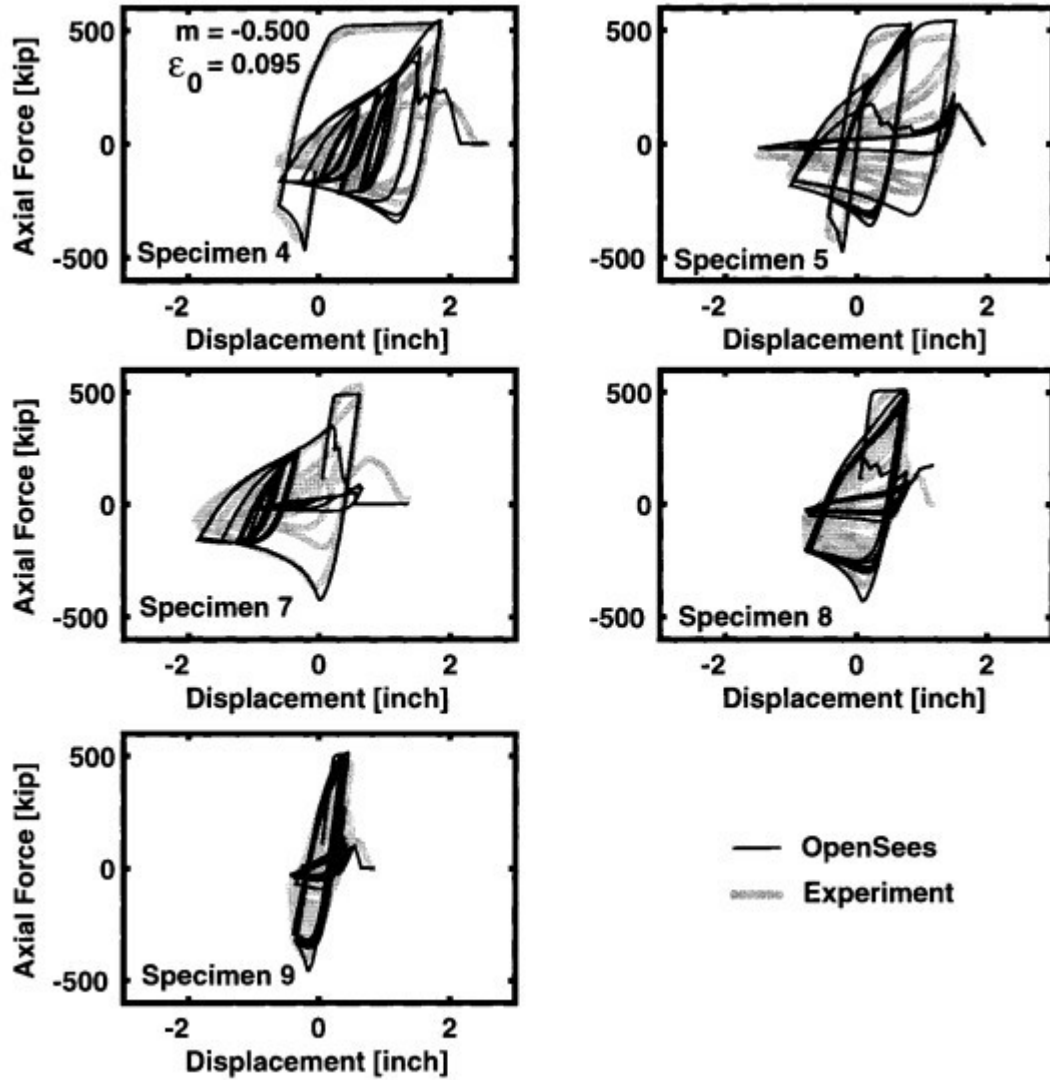


Figure 2.12 OpenSees model versus experimental test results by considering the low-cycle fatigue (Uriz and Mahin, 2008)

CHAPTER THREE: MODELING OF TUBULAR BRACING MEMBERS UNDER QUASI-STATIC LOADING

Braces are the most critical elements in typical braced frames. Thus, an accurate nonlinear brace model is in demand to simulate the seismic response of the zipper braced frame. Several researchers (Archambault, 1995; Walpole, 1996; Tremblay et al., 2001; Shaback, B., and Brown, T., 2003; Broderick et al., 2008; Haddad et al., 2009) have conducted experimental tests on the cyclic behaviour of tubular brace members in order to investigate the nonlinear brace response under cyclic loading. A comparative study of analytical brace response obtained in Drain2DX and OpenSees against experimental results under quasi-static cyclic loading is carried out in this chapter.

3.1 General characteristics of the refined brace model implemented in Drain2DX

The brace model, termed Element 05, was implemented in Drain2DX by Ikeda and Mahin (1984). This nonlinear brace element is defined by the refined physical theory model which consists of two elastic beam segments joined with a plastic hinge at mid-span (Figure 3.1 a). The beam segments allow elastic axial and flexural deformations while the state of the plastic hinge is defined by a P-M interaction curve. Empirical parameters for defining the P-M interaction curve and the tangent modulus of elasticity are included in the Ikeda and Mahin refined physical theory model (1984).

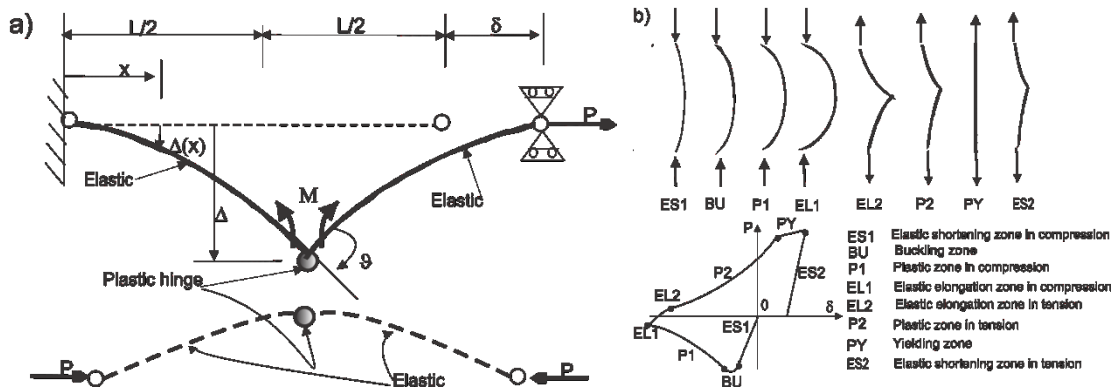


Figure 3.1 Refined physical theory model of brace: a) Refined physical theory brace models; b) Basic behaviour of a brace associated with each zone (Ikeda and Mahin, 1984)

When the brace member is loaded with axial compressive force P , a mid-span deflection Δ is raised. This deflection increases with the axial shortening deformation δ until the plastic hinge rotation is formed under the internal bending moment M . At this point, the force starts decreasing following the implemented P - M interaction curve and the rotation θ simulates the buckling of the brace.

The brace's hysteresis cycle can be divided in four zones: elastic zone, plastic zone, yielding zone and buckling zone, as shown in Figure 1 b). The elastic zone is divided into shortening (ES2 and ES1) and lengthening zones (EL2 and EL1) both in tension and compression and the plastic zone is divided into two zones in compression (P1) and tension (P2). The plastic hinge rotation is assumed to occur only in plastic zones and is defined as a function of axial force P and loading history. In Element 05, each zone is divided into a finite number of sections with constant tangent stiffness.

In Drain2DX, the tangent modulus E_t implemented in Element 05 (Ikeda and Mahin, 1984) influences the inelastic cyclic stretching and shortening of braces. For an elasto-perfectly plastic material assigned to the hinge zone, elongation δ increases under

constant tensile load. In this model, two linear empirical curves are implemented as shown in Figure 3.2. These curves are defined as a function of the normalized axial force, $p = P/P_y$, to define the ascending and descending patterns when the axial force decreases or increases. Sets of four parameters $e1$, $e2$, $e3$ and $e4$ are selected and calibrated based on available experimental data on the tangent modulus of elasticity. It is assumed that tangent modulus is constant until the specimen starts buckling or yielding; then it increases bilinearly when the axial force reverses. However, the difference between the deteriorations of the tangent modulus from cycle to cycle is ignored.

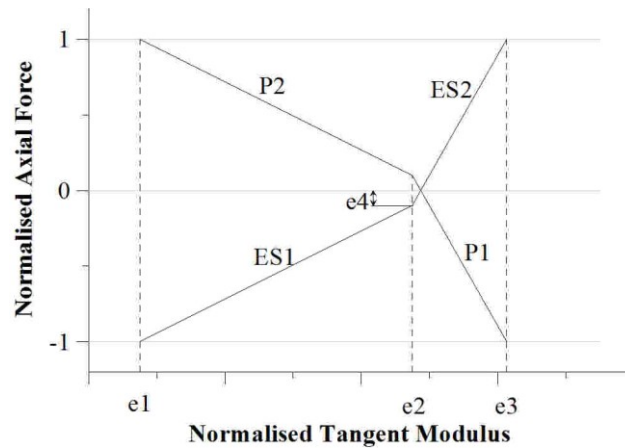


Figure 3.2 Linear Idealization Curves for Tangent Modulus History (Ikeda & Mahin, 1984)

Thus, in the nonlinear dynamic analysis, the Element 05 implemented in Drain2DX is capable of simulating the inelastic behaviour of braces with various types of cross sections. The accuracy of brace response depends on the defined P-M interaction curve, empirical parameters used to define the tangent modulus variation and the magnification factors in tension and compression.

In conclusion, the behavioural characteristics implemented in Element 05 are identified as: i) the material non-linearity per cycle, expressed by the tangent modulus of elasticity in place of the elastic modulus; ii) the deterioration of the cyclic plastic hinge rotation; iii) the consideration of residual displacement once the strength of the material starts degrading. However, local buckling and Bauschinger effect, the progressive degradation of tangent modulus during cycles and the spread of plastification along the brace's length are not considered in this model.

3.2 General characteristics of the brace model in OpenSees

In order to overcome the aforementioned limitations of Drain2DX brace model, the Nonlinear Beam-column element with fibre section was selected from the OpenSees's library to simulate the inelastic brace response. This Nonlinear Beam-column element allows plasticity to be spread along the member length. A corotational transformation method is selected to account for the large displacement and a bilinear material law known as Menegotto-Pinto material with isotropic strain hardening is used.

Uriz and Mahin (2004) have underlined that more accurate inelastic brace behaviour can be simulated with nonlinear beam-column elements combined with fibre section model, by applying an initial camber at the member mid-length and attributing the uniaxial Material Steel02, also known as Giuffre-Menegotto-Pinto model with isotropic strain hardening. The Menegotto-Pinto functions (1973) express stresses as a function of strain and the material model is defined based on the following equation:

$$\sigma^* = b\varepsilon^* + \frac{(1-b)\varepsilon^*}{(1 + \varepsilon^{*R})^{\frac{1}{R}}} \quad \text{Equation 3.1}$$

where σ^* and ε^* are the effective stress and strain depending on the unload/reload interval, b is the ratio of the final to initial tangent stiffness and R is a material parameter which defines the shape of the unload curve. The Menegotto-Pinto function for the strain stress curve is able to describe the response of the highly nonlinear model accurately. It is stated that the initial tangent stiffness E_0 is equal to the elastic stiffness E , the stress-strain relation is linear in the elastic range $\sigma_0 = E\varepsilon_0$ and under the yielding plateau, the strain increases from yielding strain ε_0 to strain hardening ε_{sh} while the stress σ_0 is constant. The Menegotto-Pinto model accounts for the accumulated plastic deformation at each point of load reversal. Thus, the hysteresis loop follows the previous loading path for a new reloading curve while the deformation is cumulated.

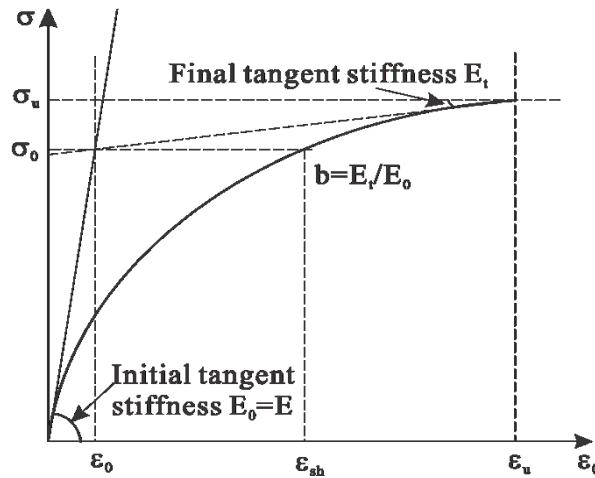


Figure 3.3 Menegotto-Pinto model for steel material

In OpenSees environment, the brace model consists of a number of force-based elements with distributed inelasticity over the length of the member. The steel fibres of

the elements are defined with Menegotto-Pinto stress-strain relationship. Thus, both Bauschinger effect and P - M interactions are considered. The force displacement relation in the standard force-based element formulation is established on the basis of local coordinates, which has been transformed to global reference system following the concept of the Corotational geometric transformation, in other words, large displacement geometry is also considered in the model. With this approach, two elements for each brace are sufficient to simulate the buckling zone. Even though the local buckling is not considered in the model, according to Uriz and Mahin (2008), the nonlinear response of hollow cross-sectional braces does not seem to be substantially affected.

3.3 Selected experimental tests from literature

For validating the accuracy of the computed models, four full-scale brace members with tubular cross-sections, loaded first in compression were selected from nine experimental studies (Tremblay, 2002). Among them, three out of twenty-four brace specimens tested at the Structural Engineering Laboratory at Ecole Polytechnique, Montreal (Archambault et al., 1995) and one out of twenty specimens tested at the University of Calgary (Shaback and Brown, 2004) were selected. The three selected specimens, belonging to the first group, have been tested in a single bracing frame configuration as pin-ended members. The test set-up is shown in Figure 3.4 and was used for experimental investigation of a single and X-bracing frame configuration. Among the three selected braces, two of them labelled $S1B$ and $S3B$ were tested under cyclic quasi-static displacement loading type H_I (Figure 3.6 a,b), while the third brace, $S1QB$, under displacement time history Q (Figure 3.6 c). The selected cyclic quasi-static loading sequence H_I is a symmetrical displacement pattern with stepwise increasing deformation

cycles, as recommended in ATC-24 (1992). Two identical cycles were defined at each second step and the increment in peak deformation between successive steps was set to 0.67 times the interstorey drift at yielding. The selected Q sequence is a displacement history developed based on the results of nonlinear dynamic time step analyses performed on typical two- and three-storey buildings subjected to several ground motion records. Specimens $S1B$ and $SIQB$ have the same rectangular hollow section RHS 152x76x4.8, while the slender brace $S3B$ has a square hollow section HSS 76x76x4.8. During the experiments, the interstorey drift Δ and the storey shear V was obtained, so that storey shear-drift hysteretic loops were built and illustrated in this study. The third selected brace has a cold-former hollow section made of CSA-G40.21M-350W steel ($F_y=350$ MPa; $F_u=450$ MPa). The deformation δ_y corresponds to the clear brace length L_B multiplied by the yield strain of the brace, $\varepsilon_y=F_y/E$ with $E=200000$ MPa. For the single brace specimens, the effective buckling length KL varies between 0.88 to 0.96 L_H . The slenderness parameter $\lambda=(KL/r)(F_y/\pi^2E)^{0.5}$ as well as the mechanical and geometrical properties of the selected braces are given in Table 3.1.

The brace effective slenderness ratio KL/r was evaluated in the plan of buckling considering end conditions. Specimens $S1B$, $SIQB$ have a slenderness of $KL/r = 92.6$ while the $S3B$ specimen has a slenderness of $KL/r = 143.2$. In Table 3.1, the length of the braces between the two ends hinges L_H is equal to the distance between the points where hinges were observed in the gusset plates during the tests.

The brace specimen labelled $2A$ was selected from the experimental tests conducted at Calgary University. The $2A$ brace specimen is a stocky HSS152x152x8.0 member with a

slenderness ratio equal to 68 this specimen was first loaded in compression under the cyclic quasi-static loading protocol as shown in Figure 3.6d and its mechanical and geometrical characteristics are presented in Table 3.1. The experimental set-up for a single brace member is shown in Figure 3.5. The yield strength F_y of the selected braces was obtained using the 0.2% offset method from stub-column testing of sample bracing member. All of the selected specimens have developed a plastic hinge at the member mid-length.

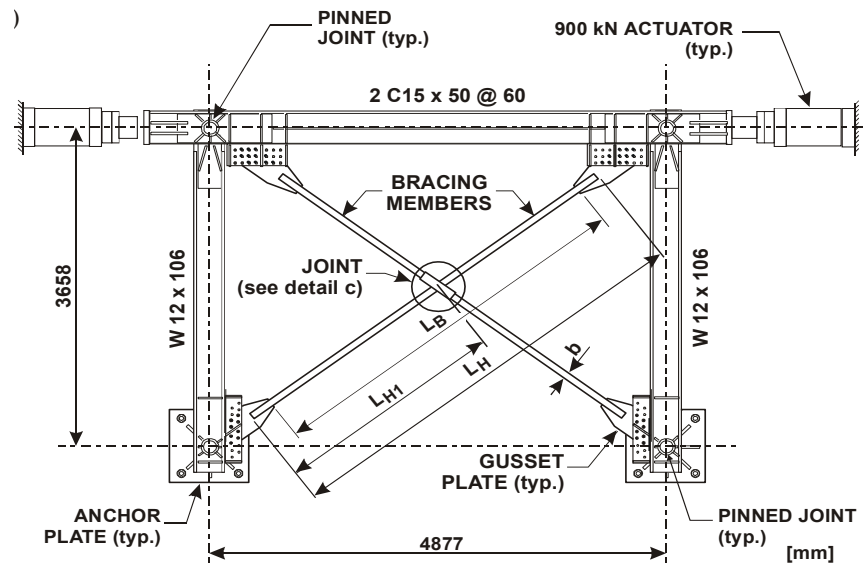


Figure 3.4 Experimental set-up for single and X bracing frame configuration (Tremblay et al., 2003)

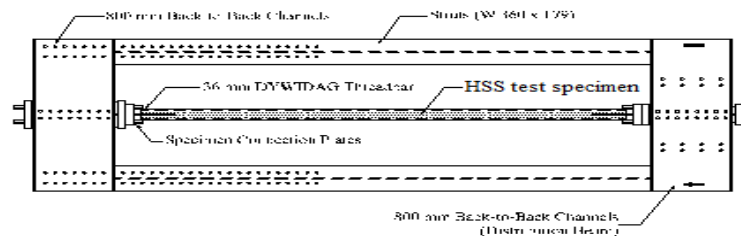


Figure 3.5 Experimental set-up for single brace 2A (Shaback, B., and Brown, T., 2003)

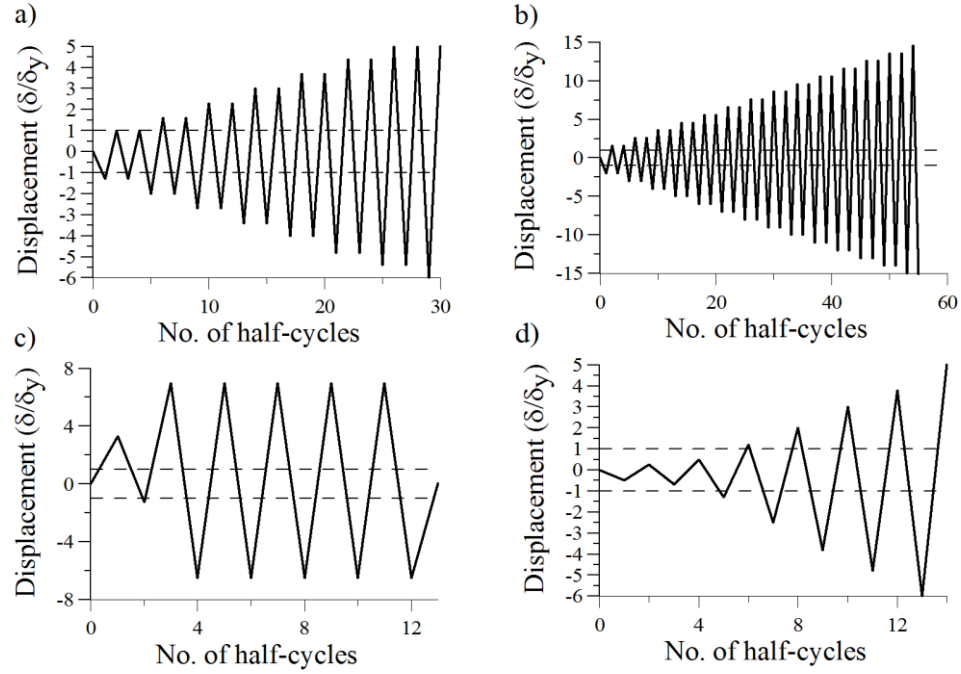


Figure 3.6 Loading protocols for specimens a) *S1B*; b) *S3B*; c) *S1QB*; and d) *2A*

Table 3.1 Properties of selected test specimens

Study no./Test specimen	Hollow cross-section	Ag mm ²	F _y MPa	I 10 ⁶ mm ⁴	Z 10 ³ mm ³	r mm	(b ₀ /t)/(b ₀ /t) _{lim}	L _B mm	L _H mm	KL/r	λ	δ _y mm
1/S1B	127x76x4.8	1790	395	3.78	73.8	45.9	0.67	4007	4610	92.6	1.312	7.922
1/S1QB	127x76x4.8	1790	395	3.78	73.8	45.9	0.67	4009	4610	92.6	1.319	7.926
1/S3B	76x76x4.8	1310	389	1.08	34.4	28.8	0.67	4179	4619	143.2	1.990	8.126
7/2A	152x152x8.0	4430	442	15.1	237	58.4	0.86	3950	3995	68	1.01	8.730

The resistance capacity of selected specimens in tension $A_g F_y$ and compression C_r (where $C_r = A_g F_y (1 + \lambda^{2n})^{-1/n}$), as well as the probable capacity in tension $A_g R_y F_y$ (where $R_y = 1.1$), compression C_u and the probable postbuckling capacity in compression C_u' are given in Table 3.2. In addition, Table 3.2 gives the horizontal projection of axial forces developed on braces during the experimental test conducted on the set-up illustrated in Figure 3.4.

Table 3.2 Calculated tensile and compressive strength of test specimens

Study no. ¹⁾ / Test specimen	Hollow cross-section shape	$A_g F_y$ kN	$A_g R_y F_y$ kN	C_r ($\phi=1$) kN	C_u kN	C_u^* kN	C_r / T_r	C_u' / C_u	$A_g R_y F_y / \cos\theta$ kN	$C_u \cos\theta$ kN	Test results kN
1/S1B	127x76x4.8	706	777	305	403	155	0.43	0.38	622	320	$T_{max}=526$ $C_u=328$
1/S1QB	127x76x4.8	706	777	304	401	155	0.43	0.38	622	318	$T_{max}=722$ $C_u=362$
1/S3B	76x76x4.8	510	561	115	152	112	0.23	0.74	449	121	$T_{max}=464$ $C_u=129$
7/2A	152x152x8	1958	2154	1156	1526	431	0.59	0.28	-	-	$T_{max}=2164$ $C_u=1507$

* $C_u^* = 0.2A_g R_y F_y$ (probable postbuckling compressive capacity)

3.4 Comparison of analytical inelastic braces response in Drain2DX and OpenSees versus Experimental

3.4.1 Empirical parameters calibration for Element 05 implemented in Drain2DX

The concentrically braced frame in single bracing configuration illustrated in Figure 3.3 was modeled in Drain2DX and tested under the same loading protocols as considered in experiments.

All the beam-to-column connections and brace-to-gusset plate connections are considered as pin connections in the model. The beam and columns are modeled as beam-column element, Element 02. Braces were modeled with Element 05 and the brace's gusset plate was modeled with Element 01 (Elastic truss element). Regarding the refined brace model (Element 05), a set of empirical parameters (p_{12} , b_1 , c_1 , a_2 , b_2) is required to define the theoretical $P-M$ interaction curve and a set of four parameters (e_1 ,

e_2, e_3, e_4) is required to define the bilinear variation of the tangent modulus curves after buckling or yielding. Parameters α_t, α_c can also be defined to adjust the magnitude of yielding forces in tension and compression.

For the refined physical theory brace model, the effective plastic hinge moment M is expressed as the product of the axial force P and the effective lateral displacement, Δ_{eff} . Based on the measured yield stress during experimental tests and assuming a elastic-perfectly plastic property for the material, two parabolic equations have been proposed by Ikeda & Mahin for the theoretical P - M interaction curve: $m = 1 + b_1p + c_1p^2$ for $0 \leq p \leq p_{12}$ and $m = a_2 + b_2p + c_2p^2$ for $p_{12} \leq p \leq 1$ (where $m = M/M_p$ and $p = P/P_y$). The empirical parameters $a_1, b_1, c_1, a_2, b_2, c_2$ and p_{12} were suggested based on the experimental tests conducted for a brace member with tubular cross-section, HSS 102x102x12.5. The values of suggested parameters are given in Table 3.3 while the P - M interaction curve is illustrated in Figure 3.7.

Table 3.3 Coefficients for defining the theoretical P - M interaction curve

Study	p_{12}	b_1	c_1	a_2	b_2	c_2
Ikeda and Mahin proposal (HSS 102x102x12.5)	0.5	0	-1.33	1.33	-1.33	0
This study	0.6	0	-1.04	0.788	0.495	-1.278

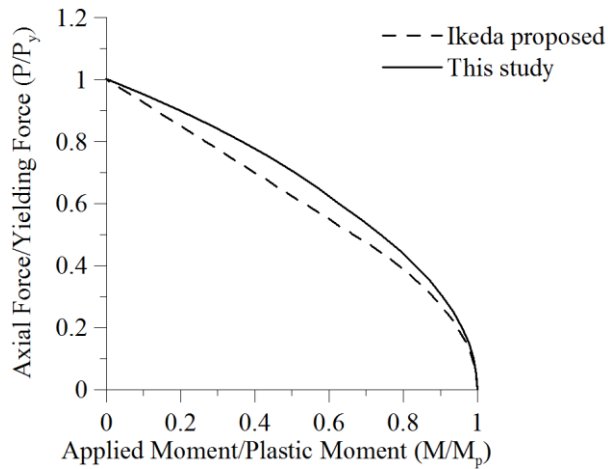


Figure 3.7 Theoretical P-M interaction curves

The empirical parameters e_1 , e_2 , e_3 , e_4 used to determine the slope of the hysteresis loops are shown in Table 3.4. In order to match the experimental curves (analyzed in this study) with the theoretical ones based on the refined model, the value of the parameters defining the tangent modulus curves has to be slightly adjusted. It is noted that Ikeda and Mahin have considered a W-shape member to calibrate the e_1 to e_4 parameters.

Table 3.4 Empirical parameters for describing the tangent modulus curves for braces with tubular sections

Study	e_1	e_2	e_3	e_4
Ikeda & Mahin proposal	0.05	0.9	1.25	-0.25
This study	0.15	0.95	1.225	0

Magnification factors, α_t and α_c are used to adjust the tensile and/or compressive capacities of brace members with values obtained in experimental tests. The magnification factors proposed by the previous and current study are shown in Table 3.5

as well as the value of the constant β , which defines the plastic hinge rotation degradation in the elastic elongation zone.

Table 3.5 Magnification factors for braces with tubular sections

Study	α_t	α_c	β
Ikeda & Mahin proposal	0.9	0.8	1.2
This study	1.0	1.0	1.2

3.4.2 Comparison of analytical results using Drain2DX with experimental results

By considering the same quasi-static loading as depicted in Figure 3.6 and the geometrical properties of the braced frame setup as illustrated in Figure 3.3, respectively Figure 3.4, the computed hysteresis loops (force versus displacement) of specimens *S1B*, *SIQB*, *S3B* and *2A* are shown in Figures 3.8 to 3.11. It is underlined that during the experimental test, the inelastic deformations were observed only in the brace member. As in the aforementioned figures, the refined Drain2DX brace model is able to simulate very well the overall cyclic behaviour of related brace members. In this study, by using the empirical parameters proposed for the Element 05, the analytical hysteresis loops are a better match to the experimental results. However, the brace model is not able to perfectly simulate the sample inelastic behaviour especially in the plastic zones of hysteresis loops, which are depicted from force-displacement parameters.

For the slender specimen *S3B* with $KL/r = 143$ the analytical results obtained in the tensile plastic zone P2 underestimate the slopes of the force displacement curves and fail to reach the tensile axial strength. This limitation can be overcome by implementing the Baushinger effect in the brace model.

During later cycles following buckling and at the junction of the elastic shortening zone in compression ES1 and the plastic zone in compression, some underestimated strength is observed for all specimens. This transition can be corrected if the model is able to consider the effect of the gradual spread of plastification across the brace length.

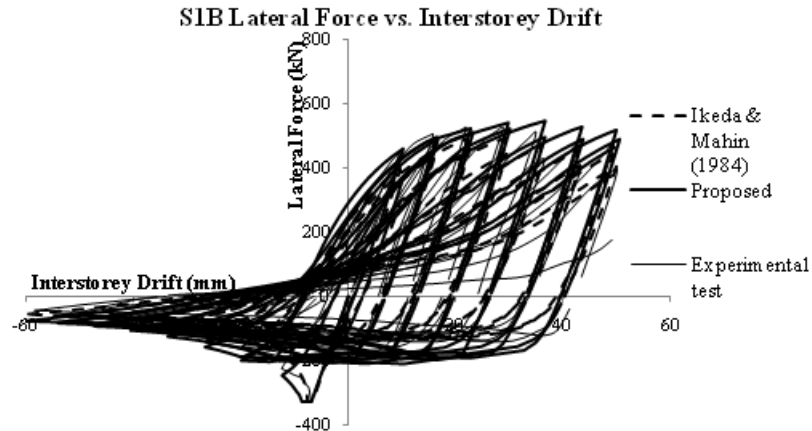


Figure 3.8 Hysteresis loops of specimen *S1B*

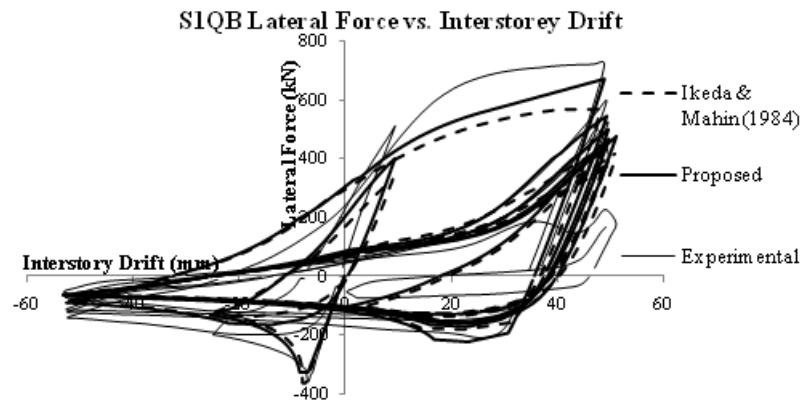


Figure 3.9 Hysteresis loops of specimen *S1QB*

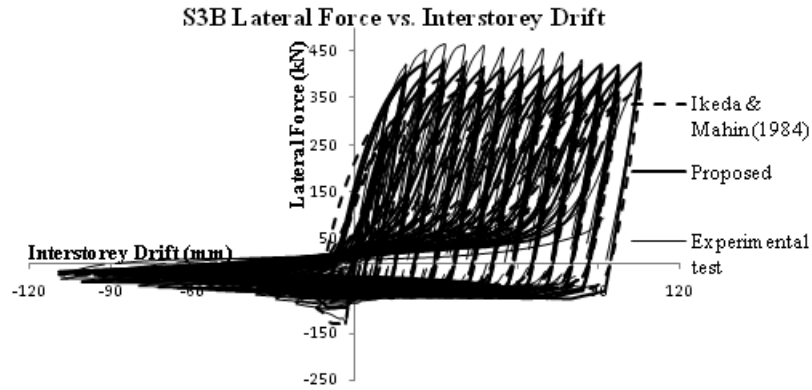


Figure 3.10 Hysteresis loops of specimen *S3B*

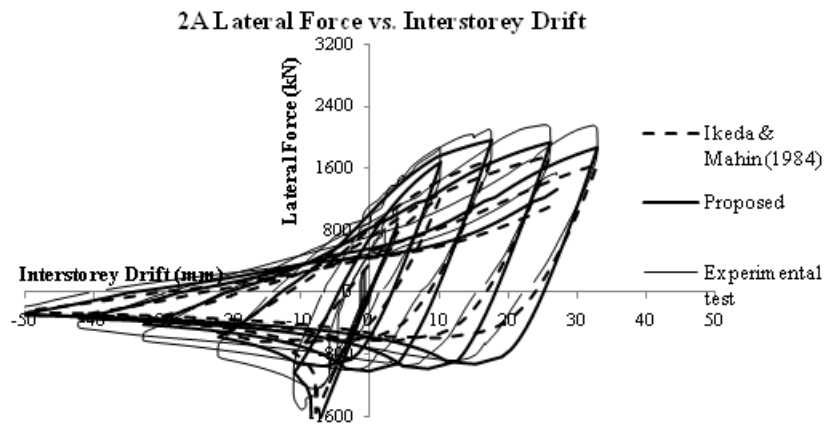


Figure 3.11 Hysteresis loops of specimen *2A*

3.4.3 The influence of parameters required in *OpenSees* for the brace model

The brace element is modeled with a force-based nonlinear beam-column element which relies on an iterative force formulation and considers distributed plasticity across the element's length. In this study, the Goffre Menegotto-Pinto material is used and the parameters considered to define the transition between elastic to plastic response are the same as given in Aguilero et al. (2006): $R_0 = 20$, $cR1 = 0.925$, $cR2 = 0.15$; $a_1 = a_3 = 0.00001$, $a_2 = a_4 = 0.00002$ for the isotropic hardening parameters; and $b = 0.01$ for the kinematic hardening parameter. These parameters used to define the steel material were

calibrated from the load-deformation response of an inner plate for a buckling restrained bracing member and subjected to quasi-static cyclic testing (Tremblay et al., 2004).

The brace member is modeled as being composed of a number of nonlinear beam-column elements. In order to percept the sinusoidal out-of-straightness deformation of braces, more than two nonlinear beam-column elements have to be considered (Figure 3.12). Herein, the gusset plate is modeled as a rigid link and its length used for the numerical model corresponds to that used in the experiment tests. The two rigid links are connected to the nonlinear beam-column elements by using zero-length rotational springs and the residual stress of the brace member is disregarded.

Simulation of the inelastic brace member behaviour (yielding in tension and buckling in compression) strongly depends on the following parameters:

- the amplitude of the initial geometric imperfection at brace mid-span (out-of-straightness), e ;
- the numbers of fibres discretization over the member's cross-section, N_f ;
- the number of nonlinear beam-column elements across the brace length, N_e and
- the number of integration points per element, N_i .

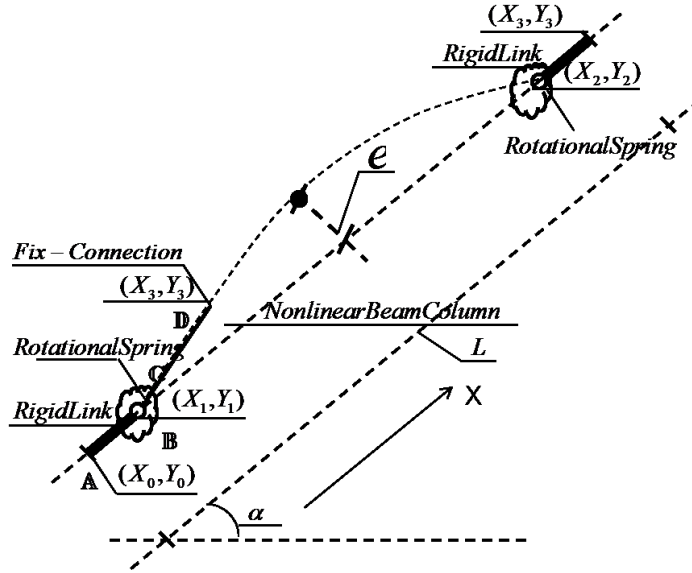


Figure 3.12 The considered brace model in OpenSees

3.4.3.1 The influence of the out-of-straightness parameter

For the specimen 2A in consideration here, the effect of initial camber (out-of-straightness) is investigated. Four different values, corresponding to $1/1000^{\text{th}}$, $1/600^{\text{th}}$, $1/350^{\text{th}}$ and $1/100^{\text{th}}$ of the brace length ($L=3.95\text{m}$) have been considered. These values applied at the brace mid-length corresponds to initial out-of-straightness parameters of $e=3.95\text{mm}$, 6.58mm , 11.28mm and 39.5mm , respectively. Herein, the brace was composed of two nonlinear beam-column elements, the brace cross-section was defined by $N_f = 16$ fibres as per discretization type “A” shown in Figure 3.14 and four integration points, N_i were used for each one of the two elements. The sensitivity of the out-of-straightness parameter (e) with the buckling load is clearly emphasised in Figure 3.13. By amplifying the initial camber, required to be specified for the brace model, the developed buckling load reduced significantly, while the postbuckling load is not affected. Therefore, if the initial camber is larger than expected (for example $L/100$) the buckling

is reached prematurely and conducts to a false inelastic deformation mechanism. By analysing the buckling load corresponding to an initial camber $L/350$ versus the brace buckling force C_u given in Table 2 it seems that $L/350$ (11.3mm) is a realistic value, even if $L/300$ (13mm) seems to be more accurate.

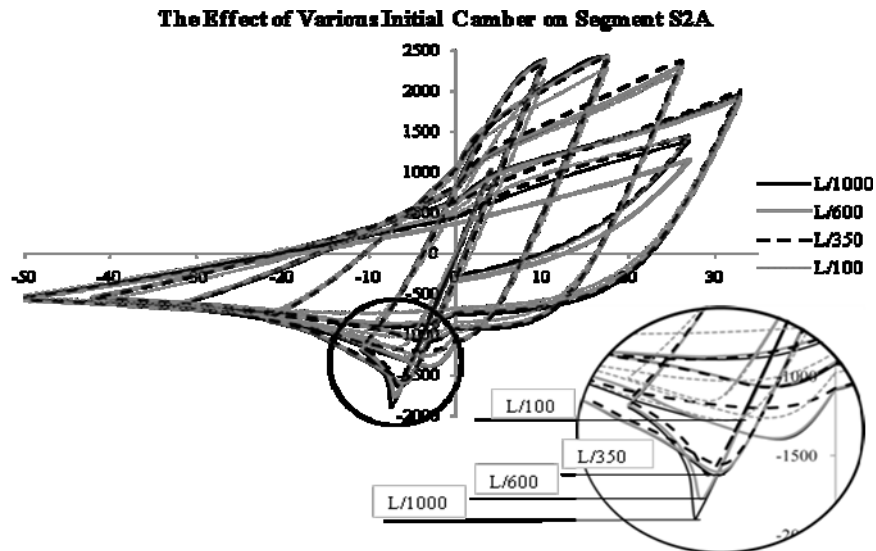


Figure 3.13 Effect of the out-of-straightness parameters with buckling load captured in the hysteresis loops

Therefore, the accuracy of the brace response at the first buckling zone is influenced by the out-of-straightness parameter, e , which needs to be applied at the middle of the brace.

In this study the out-of-straightness parameter is calculated based on the analytical equation given by Diciceli and Metha (Simulation of inelastic cyclic buckling behaviour of steel box sections, 2007), which is:

$$e = \frac{M_{pb}}{P_b} \left(1 - \frac{P_b L^2}{12EI} \right) \quad \text{Equation 3.2}$$

where P_b is buckling load of the brace, M_{pb} is the reduced plastic moment of the brace which corresponds to P_b on the proposed P-M interaction curve given in Figure 3.7, and L , E and I are the length of the brace, the modulus of elasticity and moment of inertia of the brace about the axis of buckling, respectively. For example, considering brace 2A, the M_{pb} value which corresponds to $P_b = 1507kN$ in the given P-M curve is $M_{pb} = 54kNm$; the calculated value of $e = 13mm$ matches perfectly the estimated ratio $L/300$. However, for various brace lengths and cross-sections, by estimating the out-of-straightness parameter e as being the same percentage of the length of the member is not accurate. During the member iterations, the coordinates of the fibres are constantly updated starting from the initial configuration with camber included. Thus, the employment of the above equation is recommended to evaluate the out-of-straightness parameter, which is very sensitive to the value of buckling load.

In braced frame analysis, when the exact buckling load of brace members cannot be obtained directly, an initial sinusoidal out-of-straightness with maximum amplitude corresponding to $1/500^{\text{th}}$ of the brace length are generally tested to give a satisfied buckling response.

3.4.3.2 The influence of the number of fibres

The number of fibres discretization over the element cross-sections may impact the hysteretic behaviour of braces. Two types of fibre discretization for tubular cross-sections are considered herein and are labelled in this study types “A” and “B” as is shown in Figure 3.14. Thus, in case “A” illustrated here, an arrangement of 16 fibres are distributed

as follow: 1 fibre is concentrated at each corner of the element's cross-section and the remaining 12 fibres are distributed at equal distance across the webs and the flanges of the studied tubular section (3fibres each as for HSS sections).

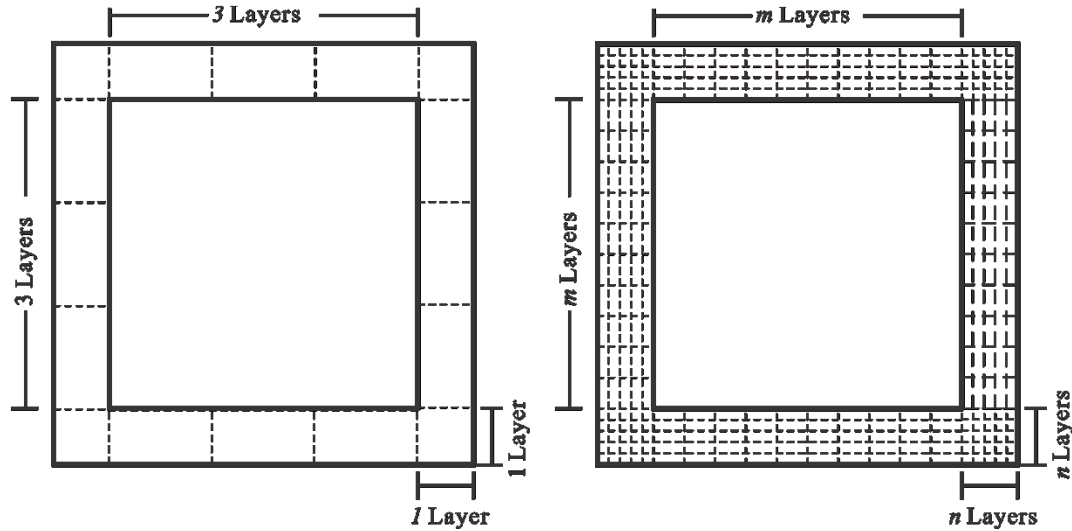


Figure 3.14 Layout of different fibre discretization: a) Type “A”, with 16 fibres; b) Type “B”, with $4 \times n(m+n)$ fibres

In case “B”, each corner of the element's cross-section is meshed with $n \times n$ fibres while the flanges and webs are meshed with $m \times n$ fibres. In comparison, m is set equal to 120 and n is set equal to 5, thus, the entire cross-section is discretized with 500 fibres.

Difference in results between both cases: $N_f=16$ and $N_f=500$, is shown in Figure 3.15 for brace *S1B*. The analytical model was built with two nonlinear beam-column elements ($N_e=2$) and four integration points per element ($N_i=4$).

The number of fibres used to mesh the brace cross-section influences the hysteresis behaviour of the brace, while, more importantly, in the case of highly nonlinear

elements, further meshing offers a better chance of convergence while slightly increases the computation time.

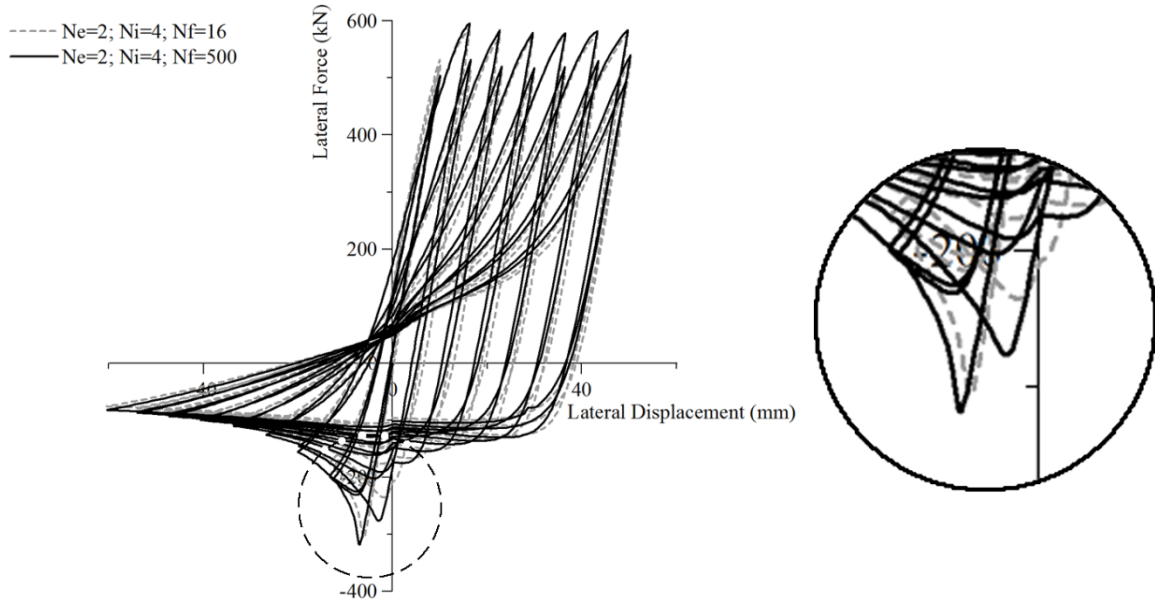


Figure 3.15 Hysteresis loops of specimens *S1B* with different fibre discretization

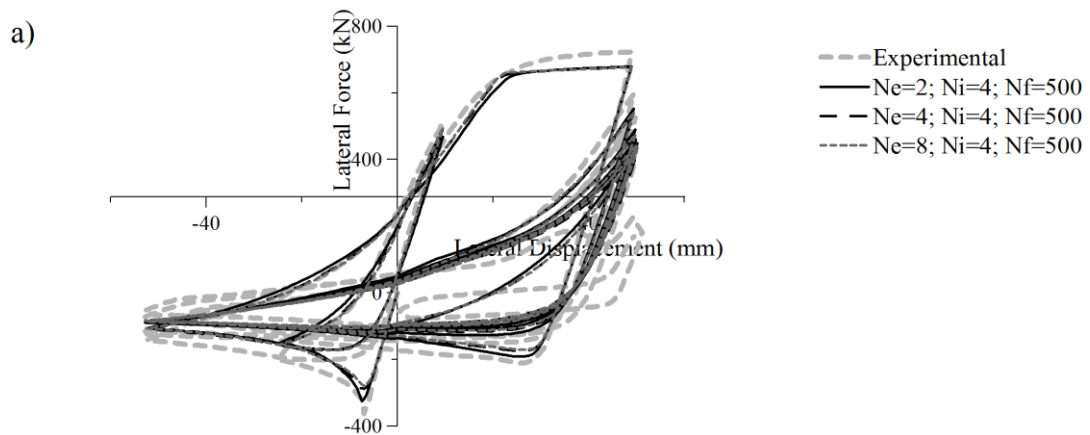
3.4.3.3 The influence of the number of elements

In this analysis, the number of nonlinear beam-column elements considered to make up the brace member and to enable the brace to accommodate a sinusoidal deflected shape is 2, 4 and 8. Recalling the Uriz and Mahin study (2008), the number of elements used with the aim to capture the displaced shape of the buckled brace was 30, 10, 4 and 2. However, 2 beam-column elements are not sufficient for modeling an adequate deflected shape. In this study, the case with 2 beam-column elements is considered for the comparison purpose. Again, the number of fibres used in this investigation is 500 and the number of integration points per element is $N_i = 4$. As is shown in Figure 3.16, the number of elements selected to model the brace *S1QB* has a small effect on the buckling force prediction and has a slightly difference in the postbuckling range. Furthermore, it

can be noticed that when more than 4 elements are used, the analytical brace response in terms of both hysteresis behaviour and energy dissipation is almost identical. On the contrary, modeling each brace member with only 2 nonlinear beam-column elements, a minimum computation time is required while the model is still able to capture larger curvature during the nonlinear global response if refined efficient meshing is applied at the level of the cross-section, however, using more than 4 elements is recommended.

A similar conclusion related to the minimum number of elements used for brace modeling was formulated by Uriz and Mahin (2008) and Aguero et al. (2006). They mentioned that different curvature distribution is obtained for 2, 4, and 6 elements with 16 fibres per cross-section and 4 integration points. Choosing more elements to simulate an accurate deformed shape is highly recommended. However, increasing the number of nonlinear beam-column elements requires an increase in the computation time.

Analytical response of specimen *SIQB* versus experimental test results



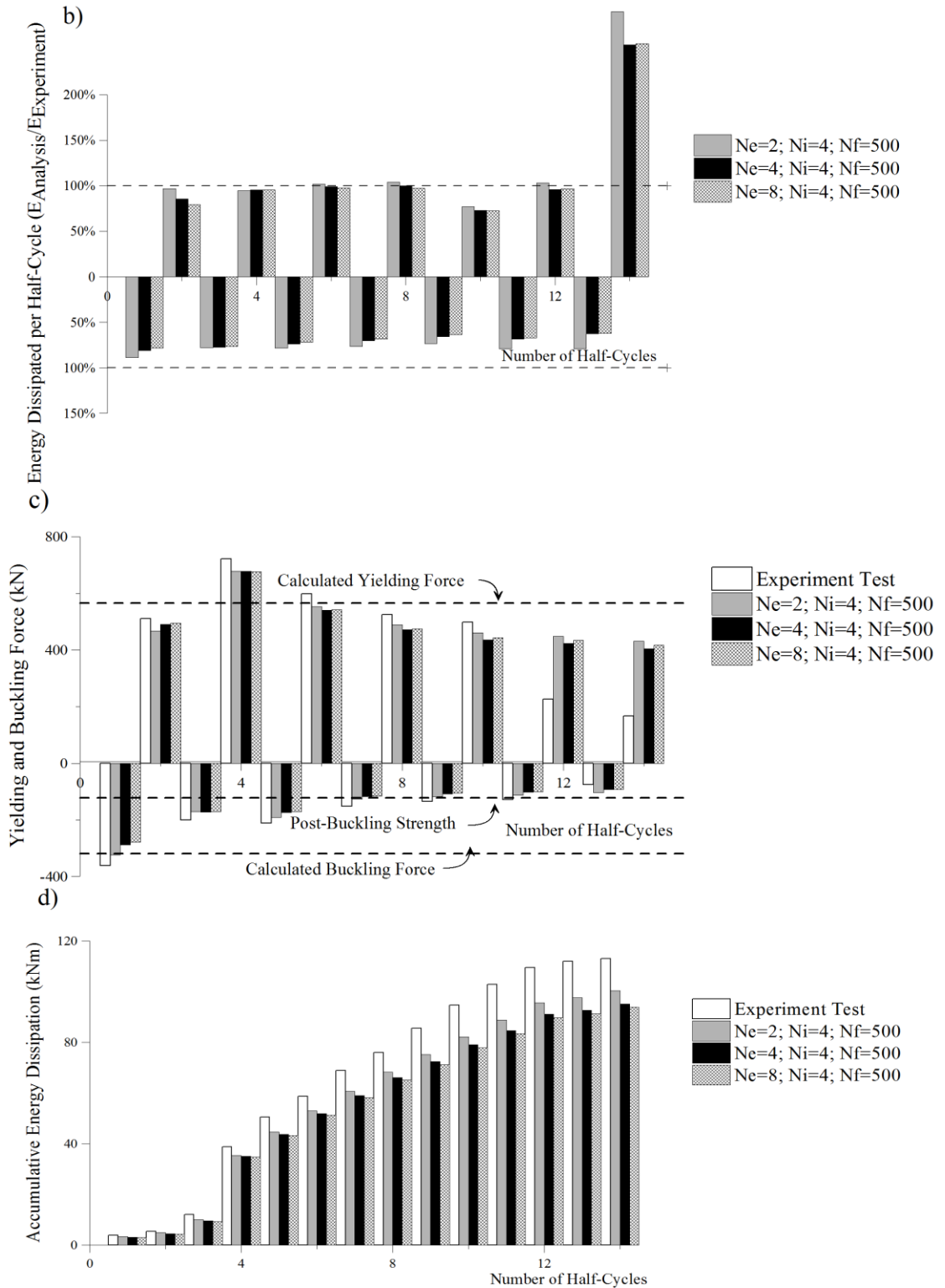


Figure 3.16 Effect of different numbers of nonlinear beam-column elements on the buckling and hysteresis response of specimen *SIQB*: a) Hysteresis loops; b) Energy dissipated per half-cycles; c) Yielding & buckling forces of each half-cycle; d) Accumulated energy dissipation.

3.4.3.4 The influence of the number of integration points

In this analysis the number of elements along the brace length was fixed to two, the number of fibres was set equal to 16 as per type “A” of discretization and the number of integration points is varied within each element such as: 2, 3, 4, 6 and 8. The initial camber was calculated based on the equation given in section 3.5.3.1, and the value corresponds to $L/350$. If two integration points are set per element the result differs significantly from others when 4, 6, 8 integration points have been considered. This comparative analysis is illustrated in Figure 3.17 for the *S2A* specimen. Therefore, to ensure the accuracy of the brace behaviour, at least 4 integration points per element are required. From Figure 3.17 it can be seen that the difference in brace response when 4, 6, or 8 integration points are selected is negligible. Aguerro et al. (2006) has also recommended that each nonlinear beam-column element to includes 4 integration points.

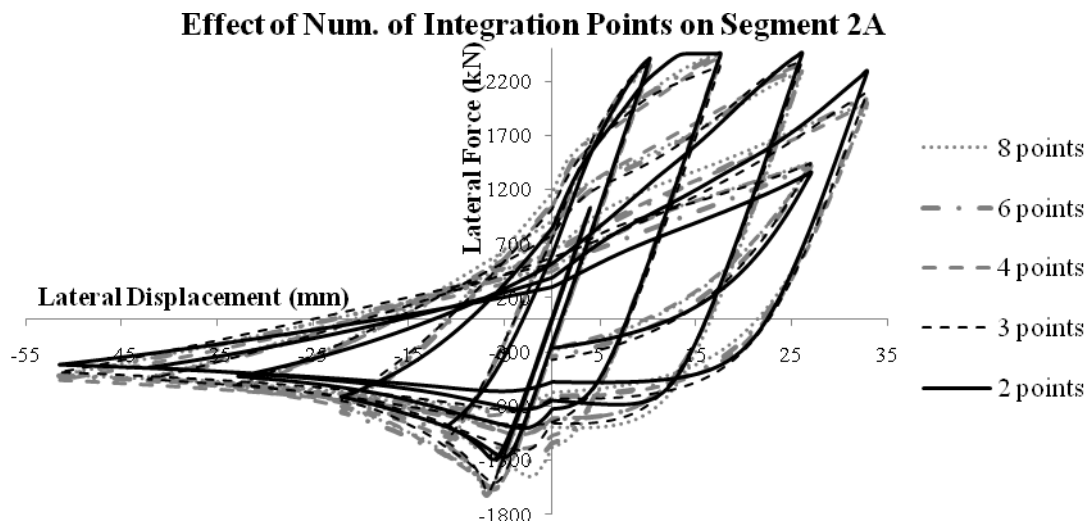


Figure 3.17 Effect of the number of integration points per nonlinear beam-column element to the specimen 2A

3.4.4 Comparison of analytical results using OpenSees with experimental results

Correlations between analytical studies and experimental test results demonstrate the ability of the proposed model to simulate the inelastic brace response under cyclic loading. In these analyses the uniaxial steel Giuffre-Menegotto-Pinto material nonlinearity is defined by integrating the stress-strain relation expressed at the material level over the area of the cross-section. Due to the large number of meshes (fibres), the computational attempt to perform the numerical integration and storage of variables render the modeling more demanding at the level of computation (De Sousa, 2000). However, by considering the characteristics of the nonlinear beam-column element to spread plasticity across the element length, the employed force-based formulation provides a good estimation of stiffness variation along the nonlinear beam-column element. This occurs in the presence of moderately large deformations. The effect of N_f and N_e are further studied and the results are illustrated in Figure 3.18. For these studies, the amplitude of initial out-of-straightness was considered $L/350$ and 4 integration points are assigned for each nonlinear beam-column element. A Newton algorithm with line search was selected from the OpenSees library in order to achieve rapid convergence (Mazzoni et al., 2005). This algorithm uses an energy increment for which the tolerance was set equal to 10^{-6} for a maximum of 500 iterations.

As shown in Figure 3.18, for element *S1B*, a good match has been observed with experimental test results in terms of forces developed in each half-cycle if 4 or 8 nonlinear beam-column elements are considered and the element cross-section is meshed with 500 fibres instead of only 16 fibres. As highlighted in the figure, if 500 fibres are used the tensile forces developed in the first few cycles are closer to the experimental

values. Similar conclusions can be formulated by considering the output of energy dissipation per each half-cycle.

Different N_f and N_e values do not have a significant influence on the brace behaviour in terms of cumulative energy dissipation. Therefore, by assigning 500 fibres to the nonlinear beam-column element cross-section, the model simulates the response more accurately, especially in the first a few cycles, even when only 2 elements are used for each brace. Therefore, $N_f=500$, $N_e=4$ and $N_i=4$ are used for future brace modeling.

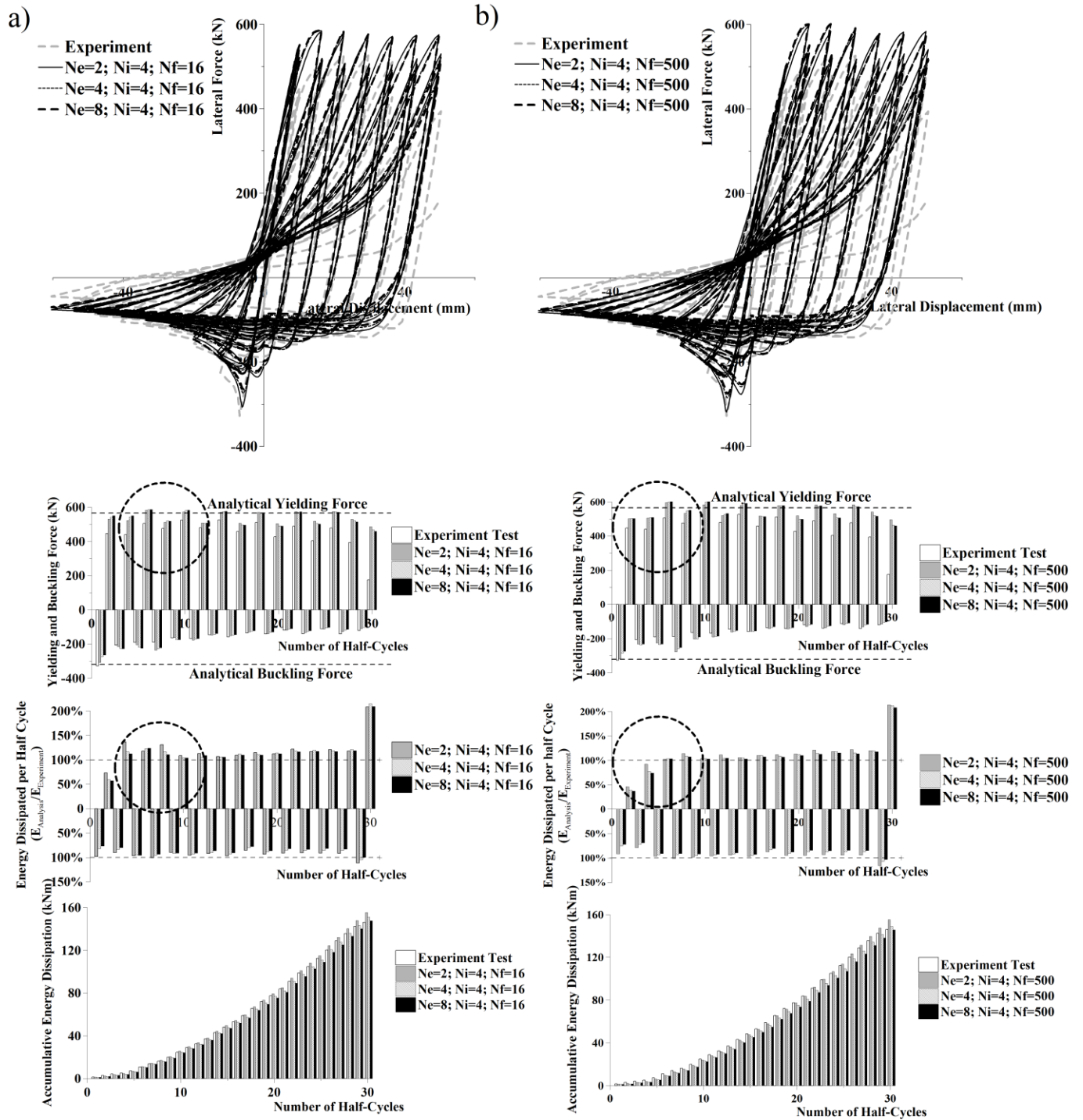


Figure 3.18 Effect of N_f and N_e on specimen *S1B*: a) $N_e=2,4,8$; $N_i=4$; $N_f=16$; b) $N_e=2,4,8$; $N_i=4$; $N_f=500$;

3.4.5 Comparative response of braces under quasi-static loading in OpenSees and Drain2DX versus experimental test results

As illustrated in Figure 3.19, both numerical models developed in Drain2DX and OpenSees are able to capture the brace's behaviour accurately. The main difference between the two brace models built in Drain2DX and OpenSees has been identified in the plastic zone P2(tension) of the force-displacement hysteresis loops (see Fig. 3.1 b) due to the omission of the Baushinger effect in Drain2DX. Even though the OpenSees model includes the Baushinger effect and the simulation is highly refined, some difference between the analytical response and experimental data under quasi-static loading still exists. The difference in simulation is explained by the omission of the low cycle fatigue, the local buckling and residual stresses.

In this study accuracy in modeling the inelastic response of a slender brace *S3B* ($KL/r = 143$), intermediate brace *S1B* and *SIQB* ($KL/r = 93$) and stocky brace *2A* ($KL/r = 68$) is emphasized. In light of this, the influence of loading parameters for the intermediate brace *S1B* versus *SIQB* has also been identified. The parameters chosen for investigation are: the yielding force, the energy dissipated per half-cycle and the total cumulative energy dissipation.

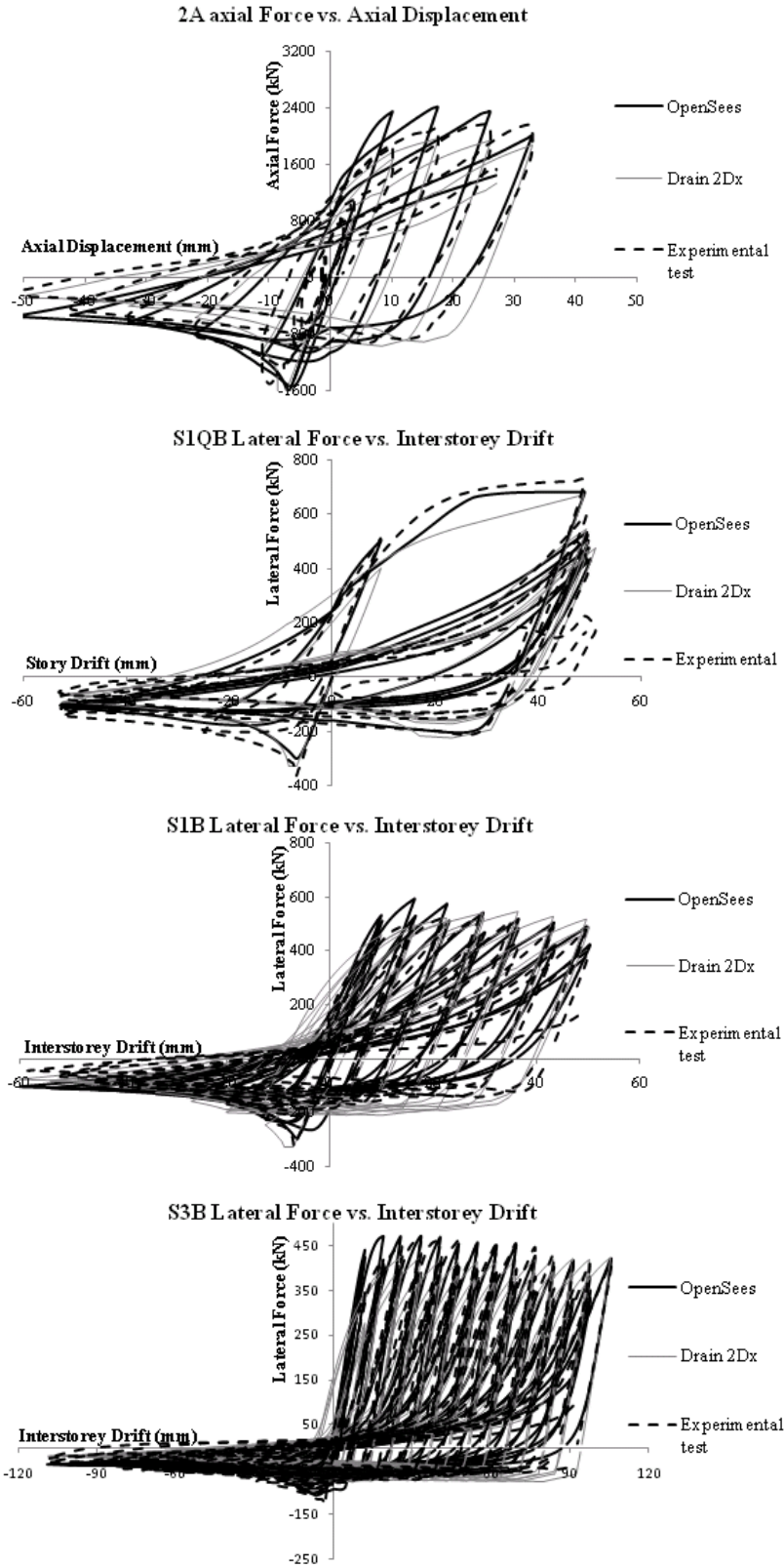


Figure 3.19 Comparative results of braces hysteresis response in terms of force-displacement: a) specimen *2A*; b) specimen *S1QB*; c) specimen *S1B*; d) specimen *S3B*

➤ Inelastic behaviour of the intermediate braces samples *SIB* and *SIQB*

Specimens *SIB* and *SIQB* belong to the same braced frame set-up, but were subjected to different quasi-static displacement control loading histories, which initiated with compression. Specimen *SIB* was subjected to 14 quasi-static cycles (28 half-cycles) incremented at each second cycle (Figure 3.6 a) upon rupture, which initiated in tension as shown in Figure 3.20a. Specimen *SIQB* was subjected to 6 similar cycles with equal loading displacement (Figure 3.6c) which were equivalent to the 13th cycle in terms of displacement loading protocol cycle developed to the specimen *SIB*. As illustrated in Figure 3.20b, the failure of this brace is in tension.

The intermediate brace *SIB* has reached the buckling load during the first cycle and didn't experience yielding in tension under the aforementioned loading protocol. As shown in Figure 3.20a, the axial forces in OpenSees are slowly overestimated, local buckling and fatigue was omitted from the model and the buckling force is 12% larger than the analytical value calculated in agreement with the S16 standard. Under a different loading protocol characterised by large displacement from the beginning of its application, the behaviour of brace is different. Thus, the brace *SIQB* has reached buckling in the first cycle followed by yielding in tension in the next cycle. In this case, the strain hardening effect has produced an increase in the tensile capacity of the member, 8% lower than T_u , as illustrated in Figure 3.20b.

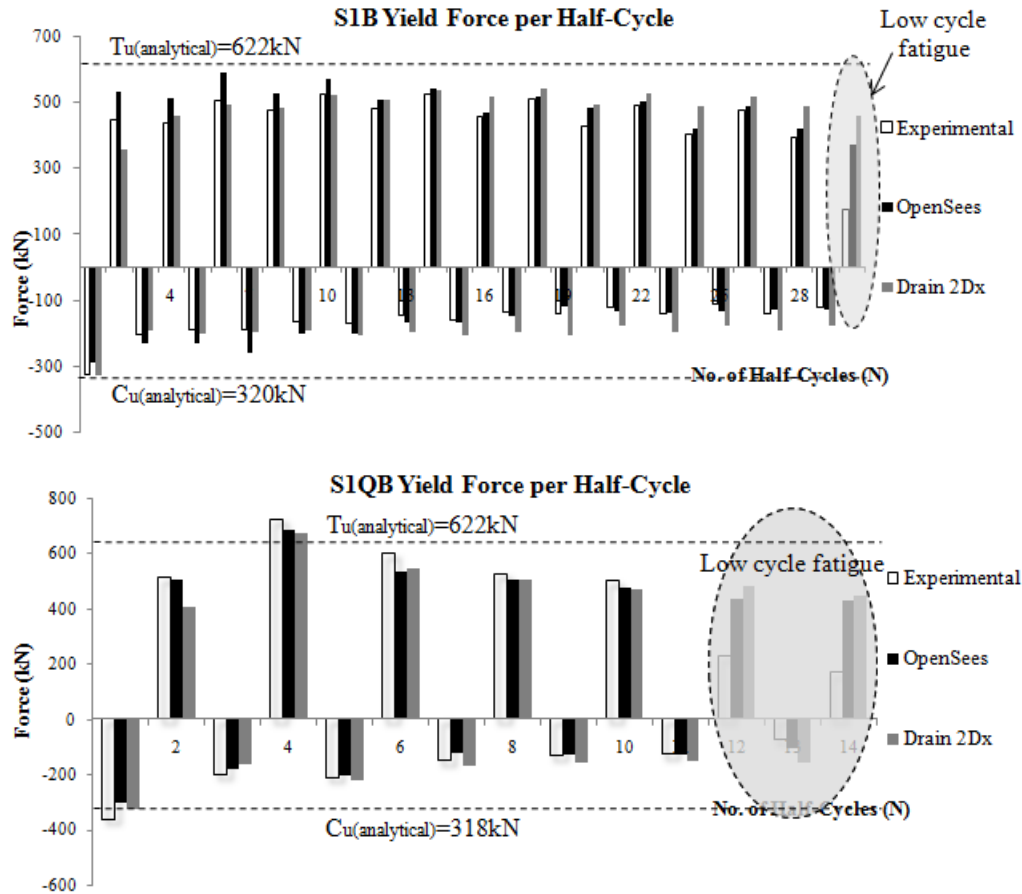


Figure 3.20 Axial force developed per half-cycle for: a) specimen *S1B* and b) specimen *SIQB*

When the *S1B* brace is subjected to an incremented loading history, a lower tensile force was developed in every odd cycle as shown in Figure 3.20a. Although the energy dissipated in tension in the OpenSees brace model *S1B* matches almost perfectly the experimental values, a small difference of 15% is observed in the compression side due to the omission of local buckling implemented in the analytical model. However, the difference in terms of the cumulative energy dissipation is about 3% between the experimental and the analytical model (OpenSees) and is overestimated up to 20% in Drain2DX due to the omission of the Bauschinger effect (Figure 3.22a). The sample *S1B* reaches 50% of the total cumulative dissipated energy during the 10th cycle out of 14

which means 67% of the total number of cycles. Comparatively, the sample *SIQB* reaches 50% of the total cumulative energy during the 3rd cycle out of 7 which means 43% of the total number of cycles. If in the first case (sample *SIB*) the cumulative energy dissipation follows a parabolic curve pointing upwards, in the second (sample *SIQB*) case the cumulative energy follows a parabolic curve pointed down. In the case of *SIQB* sample the cumulative energy in OpenSees is underestimated by 15% while in Drain2DX is underestimated by 2% (Figure 3.22b) and this difference is developed in the plastic zone in compression as is illustrated in Figure 3.21b.

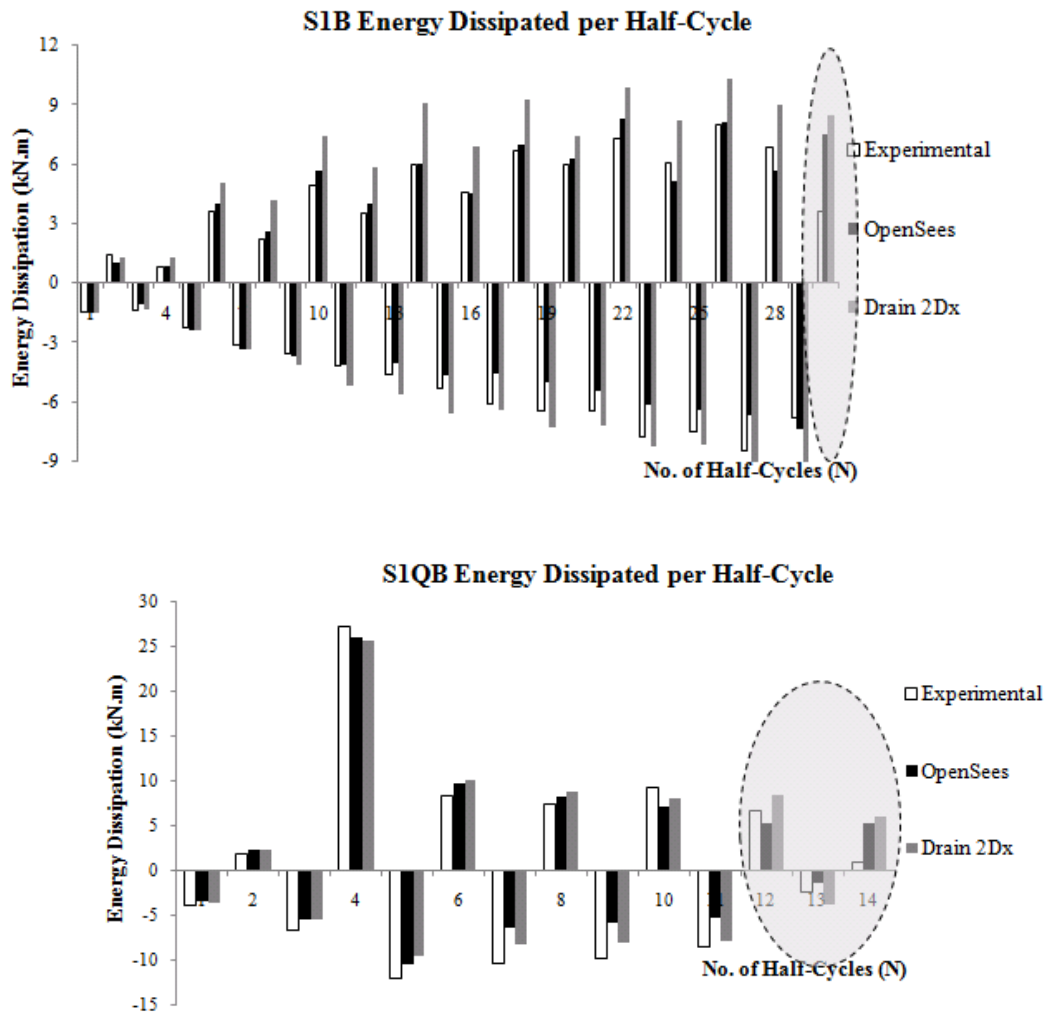


Figure 3.21 Energy dissipated per half-cycle: a) specimen *SIB*; b) specimen *SIQB*

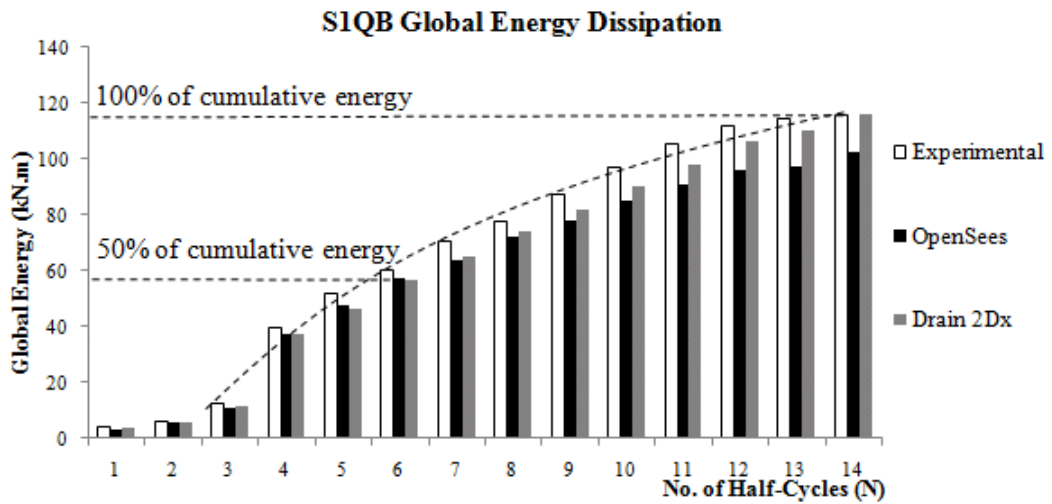
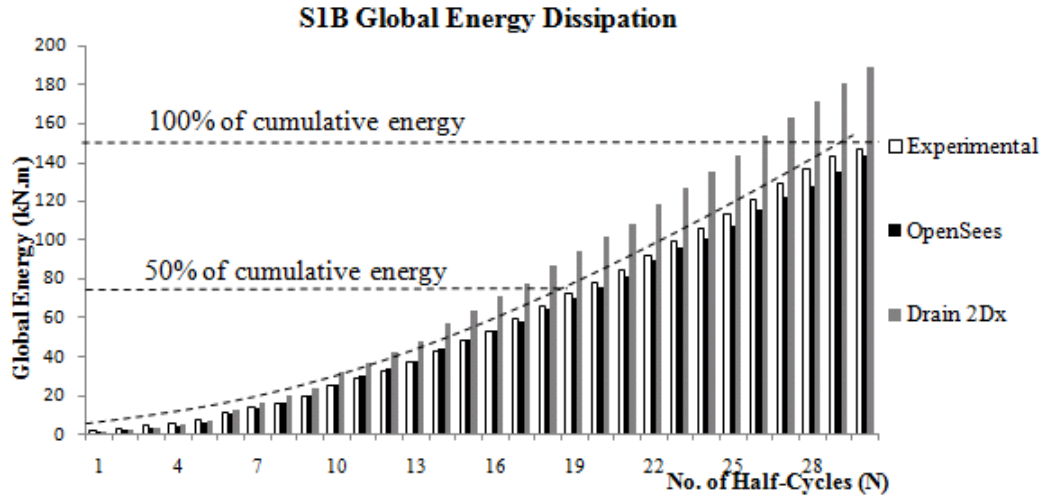


Figure 3.22 Cumulative energy dissipation per half-cycle: a) specimen *S1B*; b) specimen *S1QB*

In addition, under a smooth loading protocol the same brace 152x76x4.8 is able to dissipate 30% more energy (S1B) than under larger loading protocol (S1QB) especially when lower displacement amplitudes are applied from the beginning. For the intermediate brace *S1B*, the energy dissipated is approximately equal in tension and compression, while for the brace sample *S1QB*, a lower amount of energy is dissipated in tension.

➤ Inelastic behaviour of the slender brace sample *S3B*

The brace sample *S3B* was subjected to the same type of displacement history as the brace sample *S1B*. In comparison with the previous case (*S1B*), the number of applied cycles has doubled to 28 (56 half-cycles) for a maximum displacement of $\pm 100\text{mm}$ as illustrated in Figure 3.6b. First, the brace was loaded in compression and the buckling state was reached during the first cycle. Then, after the application of two similar cycles, the brace yielded in tension in the 3rd cycle and reached its ultimate capacity when fracture was initiated in tension in the 28 cycle. By analysing Figure 5.23, during each half-cycle, the postbuckling force is almost constant while this value is approximately as being half of the buckling load in spite of the theoretical value calculated by the expression $0.2A_gR_yF_y$. In this case OpenSees, Drain2DX and experimental tests, develop similar forces in tension and compression. In addition, the OpenSees model shows similar dissipative energy values in tension with that resulted in the experimental test, while in compression side and especially in the postbuckling zone these values are underestimated by 25%. Overall the energy dissipated in tension and compression per half-cycle is comparable (Figure 3.24) and half of the cumulative energy dissipation is reached in the 19th cycles out of 28 which means 67% of the total number of cycles as shown in Figure 3.25. The total cumulative energy is underestimated in OpenSees by 30% while in Drain2DX is overestimated by 30%.

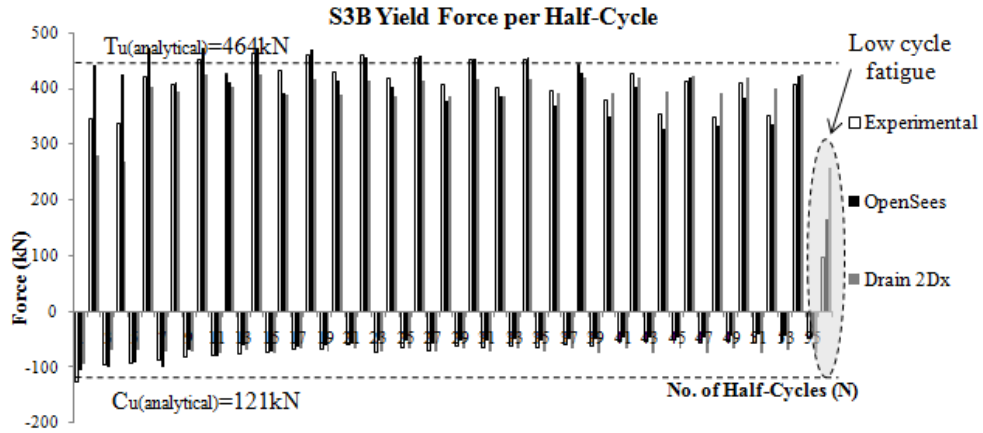


Figure 3.23 Lateral forces induced in specimen *S3B*

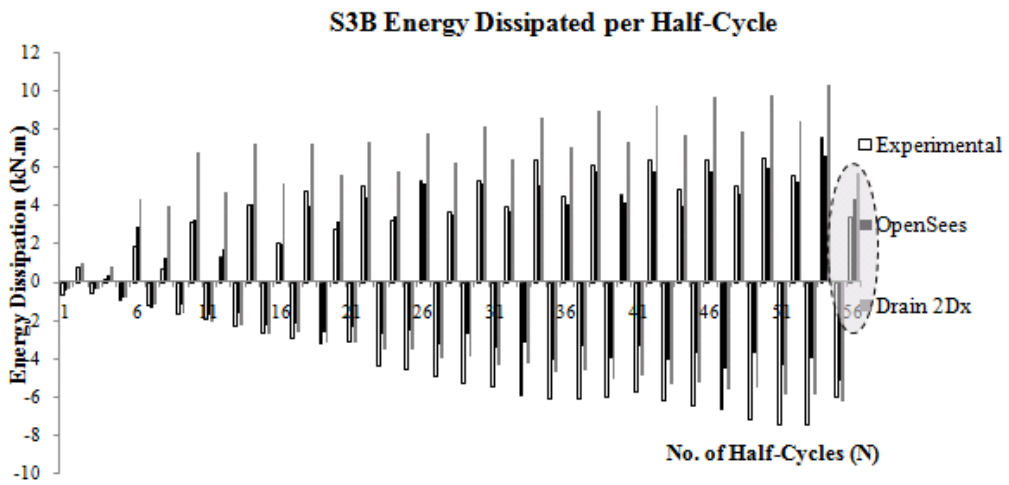


Figure 3.24 Energy dissipated by specimen *S3B* per half-cycle

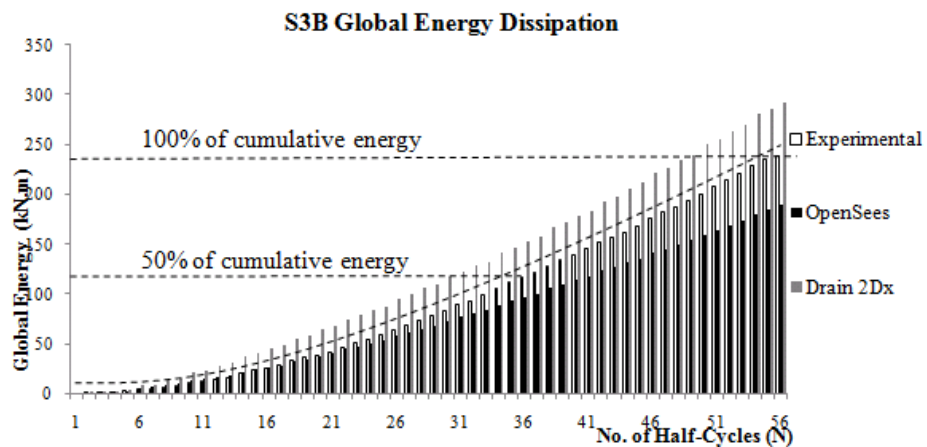


Figure 3.25 Cumulative Energy dissipation of specimen *S3B*

➤ Inelastic behaviour of the stocky brace sample 2A

This brace was subjected to 9 cycles by following an asymmetric loading history, being larger in tension than compression for the second half of cycles (see Figure 6.6). The specimen buckled in compression in the 5th cycle, yield in tension in the 6th cycle and lost its strength in the 9th cycle under an incremental increase in loading. The OpenSees model overestimates the maximum tension and compressive force in the plastic range by approximately 6% as shown in Figure 3.26 while it underestimates the maximum cumulative energy by 4% (Figure 3.28). The energy dissipation per half-cycle shows a slight underestimation in tension and overestimation in compression by 3% (Figure 3.27).

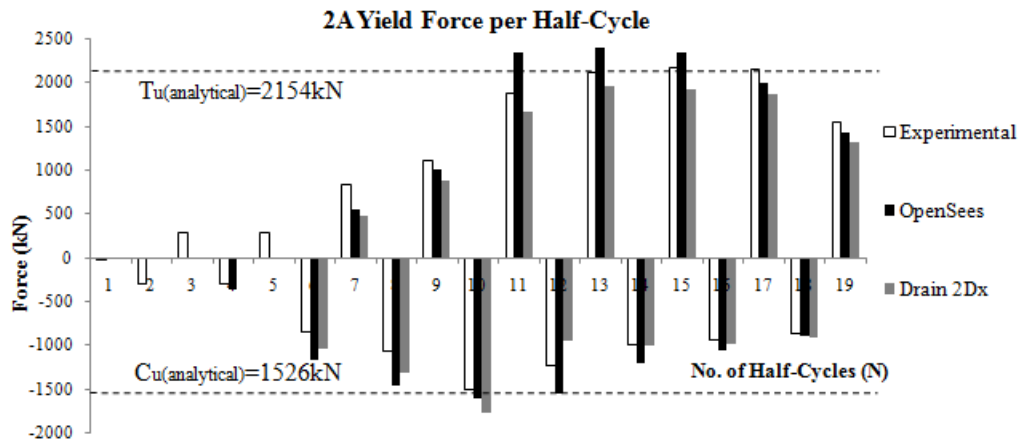


Figure 3.26 Axial force developed in specimen 2A per half-cycle

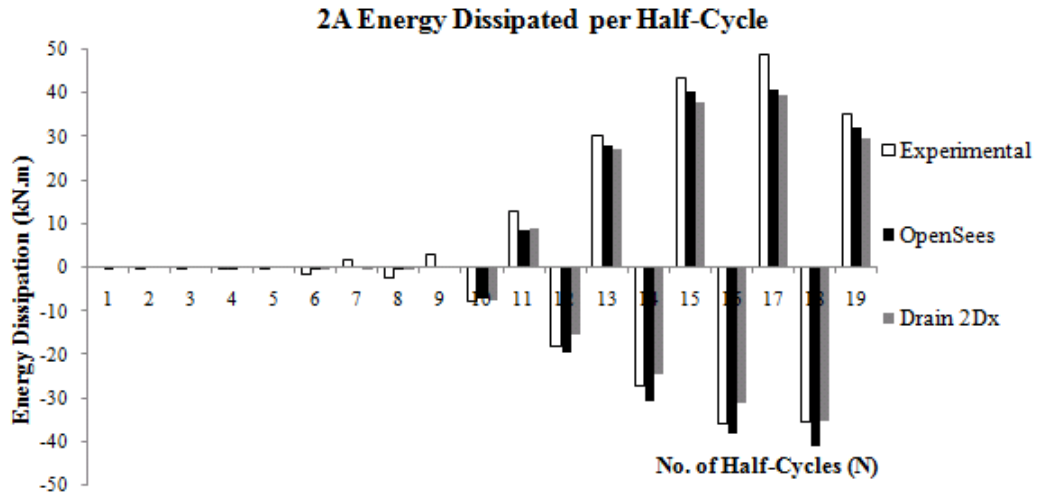


Figure 3.27 Energy dissipation of specimen 2A per half-cycle

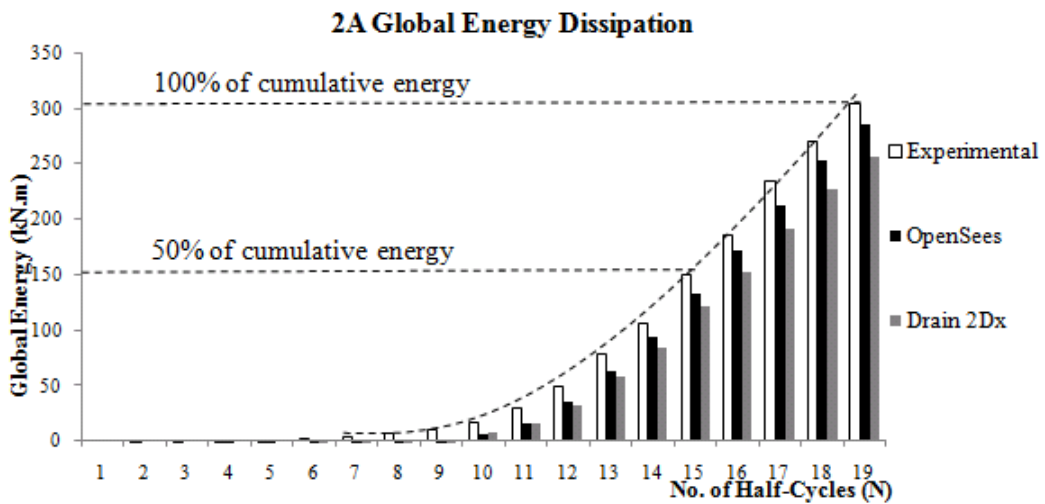


Figure 3.28 Cumulative Energy dissipation of specimen 2A

Figure 3.28 shows that half of the cumulative energy is reached in the 7th cycle out of 9 which means 78% of the total number of cycles and the tendency of cumulative energy from one to the next cycle follows a parabolic curve pointed up and open narrower than the previous cases *S1B* and *SIQB*.

CHAPTER FOUR: DESIGN METHODOLOGY OF ZIPPER BRACED FRAME STRUCTURES

In this chapter, a detailed design methodology of zipper-braced frames aiming to achieve the strong zipper effect is presented and a sample design of an 8-storey building is illustrated. The proposed design method is developed in agreement with the NBCC 2005 and S16-2009 provisions. Although the zipper frame system has been introduced in the Commentary to the structural steel seismic provisions (AISC 2005) since 1992 as a means of improving the post-elastic performance of chevron-bracing frames, it hasn't been included in the Canadian Steel Design Standard yet. Nevertheless, design recommendations for zipper braced frames have not been proposed in any building code or standard.

4.1 Design Philosophy

4.1.1 General design steps

The design of the zipper braced frame structure is divided in two steps such as:

- design of chevron braces, beams and columns by following the S16-2009 and NBC-2005 provisions for concentrically braced frame with chevron-bracing configuration and
- design of zipper columns as members acting in tension and/or compression, able to carry the loads transferred from braces and adjacent zippers.

4.1.2 Detailed design steps

4.1.2.1 Lateral seismic force and distribution

For seismic load calculation, the equivalent static force procedure has been used for the preliminary design. The base shear is proportional to the design spectral acceleration value, $S(T_d)$, the higher mode factor, M_V , importance factor, I_E , the building seismic weight, W , and it is inversely proportional to the ductility related force modification factor, R_d , and overstrength factor, R_o , as shown:

$$V = S(T_d)M_V I_E W / (R_d R_o) \quad \text{Equation 4.1}$$

For braced frame structures, NBCC 2005 requires that the minimum lateral earthquake force calculated with the above formula shall not be less than

$$V_{min} = S(2.0)M_V I_E W / (R_d R_o) \quad \text{Equation 4.2}$$

or greater than

$$V_{max} = (2/3)S(0.2)I_E W / (R_d R_o) \quad \text{Equation 4.3}$$

Then, for structures with a fundamental lateral period larger than 0.7s the total lateral seismic force is distributed such that a portion F_t is concentrated to the roof level, while the remaining $(V - F_t)$ amount is distributed to each story including the roof level in accordance with the following equations:

$$F_t = 0.07TV < 0.25V \text{ when } T > 0.7s; F_t = 0 \text{ when } T < 0.7s$$

$$F_i = (V - F_t)W_i h_i / \left(\sum_{m=1}^n W_m h_m \right) \quad \text{Equation 4.4}$$

where T is the fundamental period of the structure, h_N is the total height of the structure and F_i , W_i , are the lateral force and the seismic weight of the i^{th} floor respectively, and h_i is the height above the base to storey i . Thus, the lateral earthquake load distribution as shown in Figure 4.1 has a triangular pattern.

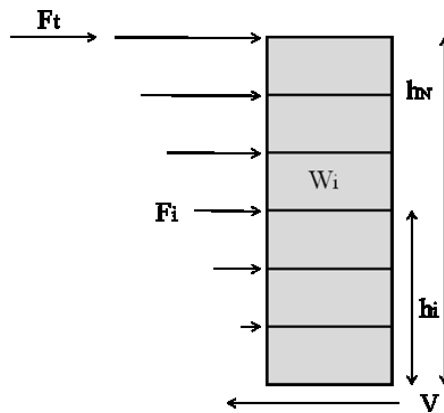


Figure 4.1 Lateral seismic force distribution

4.1.2.2 Design of braces

Braces are the first members to be designed. These elements are proportioned to resist the storey shear force in combination with the gravity load component (DL+0.5LL+0.25SL). Based on the capacity design concept, the shear force developed at the i^{th} floor is equally distributed to both tension and compression braces which belong to the same floor. Therefore, the load acting on each brace element can be calculated as:

$$T_{f(i)} = C_{f(i)} = V_i / (2 \times \cos \theta_i) \quad \text{Equation 4.5}$$

where θ_i is the angle between the brace and a horizontal line.

The brace element is designed in compression and tension such that the factored tension and compressive load (C_f , T_f) are smaller than the resisting strength of corresponding member (C_r , T_r), where $C_r = 0.9AF_y(1+\lambda^{2n})^{-1/n}$ and $T_r = 0.9AF_y$. In these formulas λ is the slenderness ratio, A is the cross-sectional area and F_y is the steel strength.

4.1.2.3 Design of beams and columns

Beams and columns shall be designed based on the capacity design concept.

For the beam design two scenarios are considered:

- Braces have reached the stage of buckling and beam has lost its braces support. Thus, the beam has to carry the reduced gravity loading (DL+0.5LL) over the entire span without considering the braces supports and must be class 1 of section. After buckling is experienced by the compressive brace, only the postbuckling load estimated as $C_u' = 0.2AF_yR_y$ can be developed in that brace. On the other hand, the tensile brace is able to carry a tensile load limited by its yielding strength, therefore, lower than the probable tensile strength, T_u .
- In the second scenario, the beam is supported by braces at its mid-span and the compressive force in the brace reaches its probable nominal compressive strength $C_u = 1.2(R_y/\phi)C_r$ where $R_y = 1.1$ and $\phi = 0.9$, and the tensile force developed in braces is considered as its probable tensile strength, T_u . In this verification the beam acts as a beam-column supporting the gravity load in combination with the axial load induced by earthquake forces and brace effects when the compression acting brace is on the verge of buckling.

Columns of the bracing bents are designed to carry the tributary gravity load in combination with brace effects. Columns are considered continuous over two stories and are designed to carry axial load in combination with bending moment, which is limited to $0.2ZF_y$, where Z is the plastic section modulus of the column section.

4.1.2.4 Design of zipper columns

Prior to the zipper column design, three assumptions are made:

- The beams are assumed to form hinges at the location where the buckled braces are connected. As stated by Tremblay and Tirca (2003), although with the presence of zipper columns, hinging of beams is delayed until the brace buckling has extended to several floors. This assumption is maintained for simplicity.
- It is also assumed that the braces can maintain their probable compression strength, C_b , upon buckling. In this way, all braces in the floors below or above the floor where the brace has buckled are able to retain their probable compression capacity when supporting the zipper column.

As stated in the previous section, the basic concept of designing zipper columns as the method proposed by Tremblay and Tirca (2003), is to consider two different scenarios which are able to capture separately the maximum tensile and compressive force developed in zippers. For low-rise structures, the zipper columns act mostly in tension and their behaviour depends on the ground motion characteristics.

Since the behaviour of the zipper frame system depends on the frequency content of ground motions, each one of the two aforementioned scenarios may occur (zippers act in

tension, zippers act in compression). However, when the higher mode effect is activated and the building has more than 8 stories, the seismic demand migrates upward, leads the upper braces to buckle, and thus drives the attached zipper columns to act in compression. When the loading reverses, the upper braces, which were previously in tension, are on the verge of buckling. The stiffness of the structure has degraded during this time sequence. When the demand is concentrated at the bottom floor and migrates upward, it drives the bottom braces to buckle and zippers to act tension. In general, it is uncertain which scenario is followed during an earthquake, and, as is shown by researchers, most of the time both scenarios may occur during the same ground motion excitation.

In the first scenario considered for zipper column design, it is expected that the bottom brace is the first to reach its buckling state, while other structural members remain elastic. Consequently, the unbalanced brace force developed at the brace to beam intersection point drives the beam to hinging and the attached zipper column to behave in tension. Since all zipper columns are designed to remain in elastic range throughout the entire ground motion, they serve as links between the lower and the upper beams and transfer the unbalanced force upwards. During this process, the compression brace located at the storey above is forced to buckle and the developed unbalanced load is transferred upward.

Note that each buckled brace will affect the remainder storey stiffness, and as a consequence, it may influence the lateral force distribution along the building height.

Based on the propagation of plastic deformation, the maximum compressive force in the zipper column must be evaluated for $(N-1)$ cases, where N denotes the number of stories.

By following Scenario No.1 shown in Figure 2.5 b) of Chapter 2, it is assumed that the bottom brace of the compression side reaches the postbuckling strength $C'_{u,1}$ and the corresponding brace on the tension side develops a force $T_{b,1}$ smaller than the probable tensile strength $T_{u,1}$. The vertical component of the developed unbalanced brace force leads the beam to hinge and to activate the zipper in tension. Once the bottom zipper (2nd floor) is activated, it drives the upper compression brace to reach its probable compressive capacity, $C_{u,2}$, while the tensile force developed in brace is limited by its probable tensile strength, $T_{u,2}$. If the brace to beam angle is θ_1 and the plastic moment of the floor beam is $M_{p,1}$, the tensile force induced in the zipper column on the floor above can be derived as:

$$T_{z,2} = (T_{b,1} - C'_{u,1}) \times \sin \theta_1 - 4 \times M_{p,1}/L_b \quad \text{Equation 4.6}$$

where $(4M_{p,1}/L_b)$ is the applied concentrated force corresponding to the development of $M_{p,1}$. This force, $T_{z,2}$ (the tensile force developed in the zipper on the second floor), is transferred to the zipper above (3rd floor) along with the unbalance force produced by the tension acting brace and compression acting brace located on the second floor. Regarding the assumption, if the compression acting brace at the second floor is on the verge of buckling, then, the tensile force developed in the zipper column located at the 3rd floor is:

$$T_{z,3} = (T_{b,2} - C_{u,2}) \times \sin \theta_2 + T_{z,2} \quad \text{Equation 4.7}$$

It is expected that after the first brace of the bottom floor reaches its postbuckling strength, buckling of braces is propagated upward and all compression acting braces on the verge of buckling will buckle simultaneously or subsequently. Therefore, the tensile force developed in the zipper column located above the floor with stiffness degradation is composed of three types of generating forces: the unbalance force caused by buckling of braces, the force required to yield the beam member and the forces transferred from the lower zippers. For any other stories, the zipper tensile force will be the summation of the unbalanced vertical force and the force developed in zippers from the stories below.

As mentioned above the force in the tension brace T_b , is always smaller than the probable tensile strength, T_u . Its value can be derived from the lateral shear force V_n induced into each storey by the ground motion, when the unbalanced force at each floor may be expressed as:

$$F_i = (T_{b,i} + C_{b,i}) \cos \theta_i - (T_{b,i+1} + C_{b,i+1}) \cos \theta_{i+1} \quad \text{Equation 4.8}$$

The expected maximum compressive forces in zipper columns are studied in a similar manner, assuming that brace buckling initiates at the top floor and propagates downward. Several scenarios base on a sequential triangular lateral force distribution pattern are shown in Figure 2.4 for both cases: zippers acting in tension and zipper acting in compression.

Six different load patterns are employed in this study in order to predict the maximum tensile and compressive forces developed in zippers. This prediction is verified for different types of ground motions which have been scaled to match the design

spectrum for a given location. The pattern load which gives a better estimation of the forces developed in zippers is proposed for design.

In this respect, the zipper frame system was analyzed based on different load distribution pattern along the building height. In light of this, a spreadsheet was developed for 4-, 8-, and 12-storey structures.

4.2 The influence of Pattern Load Selection on the Preliminary Design Methodology

Different lateral load distributions along the height of the structure have significant influence on the forces induced in braces and zipper columns. Thus, the purpose of this study is to refine the design method developed by Tremblay and Tirca (2003) with the aim of recommending a suitable zipper force envelope for both tension and compression forces. To reach this objective, 6 different pattern loads described below are considered in this study.

4.2.1 Sequential triangular pattern load

The design method proposed by Tremblay and Tirca (2003) is based on a sequential triangular pattern load distribution. It was assumed that the lateral loads vary linearly from a maximum value at the roof level to zero at the level under consideration as is shown in Figure 2.4. Since the compressive strength of buckled brace can only retain their postbuckling strength C'_u , and the brace on the verge of buckling sustains a probable compressive strength C_u , the force developed in the zipper columns at the corresponding stories is calculated.

The aforementioned design method has been verified by a series of time-history dynamic analyses. In this respect, a 4-, 8- and 12-story structure has been designed accordingly, and 3 ground motion ensembles have been selected and considered to verify the prediction of the maximum tensile and compressive forces developed in zippers under a sequential triangular load distribution pattern.

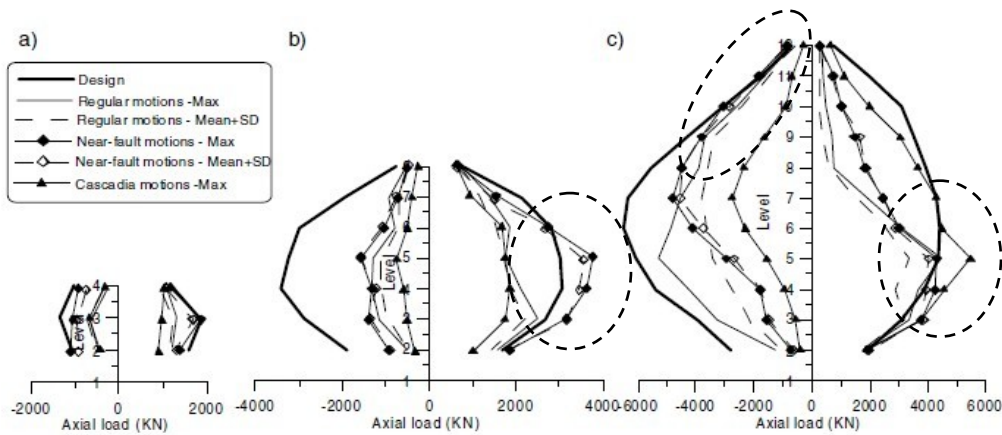


Figure 4.2 Computed peak axial loads in zipper columns for 4,8,12 storey building (Tremblay & Tirca, 2003)

As illustrated in Figure 4.2, the design load pattern employed by Tremblay & Tirca does not cover the development of the maximum force in zippers for the 8- and 12-storey buildings under the Cascadia and the Near-field ground motion ensembles. Although the predicted values mostly agreed with the peak zipper loads obtained from nonlinear time-history analyses, a few exceptions especially on the tension side at the lower levels of the 8- and 12- storey structures were found.

4.2.2 Other load distribution patterns considered in this study

In light of FEMA 356 (2000), several load distribution patterns are proposed herein with the aim to provide an accurate design envelope for the tension and compression forces expected in zipper columns.

Accordingly, the lateral load distribution concurs with the following equation:

$$F_x = C_{vx} \times V \quad \text{Equation 4.9}$$

where V is the total design base shear and C_{vx} is the vertical distribution vector which can be calculated as:

$$C_{vx} = \frac{w_x h_x^k}{\sum_{i=1}^n w_i h_i^k} \quad \text{Equation 4.10}$$

w_i , h_i and w_x , h_x denote the seismic effective weights and height of the structure on the i^{th} and x^{th} level, respectively. K is an exponent factor related to the fundamental period of the structure to define the relative lateral force distribution. Recommended by FEMA 356, for structures with a fundamental period T_1 less than 0.5 sec, k shall be taken as 1 and the lateral force distribution is based on the first mode of vibration (triangular distribution); for structures with T_1 greater than 2.5 sec, $k=2$, higher modes effect have been considered; and for any structures with T_1 between 0.5 sec and 2.5 sec, k value can be obtained by linear interpolation (parabolic distribution). The shape of these distribution vectors are shown in Fig. 4.3. Equal seismic weight and storey height are assumed for all floors.

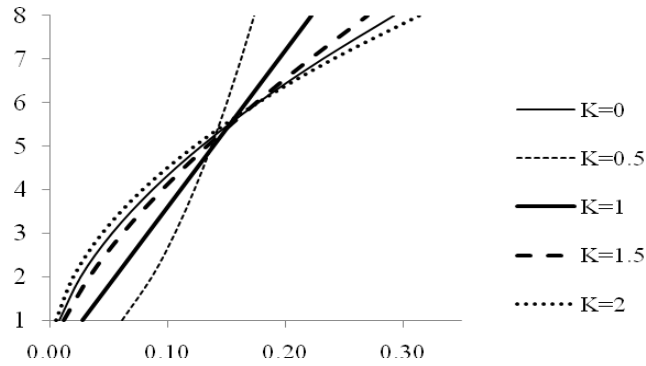


Figure 4.3 The variation of vertical distribution vector of lateral forces with different k

The three most commonly used values for the exponent factor k are 0, 1 and the one determined by T_l . These values have been chosen to determine the vertical distribution vectors. Correspondingly, uniform distribution, triangular distribution and parabolic distribution of lateral forces as shown in Figure 4.4 have been adopted in this study in order to refine the zipper force envelope in tension and compression.

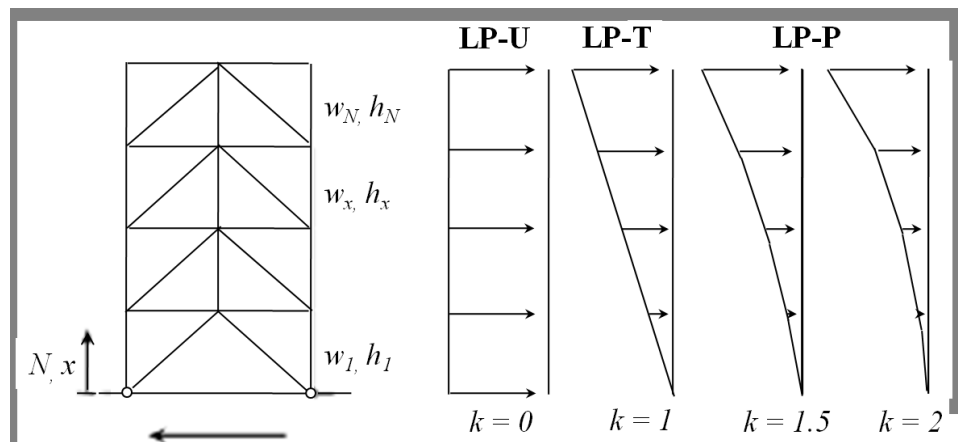


Figure 4.4 Lateral force distribution vectors

A total of six force distribution patterns are set up and compared such as the sequential load distribution pattern and the full height load distribution pattern.

Each lateral force distribution pattern is described below.

➤ LP-ST: Sequential triangular distribution pattern

The first examined load distribution pattern, labelled LP-ST, is the same as that considered by Tremblay and Tirca. For both scenarios: zippers act in tension and zippers act in compression, linear distribution of internal forces proportioned to the ratio F_i/F_n , are considered. These forces are limited by the probable buckling and postbuckling strength of braces and are shown in Figure 4.5. For example for the 4-storey zipper braced frame, when the buckling of braces initiates at the first floor, the corresponding normalized load distribution pattern is $\{1.00, 0.50, 0.0, 0.0\}^T$. While the buckling of braces propagates to the second storey, the normalized pattern vector changes to $\{1.00, 0.66, 0.33, 0.0\}^T$. Then, after the braces located at the third storey buckled, the normalized vector appears in the form of $\{1.00, 0.75, 0.50, 0.25\}^T$, in agreement with the assumption. During this time, the activated zippers are acting in tension. In the second case, when the buckling initiates at the top floor, the zippers are acting in compression. The same set of vectors has to be considered while the buckling of braces propagates downward.

Again, when the first brace buckles at the top floor, buckling of braces propagates downwards and zippers are loaded in compression. On the other hand, when the first brace buckles at the bottom floor, buckling of braces propagates upwards and zippers are acting in tension.

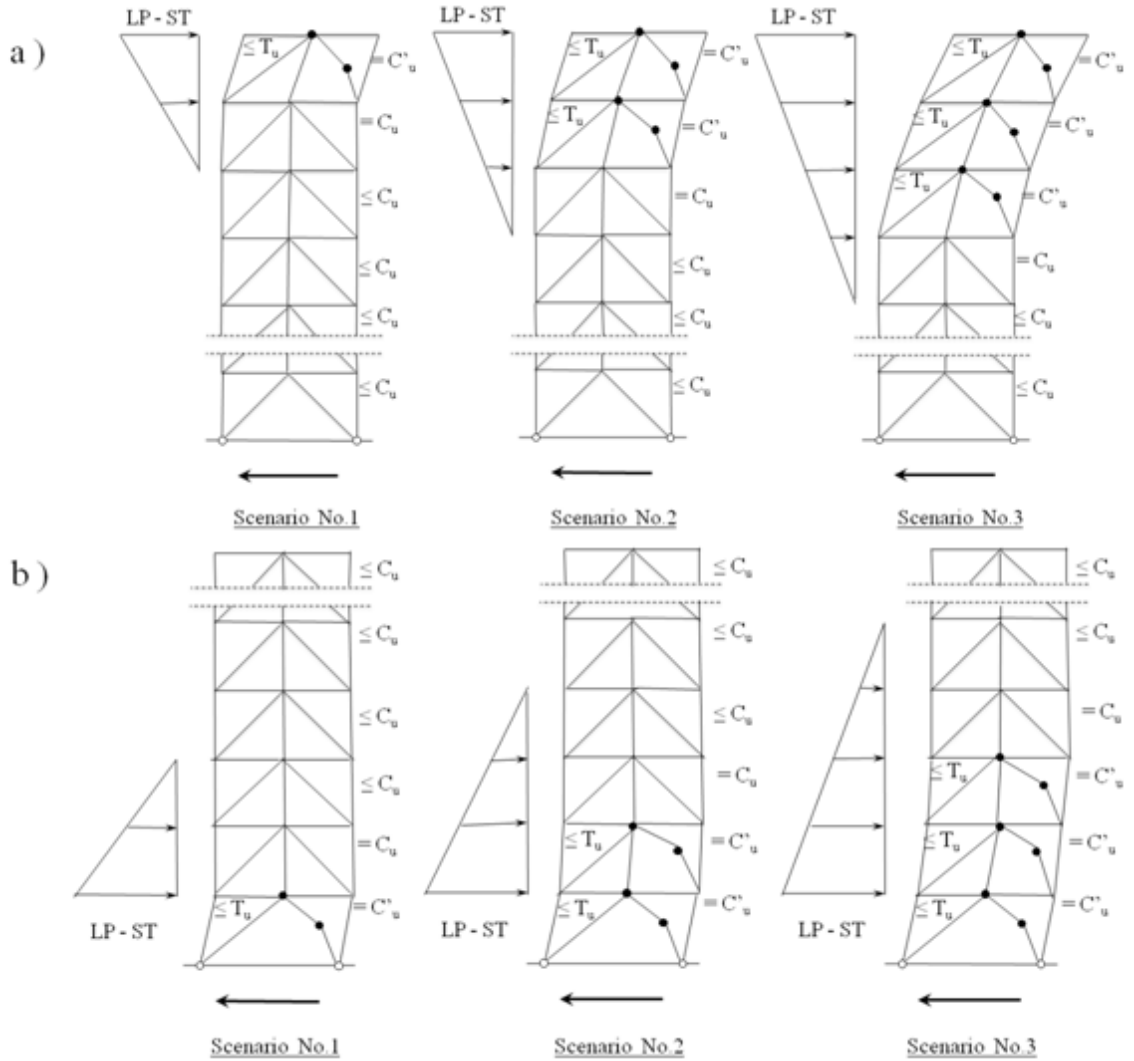


Figure 4.5 Zipper mechanics & load pattern LP-S Δ : a) buckling initiate at top; b) buckling initiate at bottom

➤ LP-SU: Sequential uniform distribution pattern

This pattern load assumes a sequential uniform distribution along the stories with buckled bracing members, followed by a linear variation within the upper or lower two stories, as shown in Figure 4.6. Also shown are both cases of buckling brace propagation, considered for estimating the tensile and compressive forces induced in zippers.

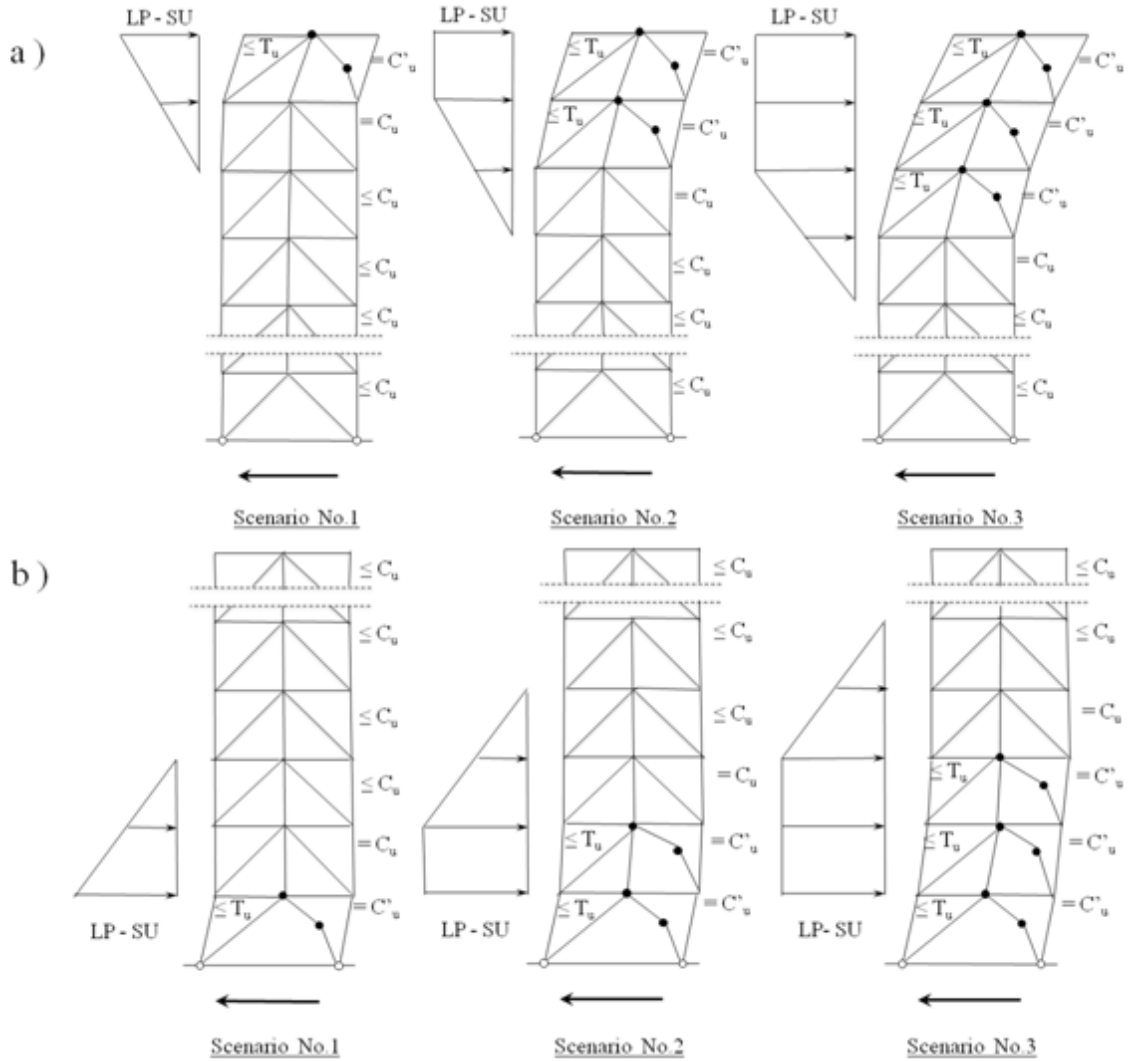


Figure 4.6 Zipper mechanics & load pattern LP-SU: a) Buckling initiate at top; b) Buckling initiate at bottom

➤ LP-SP: Sequential parabolic distribution pattern

This pattern load assumes a parabolic distribution along the stories with buckled bracing members and it decreases to zero at the level of calculation when buckling is initiated at the top floor and at the level of calculation when buckling is initiated at the bottom, as shown in Figure 4.7. Herein, the parabolic shape is governed by the equation 4.10.

To explain the LP-SP pattern load distribution, the following example is considered. A 6-storey regular chevron braced frame structure, with equal weight and height distribution among all floors, has a fundamental period of vibration calculated with the empirical equation given in NBCC 2005 as shown below:

$$T_1 = 0.025h_N \quad \text{Equation 4.11}$$

where h_N is the total height of the structure. According to National Building Code of Canada 2005 edition (NBCC2005), if the fundamental period of the structure calculated from a dynamic analysis is equal to or greater than $2T_1$, a maximum value of $2T_1$ can be used. The storey height of this structure is assumed as 4 meters for simplicity and the fundamental period of the structure, calculated from Eq. 4.11, is 1.2 seconds. Thus, the k value is obtained as 1.35.

Hence the normalized vertical distribution vector is calculated as $\{1.00, 0.78, 0.58, 0.39, 0.23, 0.09\}^T$ from Eq. 4.10, when $k=1.35$.

➤ LP-T: Triangular distribution pattern

It is assumed as a standard triangular distribution pattern load along the full height of the structure.

➤ LP-U: Uniform distribution pattern

It is assumed as a uniform distribution pattern load along the full height of the structure.

➤ LP-P: Parabolic distribution pattern

As mentioned in the previous section, this lateral force distribution is related to the fundamental period of the structure, to the stiffness and mass distribution over the

structure height. This parabolic pattern load distribution considers the level of inelastic behaviour influenced by the stiffness, masses and building height and the contribution of the higher mode effects.

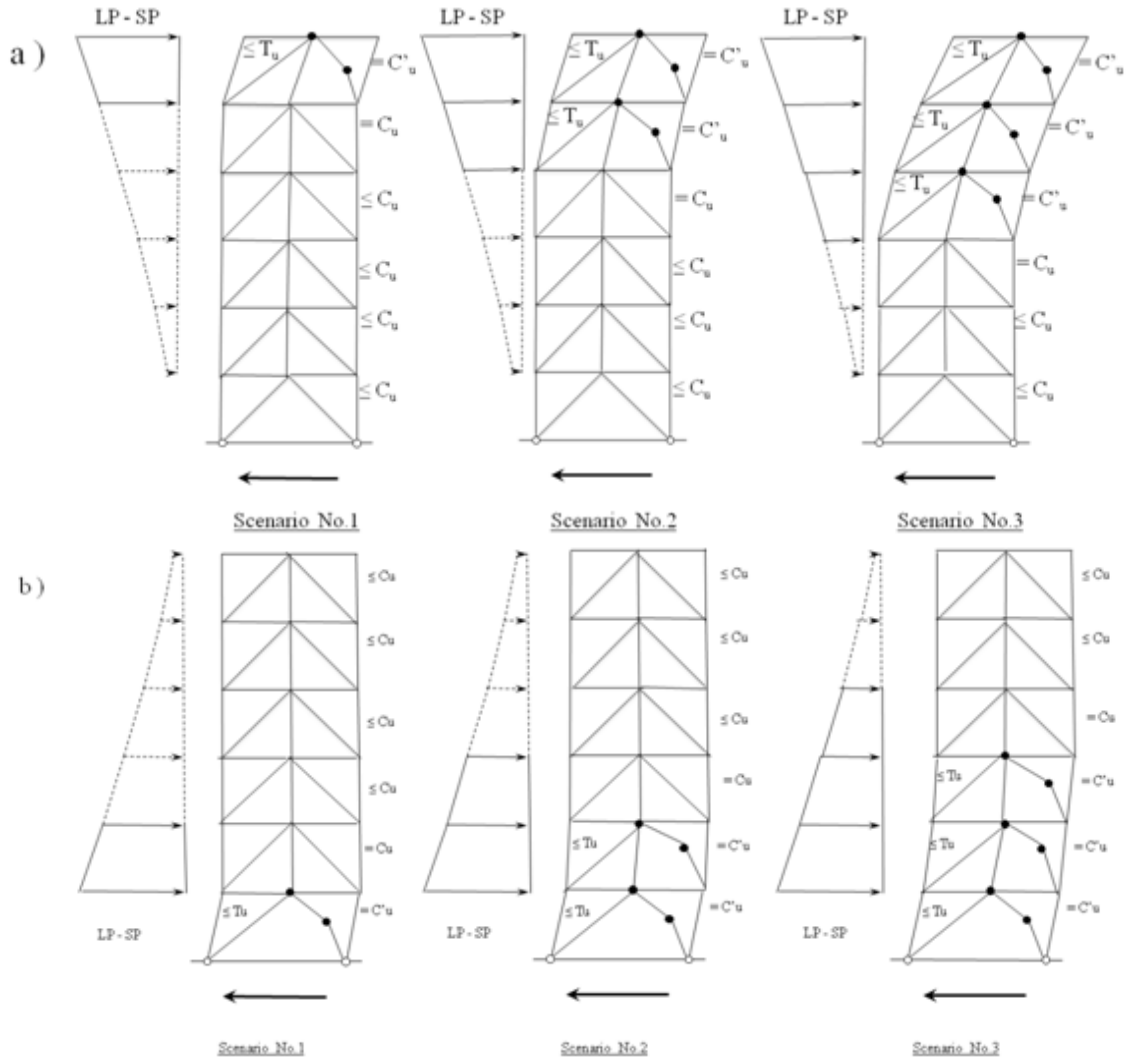


Figure 4.7 Zipper mechanics & load pattern LP-SU: a) Buckling initiate at the top; b) Buckling initiate at the bottom

4.2.3 Preliminary design & selected design load patterns

Mentioned in the previous section, a 4-, 8- and 12- storey zipper braced frame structure were designed to choose and validate the design load pattern.

4.2.3.1 Building description

The plan view of the studied structure is shown in Figure 4.8 and the modeled frame is on the N-S direction. The structures were assumed to be located on a firm ground site in Victoria, B.C., Canada. The occupancy of the building is considered as an office building, therefore, the live load is considered as 2.4 kPa according to NBCC 2005 requirement. The live load on the roof level considers only the snow load, according to NBCC 2005 and the snow load is calculated as 1.48 kPa . The dead load is considered as 3.4 kPa at the roof level, and 4.0 kPa at floor level.

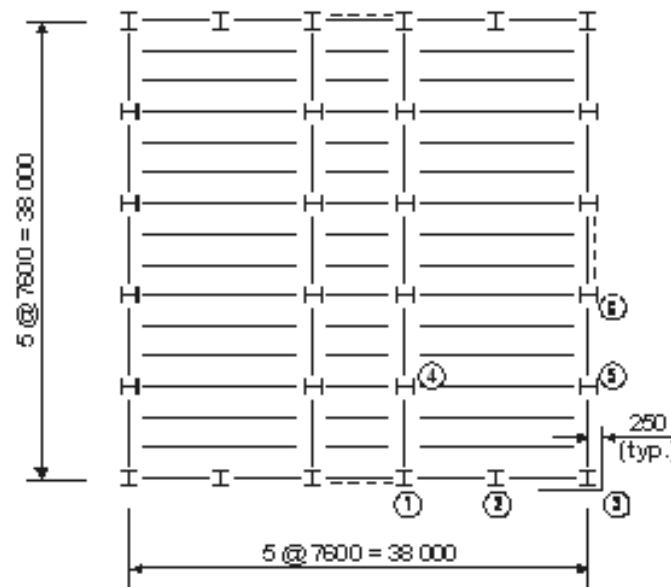


Figure 4.8 Structure plan view (Tirca and Tremblay, 2003)

The zipper braced frame is assumed to be at the same performance level as the moderately ductile concentrically braced frame, type MD (Moderately Ductile). Therefore, the ductility related force modification factor R_d , which reflects the capability of the structure to dissipate energy through inelastic incursions, is considered as 3 and

the overstrength related force modification factor R_0 is considered as 1.3. The higher mode effect factor M_v is calculated based on the building fundamental period. The analytical model of the frame is shown in Figure 4.9. Gravity columns taking into account the P-delta effect were added to the model. The gravity columns are connected to the frame through rigid links which transfer only the lateral force to the frame.

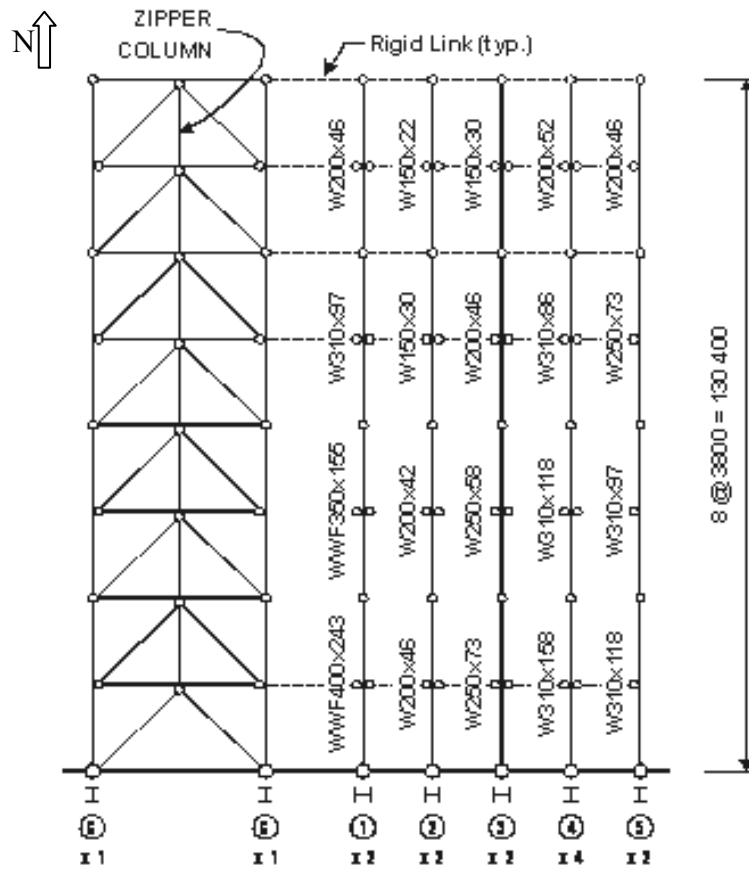


Figure 4.9 Computer model of the studied CBF with zipper columns frame (Tirca and Tremblay, 2003)

The braces, beams and columns were designed in Phase I, following the NBCC 2005 requirements. The designed sections are shown in Table 4.1 – 4.3.

Table 4.1 Member sections of the 4-storey structure

Fl.	Braces	Beams	Columns
4	HSS152x152x8.0	W360x39	W200x52
3	HSS178x178x9.5	W360x57	W200x52
2	HSS203x203x9.5	W360x57	W310x143
1	HSS203x203x13.0	W360x64	W310x143

Table 4.2 Member sections of the 8-storey structure

Fl.	Braces	Beams	Columns
8	HSS152x152x8.0	W360x39	W200x52
7	HSS152x152x9.5	W360x51	W200x52
6	HSS178x178x9.5	W360x51	W250x115
5	HSS203x203x9.5	W360x57	W250x115
4	HSS203x203x9.5	W360x57	WWF350x176
3	HSS203x203x9.5	W360x57	WWF350x176
2	HSS203x203x9.5	W360x57	WWF450x274
1	HSS203x203x13.0	W360x64	WWF450x274

Table 4.3 Member sections of the 12-storey structure

Fl.	Braces	Beams	Columns
12	HSS152x152x8.0	W360x39	W200x52
11	HSS152x152x9.5	W360x51	W200x52
10	HSS178x178x9.5	W360x51	W310x107
9	HSS203x203x9.5	W360x51	W310x107
8	HSS203x203x9.5	W360x51	W310x202
7	HSS203x203x9.5	W360x57	W310x202
6	HSS203x203x9.5	W360x57	WWF350x263
5	HSS203x203x13.0	W360x57	WWF350x263
4	HSS203x203x13.0	W360x64	WWF450x409
3	HSS203x203x13.0	W360x64	WWF450x409
2	HSS203x203x13.0	W360x64	WWF550x503
1	HSS203x203x13.0	W360x64	WWF550x503

4.2.3.2 Preliminary design of zipper columns

Concerning preliminary design, a comparison between the zipper force envelopes, as calculated from each one of the six considered load distribution patterns, is shown in Fig 4.11.

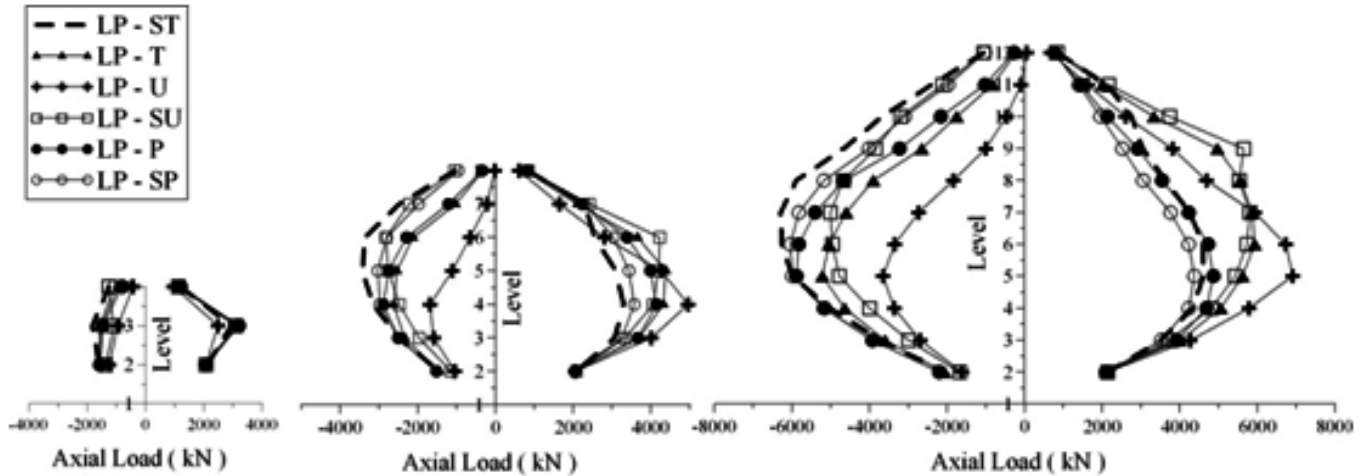


Figure 4.10 Comparison of zipper forces obtain from various load patterns

When the load distribution pattern LP-SU is considered, the envelope of the axial tension force is too large, while the corresponding values of compressive forces dropped by a considerable amount. Furthermore, as is shown in the graph, the prediction largely overestimated the tensile forces on the upper stories. On the other hand, LP-U has shown a much better prediction on the tension side of the 8-storey building, but too large a value for the 12-storey building. A similar envelope was obtained under the consideration of the LP-T pattern. In light of this, these load distribution patterns (LP-U, LP-SU, LP-T) were not selected for design. The remaining load distribution patterns, which can potentially be used in zipper column design, are LP-ST (sequential triangular), LP-SP (sequential parabolic) and LP-P (parabolic).

In the compression side, the larger force is generated under the LP-ST pattern followed by the LP-SP pattern and LP-P pattern. It is noted that these three envelopes overlapped at the lower half of the structure and slowly diverged in the upper part. In the tension side, while the LP-SP pattern offers a slightly larger envelope than the one given by LP-ST, only the LP-P pattern made a satisfying prediction.

Therefore, LP-ST pattern is recommended to be considered for the axial compressive envelope and LP-P for the tensile envelope. However, analyses of the influence of these load patterns on higher structures are still required. Preliminary designs of zippers are carried out following the methodology discussed in this chapter, and the sections chosen are as shown in Table 4.4.

Table 4.4 Member sections of the 4-, 8-, 12-storey structure

Fl.	Zippers	Zippers	Zippers
12	HSS127x127x13.0		
11	HSS203x203x13.0		
10	HSS254x254x13.0		
9	HSS305x305x13.0		
8	(2)HSS254x254x9.5*	HSS127x127x13.0	
7	(2)HSS254x254x9.5*	HSS203x203x9.5	
6	(2)HSS254x254x9.5*	HSS254x254x9.5	
5	(2)HSS254x254x9.5*	HSS254x254x13.0	
4	(2)HSS254x254x9.5*	HSS254x254x13.0	HSS127x127x13.0
3	HSS305x305x13.0	HSS203x203x13.0	HSS203x203x13.0
2	HSS254x254x13.0	HSS178x178x13.0	HSS203x203x9.5
1	-	-	-

*Built-up sections

CHAPTER FIVE: SEISMIC ANALYSIS AND STRUCTURAL RESPONSE OF MULTI-STOREY ZIPPER BRACED FRAMES

The 4-, 8-, and 12-storey zipper braced frames designed in Chapter 4 based on the proposed methodology developed on the Excel spreadsheet under the considered 2 scenarios: zippers in tension and zippers in compression, is analyzed herein with Drain2DX and OpenSees. The purpose of these analyses is to validate the design method as well as to assess the performance of this innovative structural system. A detailed description of analytical models is provided in the first part of the chapter, and a comparative discussion related to the time-history responses as obtained in Drain2DX and OpenSees is conducted in the second part.

5.1 Zipper braced frame modeling

In order to validate the proposed design method, results from numerical analyses performed with ETABS (elastic analysis) and two finite element programs: Drain2DX and OpenSees are considered. As presented in Chapter 2, most of the zipper braced frame analyses conducted by following researchers: Sabelli (2003), Tirca and Tremblay (2003, 2004), Leon and Yang (2003)), were performed by using Drain2DX. Thus, for a consistent discussion related to the previous researches, the Drain2DX program, developed at UC Berkeley, was selected as being the first analytical tool. In addition, the second computer program selected to overcome the limitations of Drain2DX was the most popular earthquake engineering simulation platform, OpenSees.

Prior to numerical modeling of zipper braced frames, the following assumptions have been made:

- For simplicity, the building sample has a symmetrical layout and the accidental in plan torsion was omitted.
- In Drain2DX, the zipper braced frame is modeled in 2 Dimension. Therefore, the out-of-plane buckling of brace elements was neglected.
- To take into account the effect of gravity columns, all the gravity columns were considered along with the braced frame in a 2D layout. The gravity columns were connected to the brace frame through rigid links to simulate their behaviour in the structure. The lateral shear forces were transferred to the braced frame through these links.
- All the connections within the structures are assumed to be pin connections, which include the brace end connections, beam to column connections, and the column ends connections.
- Gusset plates are modeled as rigid extensions. The yielding and buckling effect of gusset plates is neglected.

An analytical model built based on these assumptions is shown in Figure 5.1.

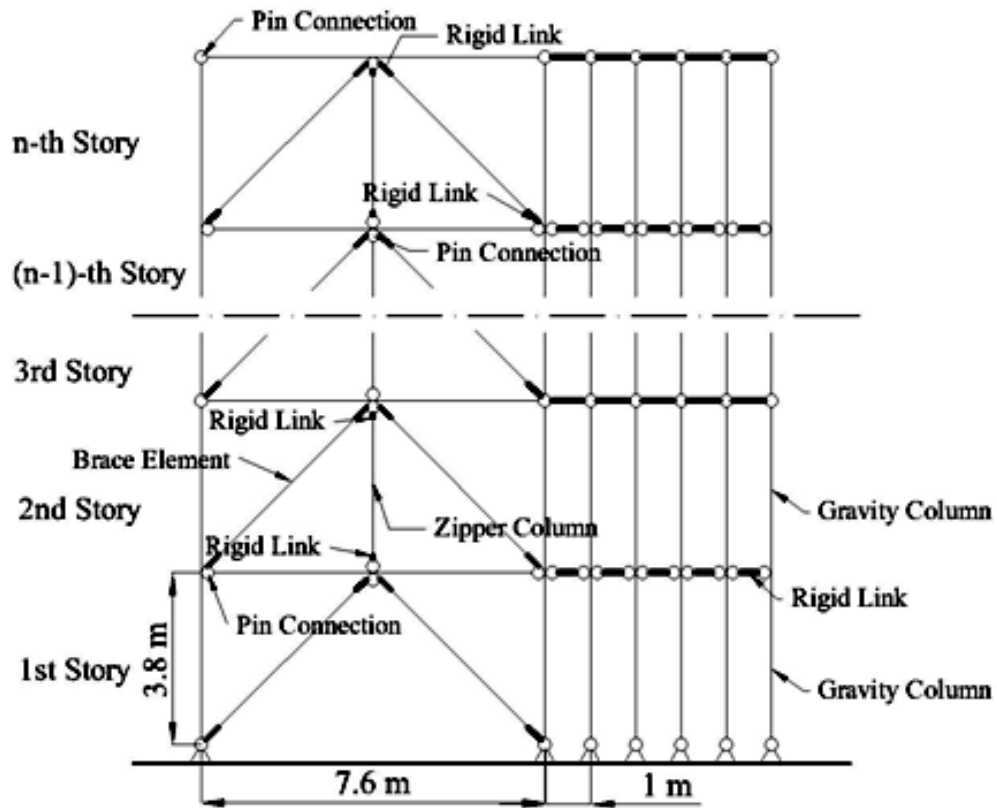


Figure 5.1 Computer model of CBF with zipper columns

5.2 Ground motions selection and scaling procedure

5.2.1 Ground motion selection

The studied buildings were subjected to three different ensembles of ground motions such as: regular, Cascadia subduction and Near-field ground motions. The first ensemble is composed of 8 regular ground motions selected to match the two dominant magnitude-hypocentral scenarios for the Victoria region which are: M6.5 recorded at 30km and M7.2 at 70km. Among them, 4 are simulated and 4 are historical ground motions, as shown in Table 2. The second ensemble contains 2 artificial ground motions simulating a Cascadia subduction scenario for a M8.5 and a hypocentral distance of 130km. The third

ensemble is composed of 6 Near-field ground motions characterized by pulse effect and forward directivity. Note, this last ensemble was employed for analyzing purposes and not as being characterized for the Victoria region. In addition to the magnitude, M_w , and the hypocentral distance, R , Table 5.1 shows the peak ground acceleration (PHA), the

Table 5.1 Ground motions characteristics

No.	Event	M_w	R (km)	Station	Comp. (degree)	PHA (g)	PGV (m/s)	PGV/PHA	t_d (s)	t (s)
Regular ground motions										
R1	Simulated Trial #1	6.5	30	-	-	0.53	0.57	1.08	4.7	8.53
R2	Simulated Trial #4	6.5	30	-	-	0.31	0.31	1.00	5.7	8.53
R3	Simulated Trial #1	7.2	70	-	-	0.30	0.30	1.00	12.5	18.18
R4	Simulated Trial #2	7.2	70	-	-	0.24	0.24	1.00	13.1	18.18
R5	1984 Morgan Hill	6.1	38	San Ysidro, Gilroy #6	90	0.37	0.37	1.00	6.5	60.02
R6	1994 Northridge	6.7	44	Castaic, Old Ridge	90	0.52	0.52	1.00	9.1	60.00
R7	1965 Puget Sound	6.7	87	Olympia, Test Lab	266	0.20	0.13	0.65	20.8	81.96
R8	1949 Western Wash.	7.1	76	Olympia, Test Lab	86	0.28	0.17	0.61	18.8	89.06
Cascadia subduction ground motions										
C1	Simulated Trial #1	8.5	120	-	-	0.10	0.17	1.70	65.1	100.00
C2	Simulated Trial #2	8.5	120	-	-	0.09	0.24	2.67	51.4	100.00
Near-field ground motions										
N1	1995 Kobe	6.9	0.6	JMA	90	0.83	1.04	1.25	-	150.00
N2	1995 Kobe	6.9	2.0	Takatori	90	0.61	1.75	2.87	-	40.96
N3	1994 Northridge	6.7	7.1	Rinaldi	228	0.84	1.75	2.02	-	14.95
N4	1994 Northridge	6.7	7.1	Newhall	90	0.58	1.18	2.03	-	40.00
N5	1994 Northridge	6.7	9.9	Sylmar County Hosp.	90	0.85	1.38	1.62	-	30.00
N6	1994 Northridge	6.7	6.4	Sylmar Converter St	52	0.60	1.22	2.03	-	60.00

peak ground velocity (PHV), the ratio of PHV/PHA, the Trifunac duration, t_d , and the total duration of the selected records, t .

5.2.2 Scaling of ground motion

Since the design spectra indicates the seismic hazard at a site for design purposes, the seismic design codes and guidelines require scaling of the ground motion accelerograms to match or the design spectrum to be within a period range of interest, T_0 and T_n (Baker, 2009).

FEMA 356 suggests that the ground motions used for dynamic analyses shall be scaled in such a way that the 5% damped response spectra of the ground motion considered does not fall below 1.3 times the 5% damped design spectrum ordinates for the interval delimited by the following period: T_0 and T_n . For conventional buildings, T_0 and T_n are assigned to be $0.2T$ and $1.5T$ respectively, where T is the fundamental period of the structure.

The proposed method for scaling ground motion accelerograms is shown below and was considered herein to scale all selected ground motions of the regular, Near-field and Cascadia ensembles.

The first step consists of equating the energy developed under the ground motion acceleration spectrum within the interval $0.2 T_1$ and $1.5 T_1$ with the code design spectrum. For most structures, during the inelastic behaviour, the fundamental period degrades toward $1.5 T_1$, while during the inelastic behaviour the higher modes oscillate with a period $> 0.2T_1$. Therefore, instead of matching the entire input energy of a given spectrum with the code spectrum, only the region between $0.2T_1$ and $1.5T_1$ is considered.

The lower limit accounts for the influence of the higher modes effect, while the upper limit accounts for the stiffness degradation of the structure in plastic range. In general, ground motions can be scaled by equating the energy content of the selected ground motion acceleration spectrum with the damage spectrum within these periods of interests. However, this method is not recommended to be applied without checking the magnitude of the scaled acceleration spectrum ordinate corresponding to T_I .

According to FEMA 356 provisions, the spectrum acceleration ordinate at T_I cannot differ more than $\pm 30\%$ of $S_a(T_I)$ where S_a is the design spectrum for the given location. Therefore for those ground motions which have spectral ordinates $S(T_I)$ outside the ranges specified by $\pm 30\%$ of $S_a(T_I)$, an adjusted scale factor is required.

Thus, for the 4-storey building, all ground motions were scaled within the period of interest $T_0=0.15s - T_n=1.1s$ and the design spectrum. The mean of the ground motions considered for each ensemble and the mean \pm one standard deviation is shown in Figure 5.2 a). For the 8- and 12-storey building, all ground motions were scaled within the period of interest $T_0=0.32s - T_n=2.6s$ and $T_0=0.5s - T_n=4s$, respectively. The results are shown in Figure 5.2 b) & c).

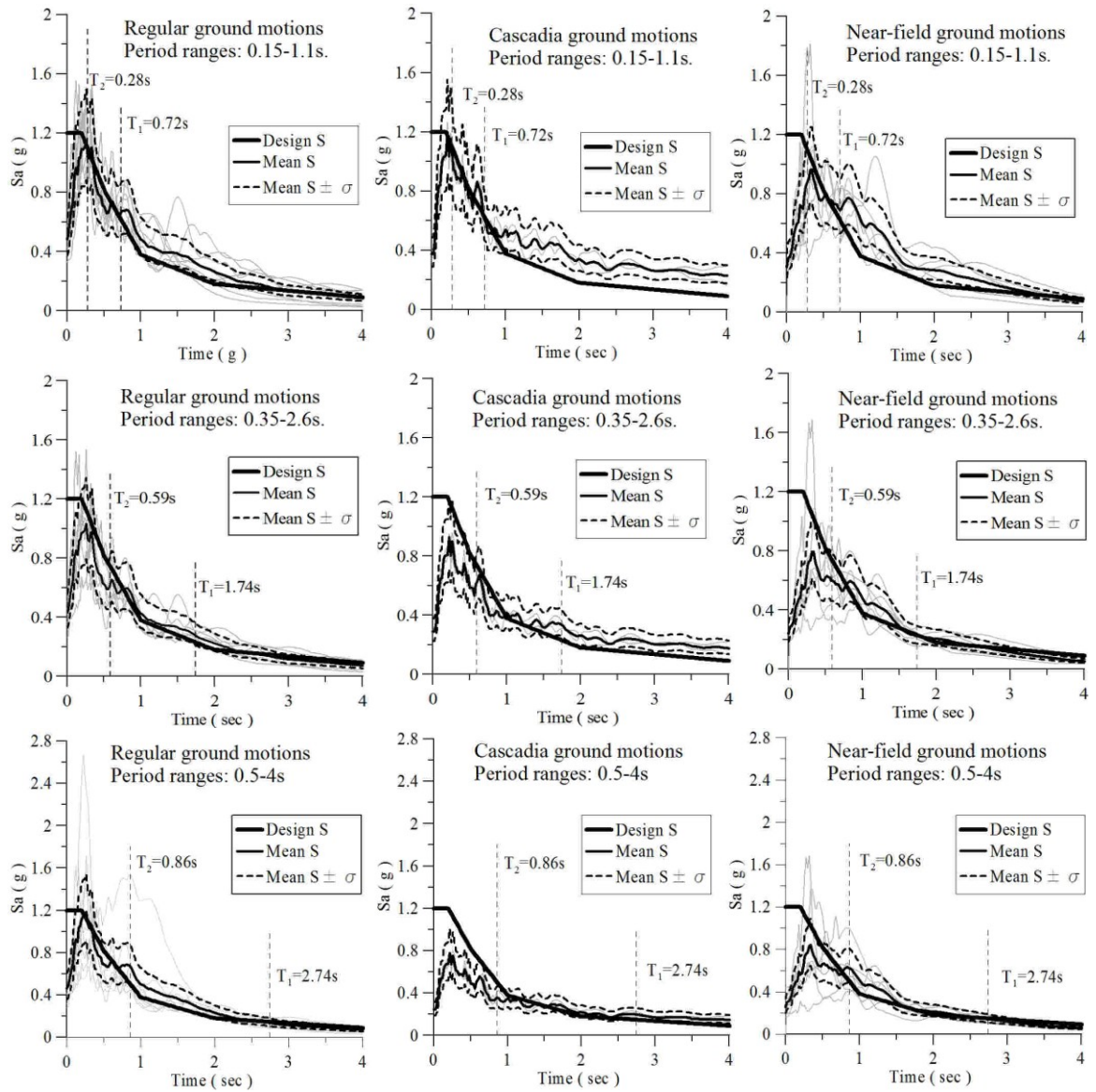


Figure 5.2 Design and scaled response spectrum of the selected accelerograms for: a) 4-storey building; b) 12-storey building; c) 12-storey building

All scale factors calculated based on the above procedure are shown in Table 5.2.

Table 5.2 Scale factors applied to the selected ground motions

No.	Event	4-story building		8-story building		12-story building	
		T ranges: 0.15s–1.1s Scale factor	PHA(g)	T ranges: 0.35s–2.6s Scale factor	PHA(g)	T ranges: 0.5s–4.0s Scale factor	PHA(g)
Regular ground motions							
R1	Simulated Trial #1	1.213	0.643	1.006	0.533	0.933	0.494
		-	-	-	-	(0.880)*	(0.466)*
R2	Simulated Trial #4	1.254	0.389	1.091	0.338	1.054	0.327
R3	Simulated Trial #1	1.697	0.509	1.201	0.360	1.130	0.339
		-	-	(1.072)*	(0.322)*	-	-
R4	Simulated Trial #2	1.867	0.448	1.347	0.323	1.221	0.293
R5	1984 Morgan Hill	1.146	0.424	1.116	0.413	1.185	0.439
		-	-	(1.190)*	(0.440)*	(2.280)*	(0.844)*
R6	1994 Northridge	0.755	0.392	0.767	0.399	0.858	0.446
		-	-	-	-	(0.970)*	(0.504)*
R7	1965 Puget Sound	2.882	0.576	2.830	0.566	3.006	0.601
R8	1949 Western Wash	1.843	0.516	1.802	0.504	1.736	0.486
		(2.064)*	(0.578)*	-	-	(1.564)*	(0.438)*
Cascadia subduction ground motions							
C1	Simulated Trial #1	3.921	0.392	2.948	0.295	2.445	0.245
C2	Simulated Trial #2	3.744	0.348	3.006	0.280	2.528	0.235
Near-field ground motions							
N1	1995 Kobe	0.418	0.347	0.371	0.308	0.416	0.345
		-	-	-	-	(0.523)*	(0.434)*
N2	1995 Kobe	0.507	0.309	0.326	0.199	0.311	0.190
N3	1994 Northridge	0.407	0.342	0.319	0.268	0.321	0.269
N4	1994 Northridge	0.625	0.363	0.615	0.357	0.643	0.373
		(0.690)*	(0.400)*	-	-	-	-
N5	1994 Northridge	0.753	0.640	0.582	0.495	0.554	0.471
N6	1994 Northridge	0.583	0.350	0.401	0.241	0.327	0.196
		(0.466)*	(0.280)*	-	-	(0.265)*	(0.159)*

()* rescaled ground motions

5.3 Numerical analyses in Drain2DX

5.3.1 Modeling in Drain2DX

The Drain2DX model was made up with two types of elements: Element 02, and Element 05.

Element type 02 is a simple inelastic beam-column element used to model steel and reinforced concrete beams and beam-columns. The element is made up of an elastic beam and two rigid-plastic hinges at its ends. All plastic deformations are concentrated within the plastic hinges. This element is used to model the beams and columns in the braced frame.

Element type 05 is a refined physical theory brace model developed by Ikeda and Mahin (1986), which achieved efficiency by combining analytical formulations describing plastic hinge behaviour with an empirical formula developed based on a study of experimental data. Element 05 was calibrated by Ikeda and Mahin based on experimental test results. However, as shown in Chapter 3, these parameters were recalibrated in this study to match the hysteresis behaviour of braces with hollow sections as per experimental tests.

This element has been used to model both braces and zipper columns.

In this study a 3% Rayleigh damping was assigned to the model. All the zipper columns and braces are pin connected to a gusset. P-delta effect has been considered for both frame columns and gravity columns. A typical analytical model is shown in Figure 5.1.

5.3.2 Drain2DX results

5.3.2.1 General behaviour

The response of the studied structures depends on the frequency content, the ratio peak ground acceleration over the peak ground velocity and the duration of the selected ground motions. For example, under the regular ground motion excitations, the largest tensile forces developed in the zipper columns occur at the lower part of the structure (levels 3rd, 4th), while the maximum compressive forces occur at the upper part. However, during Cascadia ground motion, larger seismic demand is required at the bottom part of the structure forcing zippers to act mostly in tension, while the Near-field ground motions excite the upper modes and drive the largest demand towards the upper part of the structure. For the studied buildings, the maximum and the mean + standard deviation magnitude of axial tension and compressive forces developed under the three considered ground motion ensembles are illustrated in Figure 5.3. As explained in Chapter 4, the braces, beams and columns of the braced frame structure with zipper columns were designed in agreement with S16-2009 seismic design requirements for moderately ductile CBF with a chevron bracing scheme. Several distribution patterns of internal forces generated by the unbalanced brace force propagated upward or downward were considered in order to capture the maximum demand in zippers. However, the demand in zippers varies from one pattern load to the other as is shown in Figure 5.3. By analyzing the compression side, the demand coming from both pattern loads: sequential triangular and sequential parabolic differs about 10% for the upper part of the structure. In this respect, the sizes of zippers were chosen to cover the demand resulting from the

sequential triangular (LP-ST) distribution, which is in agreement with the method proposed by Tremblay and Tirca (2003).

In the tension side, two load distribution patterns were retained for sizing the zippers such as sequential triangular (LP-ST) and parabolic (LP-P). For the 12-storey building, both envelopes are very close, while the some difference is shown for the 8-storey building. Therefore, the sizes of zipper columns was already selected to resist the compression demand as computed from LP-ST load distribution pattern verified against the maximum tensile force developed during the application of the LP-P load distribution pattern. All selected zippers have satisfied the tensile demand.

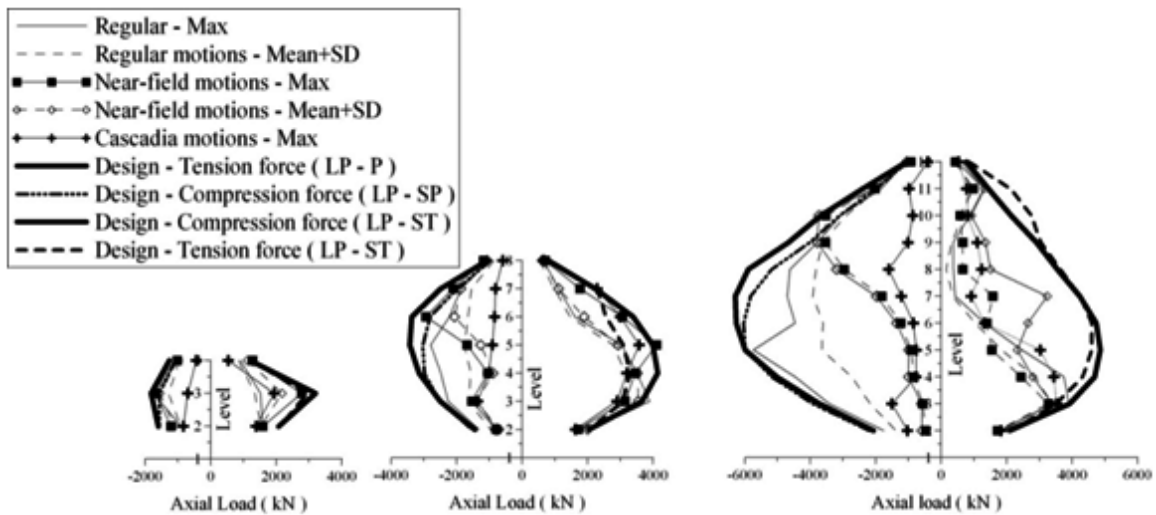


Figure 5.3 Axial force in zipper columns obtained from nonlinear dynamic time-history analyses of: a) 4-storey building; b) 8-storey building; c) 12-storey building

This exercise is able to demonstrate that by considering a parabolic distribution versus the sequential triangular distribution pattern, a slightly larger tensile demand is obtained in zippers. Therefore the concern raised by Tremblay & Tirca (2003) in their

study as shown in Figure 4.2 is overcome by adopting a different lateral load distribution pattern LP-P.

Therefore, the LP-ST load distribution pattern was retained to compute the compressive demand of zipper columns in order to size the zipper cross-sections and the LP-P load distribution pattern was retained to compute the tensile demand and to verify the selected cross-sections.

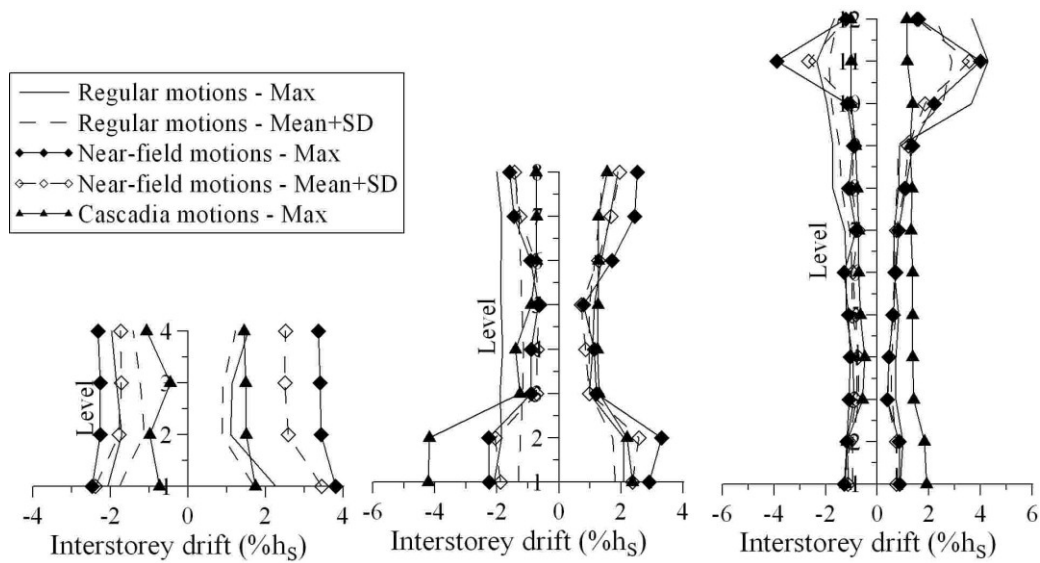


Figure 5.4 Computed interstorey drift: a) 4-storey building; b) 8-storey building; c) 12-storey building

For the studied buildings, the maximum and the Mean+SD (standard derivation) interstorey drifts have been selected as seismic response parameters. As shown in Figure 5.4, these structures show almost uniform distribution of the interstorey drift along the height of the building. During regular ground motions, the maximum interstorey drifts for the 4- and 8-storey buildings are around 2% h_s , where h_s is the storey height. The 12-storey building showed a different behaviour influenced by the higher modes effect. Thus,

the top three stories are prone to larger deformation. Under the Near-field and Cascadia ground excitations, the 8-storey structure undergoes a larger demand at the lower storeys. When the bottom braces buckle, and beams lose their brace support, the zippers are activated in tension and transfer the load to the upper undamaged floors. When Mean+SD values are considered instead of the maximum interstorey drift values, upper limit recommended by the building code (2.5% storey height) is satisfied.

5.3.2.2 Performance assessment of the 4-storey building

The 4-storey building generally deflects into the first mode of vibration. As shown in Figure 5.5, the buckling of braces initiates at the first storey, and then propagates upward. It is interesting to note that the buckling of braces and hinging of beams happen in different stages. In general, braces on the compressive side buckle first, then, in the subsequent cycle, the braces on the other half of the CBF reach the buckling force. Once the stiffness degrades, beams start hinging usually in the same sequence.

The behaviour of the 4-storey building follows the prescribed zipper mechanism (Chapter 4). The effect of higher modes is hardly noticeable due to the relatively short period of the structure. However, because of different characteristics of the selected ground motions, cases in which the brace buckling initiates at the top floor are also observed, under the R5, R7 and R8 ground motions. Under all considered Near-field ground motions but one (N5), the buckling of braces were initiated at the base. However, under both Cascadia ground motions the first brace buckled almost simultaneously at the first and at the second floor. As shown in Figure 5.3, the peak axial tensile forces computed in the zipper columns under the regular and the Cascadia ensembles were

lower, especially at the 3rd floor, than those values estimated in design. The larger values of both tensile and compressive forces were obtained in zippers under the Near-field ensemble. Under all regular and Cascadia considered ground motions, the maximum interstorey drift was remaining within the code limit (Figure 5.4).

Another interesting phenomenon which has to be noted is related to the sequences of braces buckling, which occurs within 1 second as illustrated in Figure 5.5. This typical response of zipper braced frames proves the efficiency of adding zippers to CBF systems. The zippers transfer the unbalance forces from the damaged floor to the adjacent undamaged floor. The capability of zippers to control the redistribution of lateral forces after braces have buckled has been demonstrated.

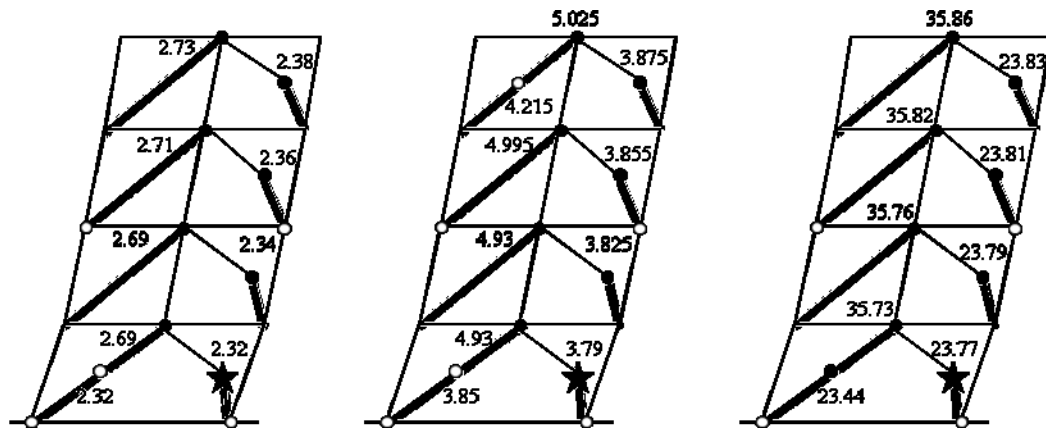


Figure 5.5 Time-history response of brace buckling and beam hinging for the 4-storey building under: a) R1 regular ground motion; b) N6, Near-field ground motion; c) C2, Cascadia simulated ground motion. (★ the first buckled brace; ● subsequently buckled brace and beam hinging; ○ yielding of brace)

5.3.2.3 Performance assessment of the 8-storey building

Considering interstorey drift as being the main parameter for assessing the structural performance of the middle-rise building, it is noted that the maximum response of the

structure under the eight selected regular ground motion excitations, and the Mean+Standard deviation values of the Near-field records are within the 2.5% limit (Figure 5.6). In general, under the six out of the eight regular ground motion excitations, the first buckling occurs at the bottom floor and the buckling is then propagated upwards. Thus, the structural response under the R2 and R6 excitation is characterised by a large demand concentrated at the upper part which forces the top floor brace to buckle. Contrary, under the Cascadia subduction ground motions, a larger demand is observed to occur at the bottom of the building. For example, the mechanism of braces buckling and beam hinges is illustrated in Figure 5.6a under the ground motion record R1. Herein, the first bottom floor brace buckles at the 2.28th second, and the unbalanced force is transferred to the upper floor through the zipper column. Due to this redistribution of forces, the brace located at the second storey on the verge of buckling reaches its probable compressive capacity at the 2.32nd second. The buckling of braces is propagated upward within 0.35 seconds. After all braces belonging to the same half-span of the framed bay buckled, the unbalance forces in braces produced hinging of the beams at their mid-span. As illustrated in the aforementioned figure, all the beam hinges developed within the time interval 2.79 seconds to 3.11 seconds.

In addition, Figure 5.6b and c shows the behaviour of the same 8-storey building under the N6 (Near-field) ground motion and Cascadia record C2. Although in these cases the first buckled brace is located at the first floor, the building behaviour is different. Under the Near-field time history acceleration the building behaves mostly after the second vibration mode with larger demand at the bottom and the top parts.

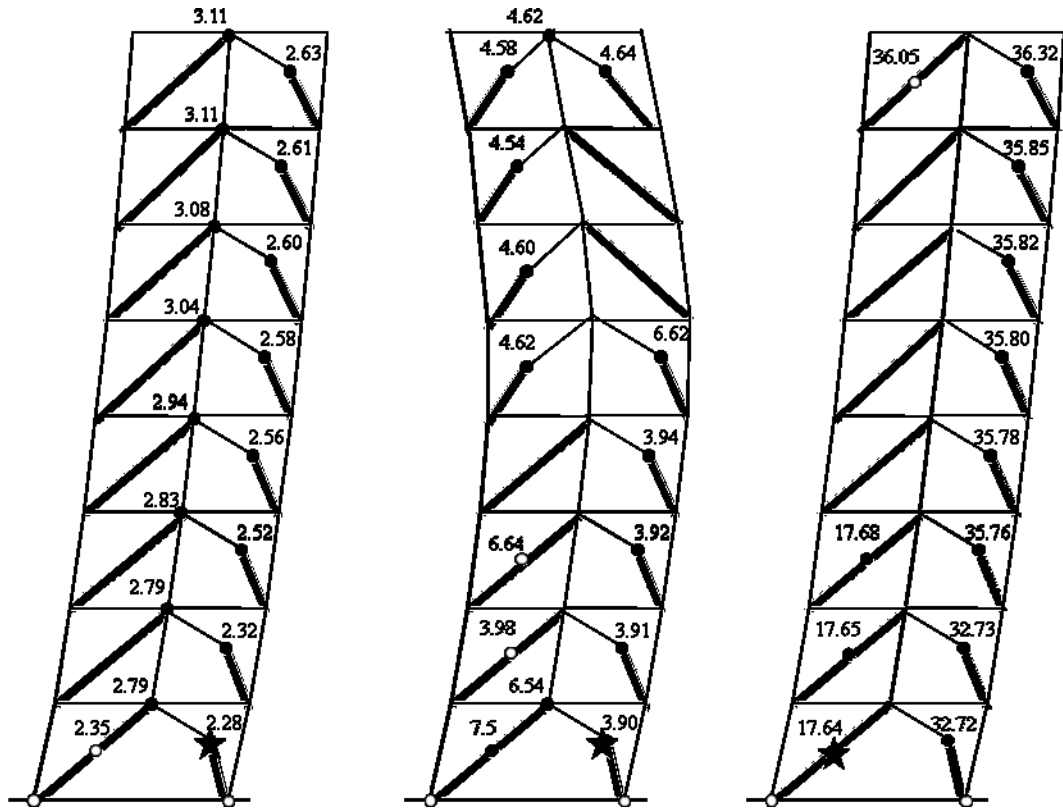


Figure 5.6 Time-history response of brace buckling and beam hinging for 8-storey building under: a) R1 regular ground motion; b) N6 Near-field ground motion; c) C2 Cascadia simulated ground motion. . (★ the first buckled brace; ● subsequently buckled brace and beam hinging; ○ yielding of brace)

Close observation of Figure 5.7 reveals that under the R1 time history accelerogram (Figure 5.7a) all floors experienced almost equal interstorey drifts and the overall deformation was observed to be sideway. The larger deformation was reached at $t = 3.45s$ under the larger asymmetrical acceleration pulse with a magnitude of 0.46g.

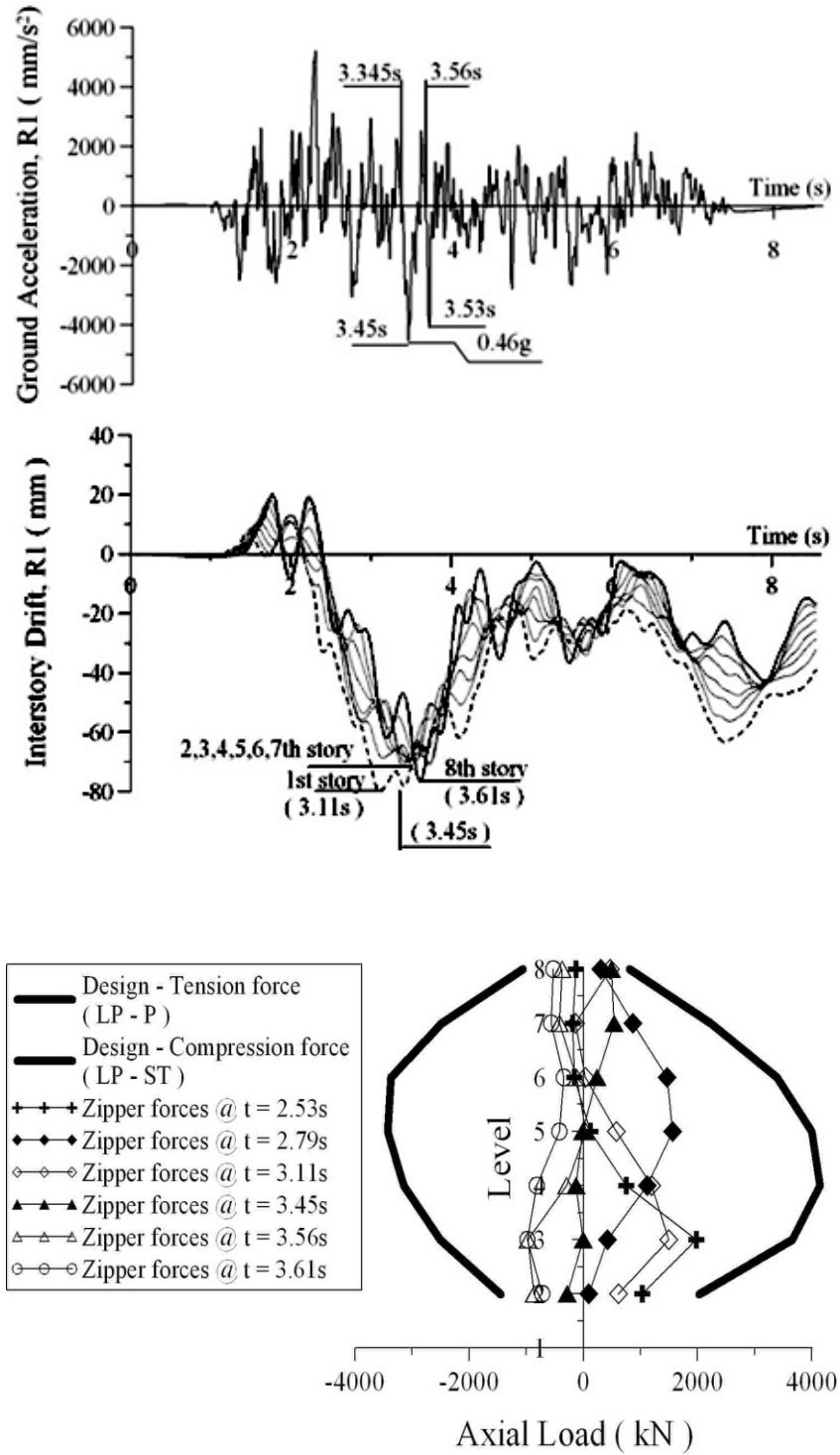


Figure 5.7 Inelastic response of the 8-storey building under the R1 ground motion: a) simulated accelerograms, R1; b) time-history of interstorey drift; c) axial forces in zipper columns

The history of axial forces developed in zipper columns over the building height are shown in Figure 5.7c for the following time steps: $t = 2.28\text{s}$; $t=2.53\text{s}$; $t=2.79\text{s}$; $t=3.11\text{s}$; $t=3.45\text{s}$ and $t=3.56\text{s}$. The axial force in the zipper columns corresponding to the maximum displacement is lower. The maximum interstorey drift corresponding to 2.2% storey height and 2.1% storey height, occurred at $t=3.345\text{s}$ at the first floor and at 3.56s at the roof respectively (Figure 5.7b).

Cascadia subduction ground motions cause a larger seismic demand at the bottom of the building rather than at the upper floors.

5.3.2.4 Performance assessment of the 12-storey building

Under the regular ground motion ensemble, the Mean+SD interstorey drift values of the 12-storey building are below the code limit (2.5%hs) and are equally distributed over the building height. However, under the R4 regular ground motions, the interstorey drift of the top 3 storeys have reached 3.5%hs. During Near-field excitations, the top stories are always influenced by the higher modes effect and experienced large interstorey drift demand in the interstorey drifts. The building response under two out of four Near-field ground motions showed a greater demand at the 11-th storey. Contrary to the behaviour of the 8-storey, building under Cascadia ground motions, the 12-storey structure shows a uniform interstorey drift distribution over the structure height with peaks below the code limit (Figure 5.4 c).

Regarding the seismic demand, in terms of axial force in the zipper columns, Figure 5.3 is analyzed. It illustrates a larger demand in the axial compression versus tensile forces in the zipper columns of the 12-storey frame, contrary to the tendency

observed for the 4-, and 8-storey response. This typical behaviour of the 12-storey building suggests a larger participation of the higher modes. Time-history response of brace buckling and beam hinges is shown in the deflected shape of the 12-storey frame illustrated in Figure 5.8. For example, under the R1 accelerogram all braces on the verge of buckling were able to dissipate a large amount of energy in less than 1 second. Although in two ground motion ensembles (regular and Cascadia) out of three, the first brace buckles at the bottom floor, while under Near-field the demand is moving to the upper floors.

As shown in Figure 5.8 a) braces of the right half-span of the structure have buckled in sequence. Due to the higher modes effect, the buckling sequences are not strictly as predicted. However, it can still be observed that all braces of the half-span buckled within 0.4 seconds. With the participation of zipper columns, the inelastic response of braces is spread into all braces of the structural system. Thus, the pure behaviour of CBF's with a chevron bracing configuration, characterised by limiting the inelastic response within a few stories, is overcome. Under the ground motion N6, the braces on the top three stories buckled simultaneously, then the buckling of braces progress downwards. Since the maximum interstorey drift developed under this ground motion is still lower than 1.3% storey height, the plastic deformation did not extend to the bottom part of the structure. When the ground motion reverses direction, braces on the other half-span of the structure start to buckle.

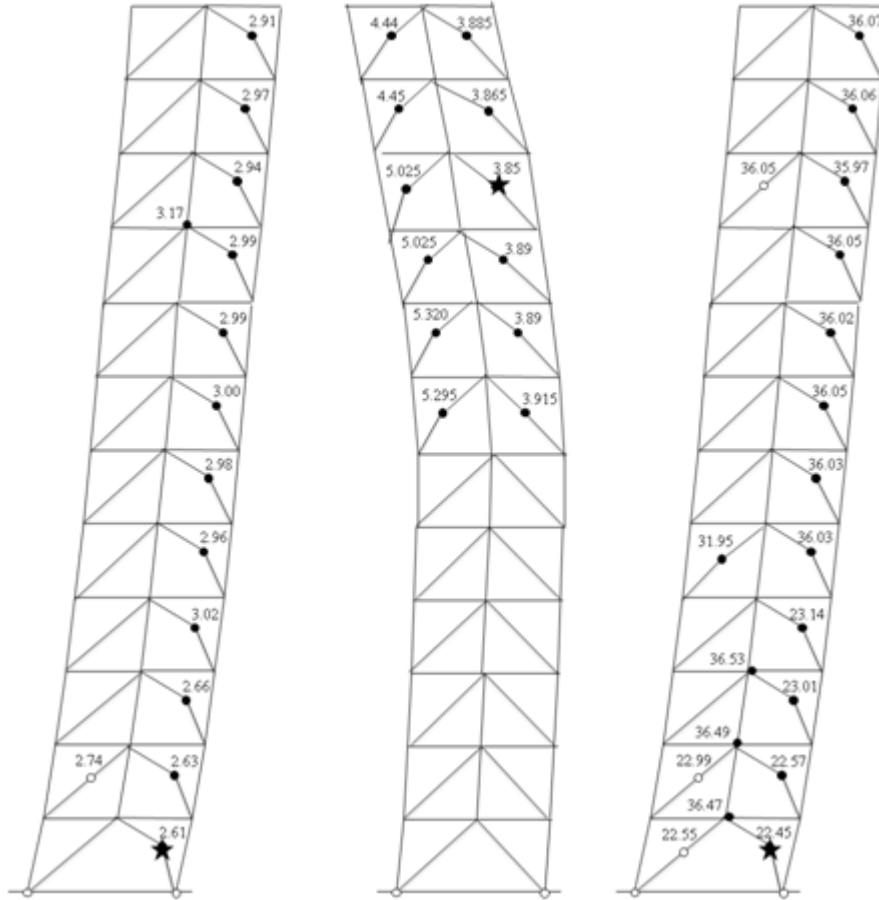


Figure 5.8 Time-history response of brace buckling and beam hinging for 8-storey building under: a) R1 regular ground motion; b) N6 Near-field ground motion; c) C2 Cascadia simulated ground motion. (★ the first buckled brace; ● subsequently buckled brace and beam hinging; ○ yielding of brace)

Although Cascadia ground excitations did not show a great demand in terms of interstorey drifts, brace buckling and beam hinging were still observed, which suggests that significant amount of energy had been dissipated through the plastic deformations. Therefore, the effect of zipper columns clearly demonstrates the spreading of inelasticity all braces.

Figure 5.9 illustrates in detail the seismic response of the 12-storey building under the ground motion excitation R1. It is shown a similar behaviour with the 8-storey

structure. In this case, all floors undergo similar interstorey displacement and the maximum interstorey drift, 1.7%hs occurs at the top floors as shown in Figure 5.9 (b) at the 3.36s after experienced a 1.4%hs at 2.93s. The upper 4 floors have a similar deflected shape due to the softening of the 8th floor where a plastic hinge was formed in the beam. This stage of inelastic behaviour is dictated at the sequence of time 3.45s when the peak ground acceleration 0.46g is reached. At the end of the ground motion, some residual drifts can be observed. Forces in the zipper columns are shown for each step of the time when braces buckle. When braces in one side have buckled and reached the postbuckling strength a large tensile force is developed in the tensile brace close to the probable tensile strength. The vertical projection of the unbalance force ($T_u \sin\theta - C'_u \sin\theta$) induces compression in zippers as is shown in Figure 5.9c. Therefore, the loop of transferring the unbalanced forces, developed in braces belonging to the same floor, to zippers at the brace to beam intersection point is observed. When the motion reverses direction, the braces of the previous tensile side are in compression and reach the buckling strength. Again, the unbalanced force is transferred to the zippers, which deflects the beams until plastic hinges are formed. In this regard, the full zipper mechanism is defined when all braces have buckled and beams have hinged

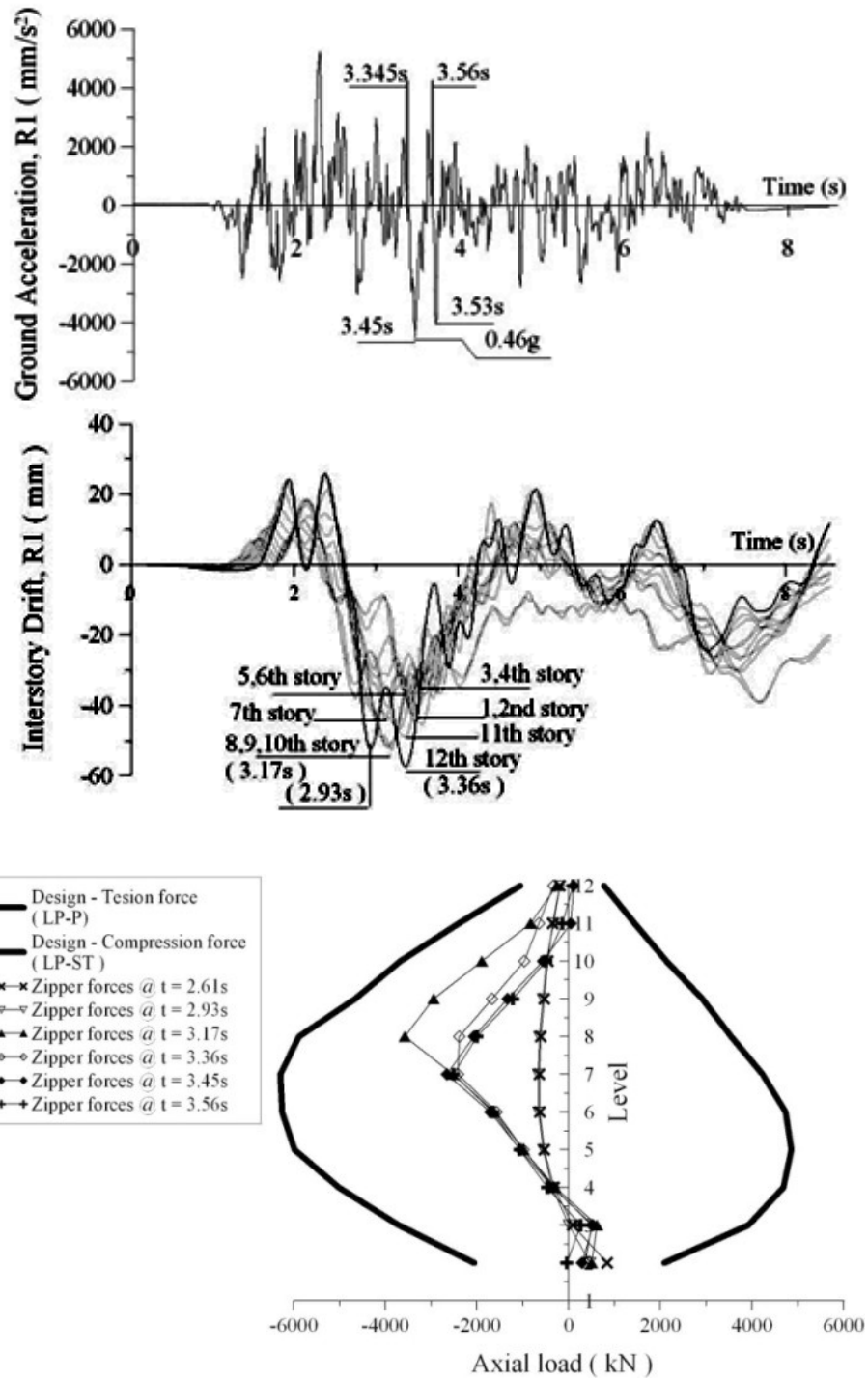


Figure 5.9 Inelastic response of the 12-storey building under the R1 ground motion: a) Simulated accelerograms, R1; b) Time-history of interstorey drift; c) Axial forces in zipper columns

It is concluded that by increasing the number of storeys, the amount of compressive forces transferred to the zippers is increased. Recalling Figure 5.3 (c), the tensile demand in zipper columns, as shown in the analysis is much smaller than predicted.

5.3.3 OpenSees results

5.3.3.1 General behaviour

This part focuses on analysing the magnitude and time-history evolution of the following main parameters: axial forces in zippers, interstorey drifts, brace force-displacement hysteresis behaviour and story shear forces.

As demonstrated above the structure response is influenced by the type of ground motions inter-plate subduction or near-field and their frequency content. The envelope of axial forces developed in the zipper columns of the 4-, 8- and 12-storey buildings, under the 16 selected accelerograms, divided in three ensembles, is expressed as maximum and mean + one standard deviation and is illustrated in Figure 5.10. These results obtained from OpenSees and the resulted from Drain2DX, shown in Figure 5.3, are almost equal. Thus, through simulation, the computation is validated. Under regular ground motion excitations, greater axial tensile force demand in zipper columns is observed at the third floor of the 4-storey structure, at the third to fifth floor of the 8-storey structure and the third to the fourth floor of the 12-storey structure. The maximum compression envelope developed in zipper columns of the 8-storey building shows a parabolic demand with the vertex located at the fifth floor, while for the 12-storey structure the distribution seems to be linear from the bottom to the 5th floor where the peak has reached and from the roof to the 8th floor where a second peak has been identified. During the Near-field excitations,

the responses of the 8-storey structure and the 12-storey structure are almost identical. In this case, the compression demand moves towards the top of the building, while the tension demand is much larger at the bottom (at the 3rd respectively the 5th floor). Interestingly, under Cascadia ground motion excitations, the zipper columns belonging to the 8-storey building behave mostly in tension, while the compressive force is almost negligible. On the contrary, for the 12-storey building, a peak in the axial compressive force envelope is identified at the 5th floor, which corresponds to a drop in the tensile force envelope.

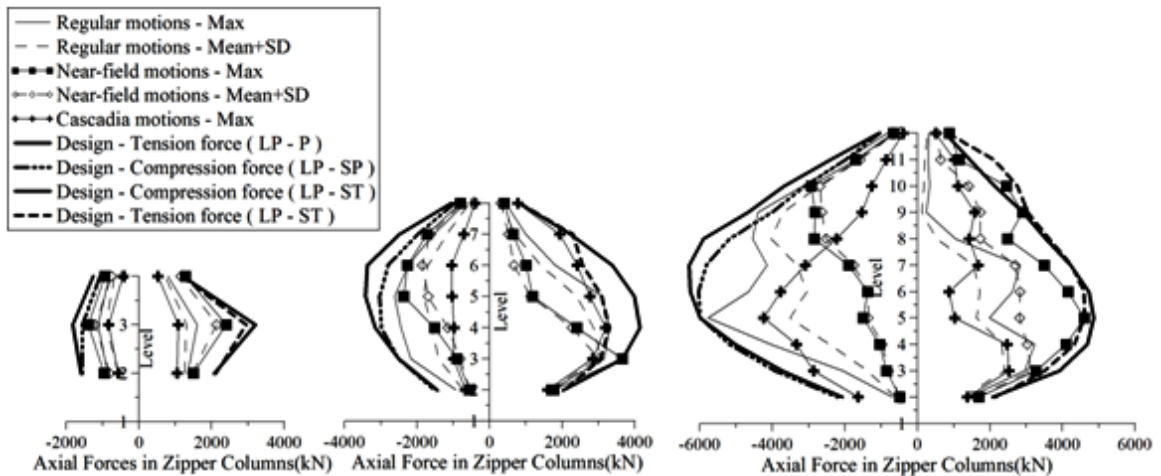


Figure 5.10 Axial force in zipper columns obtained from nonlinear dynamic time-history analyses in OpenSees of: a) 4-storey building; b) 8-storey building; c) 12-storey building

In the compression side, the predicted envelope LP-SP is identical with the forces resulted from time-history analysis for the upper 2-3 floors. There is only a small difference between the LP-SP and the LP-ST envelop for the upper half of the structure. Regarding the tension side, the two envelopes (LP-P, LP-ST) have shown very close predictions.

The maximum drifts obtained from all the dynamic analyses under the design level of lateral forces shows the same patterns as those obtained in Drain2DX (Figure 5.11). Refining the modeling of inelastic behaviour, the interstorey drift values are below the code limit, 2.5%hs. There are some differences between the maximum values of interstorey drifts obtained in OpenSees and Drain2DX. The main reason of the existence of these differences has been covered in Chapter 3. It is noted that modeling braces in Drain2DX conducts a larger incremented amount of cumulative dissipated energy than that obtained in experimental results, while the same computation in OpenSees shows a lower amount of cumulative dissipated energy. However, since the brace model in Drain2DX dissipates a larger amount of energy than that in the experimental tests, it influences the stiffness degradation and larger displacement is expected. Therefore, under various ground motion excitations, the maximum interstorey drift values are below the 2.5%hs limit, although for the 8-storey building, the demand is at the bottom floors and for the 12-storey building the larger demand is at the upper floors.

In conclusion, adding zipper columns to CBF structures with chevron bracing configuration protects the building against storey mechanism formation and assures a uniformly distributed interstorey drift over the storey height under all selected ground motions considered typical for Victoria region.

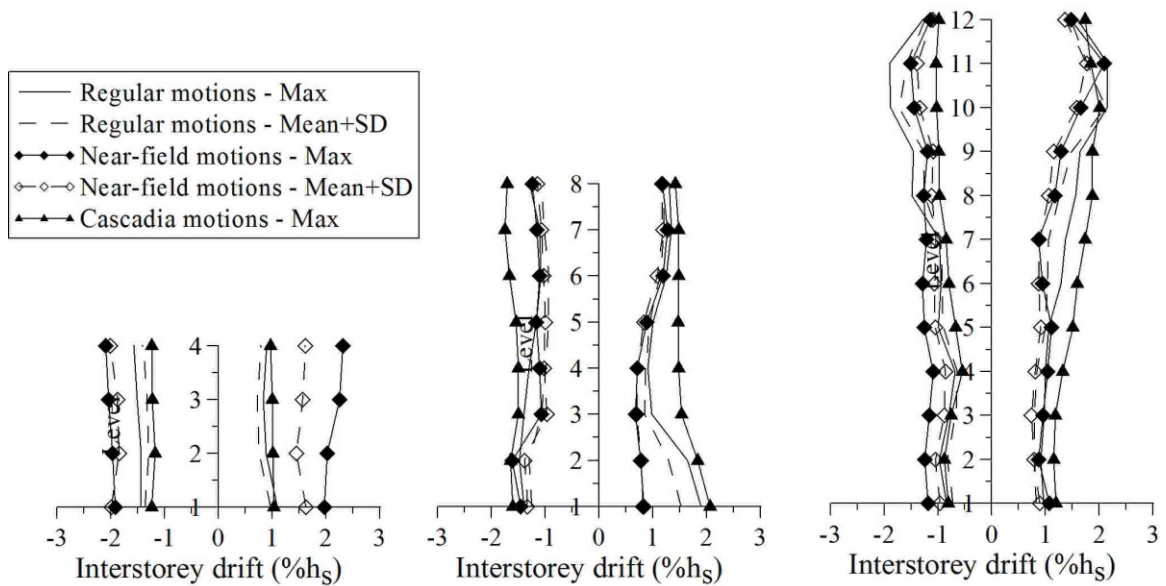


Figure 5.11 Computed interstorey drift: a) 4-storey building; b) 8-storey building c) 12-storey building

5.3.3.2 Performance assessment of the 4-story building

Close examination of inelastic behaviour of the structure revealed that, in general, the first brace starts buckling at the base or at the top of the building. More specifically, for low-rise buildings, the first buckling of brace is more likely to happen at the first floor, especially under regular ground motion due to the overall tendency of these buildings deflecting in the first vibration mode.

Thus, under all regular ground motions, R1 – R8, buckling of braces initialized at the base of the structure has been observed. The hysteresis behaviour of braces on the verge of buckling under the R1 ground motion is shown in Figure 5.12. In addition, at the time sequence when the compressive brace buckles, the behaviour of the corresponding tensile brace is also illustrated. Some yielding is detected in the tensile brace belonging to the top and bottom floors.

The seismic behaviour of the studied structure subjected to the R1 ground motion is similar in both OpenSees and Drain2DX. The time sequences indicating buckling of braces in Drain2DX are almost identical to that shown in OpenSees (Figure 5.12).

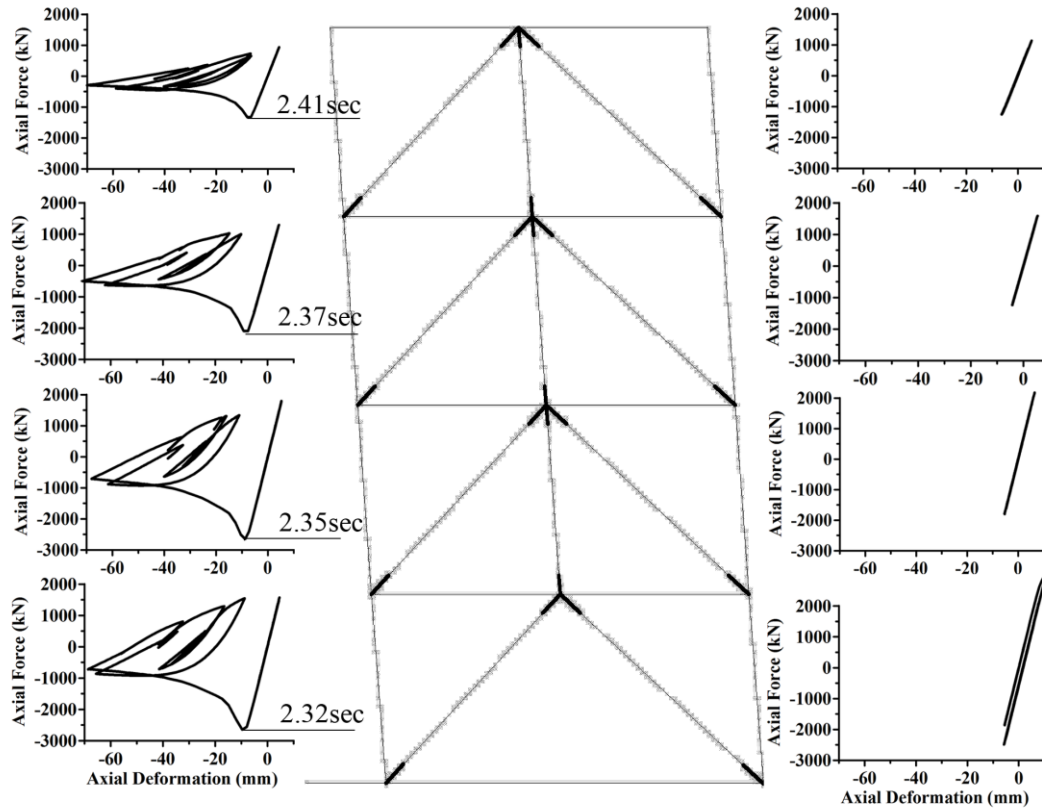


Figure 5.12 Hysteresis behaviour of brace elements in 4-storey zipper braced frame under ground motion excitation R1

To understand the structural behaviour, additional parameters such as: shear force, storey force and interstorey drift time-history are considered for investigation. The results are shown in Figure 5.13.

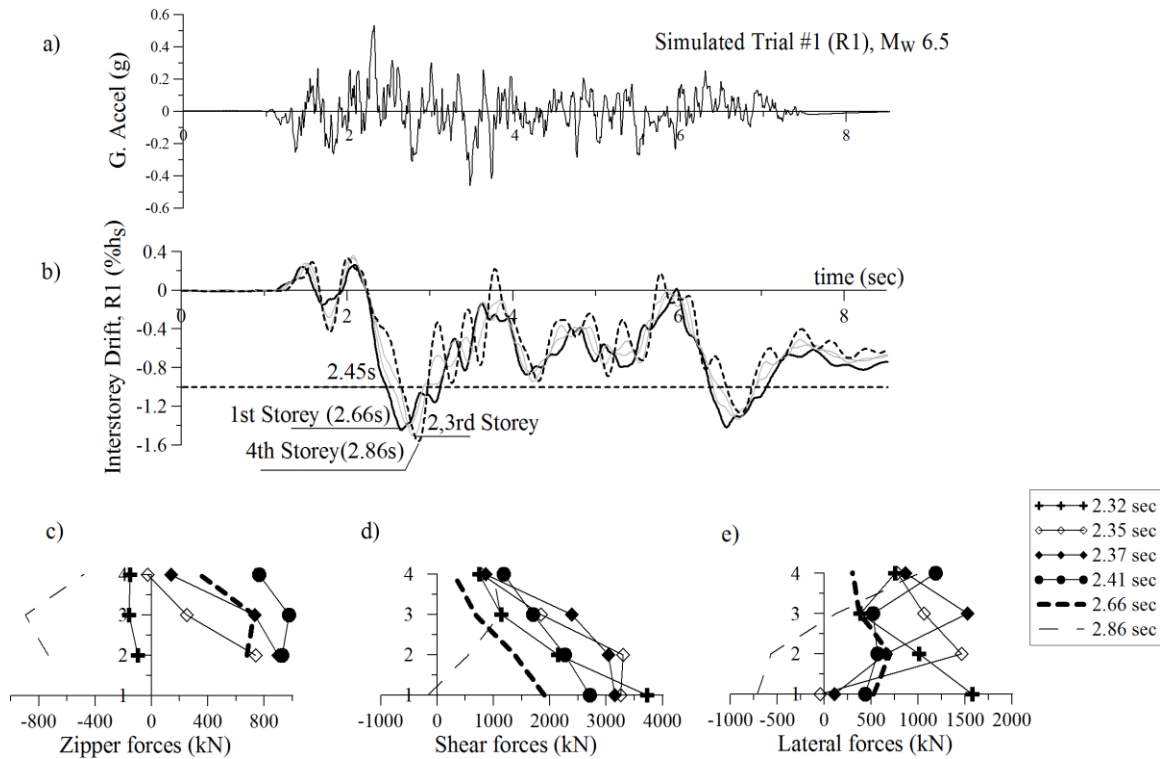


Figure 5.13 Structural response of the 4-storey zipper braced frame under ground motion R1: a) Regular ground motion excitation R1; b) Interstorey time-history record under ground motion excitation R1; c) Axial forces in zipper columns at specified time steps; d) Shear forces distribution along the building height at specified time steps; e) Storey forces induced into structure at specified time steps.

At the time sequence $t = 2.32\text{s}$, a larger storey force and a maximum base shear were reached at the 1st floor, which drove the bottom brace to buckle. After the braces buckled (from $t = 2.32\text{s}$ to $t = 2.41\text{s}$), the structure lost part of its lateral stiffness. Thus, a significant increase in story drift was observed within a fraction of a second. From Figure 5.13b, it is observed that the 4th storey brace buckles at 2.41s under a lateral interstorey drift deformation of 0.8%hs and a maximum storey force, which reached its peak after migrating from the 1st floor to the 4th floor (Figure 5.13e). The maximum interstorey drift value at the roof level increased to 1.58%hs at $t = 2.86\text{s}$. A larger axial tensile force was detected in zippers (Figure 5.13c) at the time when braces reached the buckling strength.

Herein, it is clearly shown that before the step of time 2.32s until the first brace buckled zippers were carrying only a small compression caused by the gravity loads, therefore they were not activated. At 2.35s, when the brace of the second floor buckled, both zipper columns belonging to the second and the third floor were activated in tension. As the buckling of braces propagated upwards, the tensile forces developed in zipper members increased.

Meanwhile, the storey force distribution is highly depended on the inelastic deformation of braces as is shown in Figure 5.13 e). At 2.32s, the largest storey force developed in the structure was on the first floor and then the peak migrated to the second floor followed by the upper floor at 2.37s. Again, at 2.41s, under the same cycle of the ground motion, the brace of the top floor buckled while the maximum lateral force migrated to the fourth floor. The shear force distribution for the aforementioned time sequence is shown in Figure 5.13d.

In general, the 4-storey structure showed a first-mode based deformed shape and a similar behaviour was found when the structure was subjected to Near-field ground motions. The seismic response of the 4-storey building under the ground motion excitation N3 is shown in Figure 5.14, while the sequence of brace buckling is shown in Table II-1 of Appendix II. The first brace buckled at the bottom floor at 2.36s. Then, when the ground motion reverses direction, the brace on the other side of the same floor began to buckle and the buckling of braces propagated upwards successively.

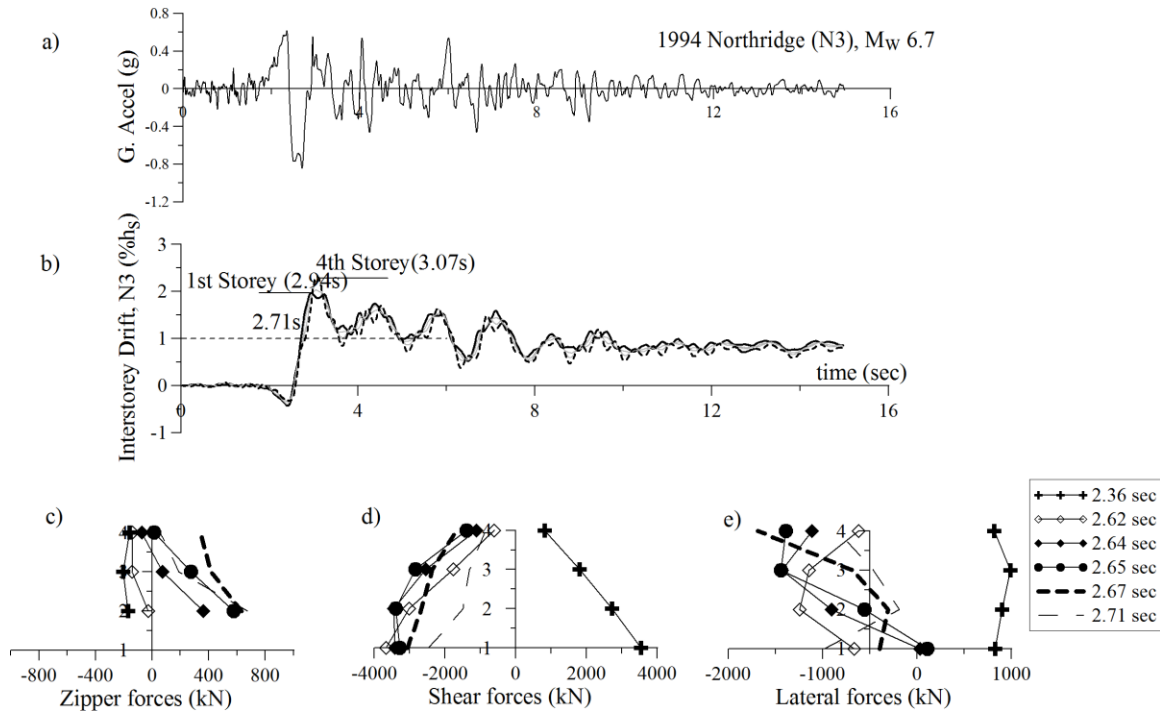


Figure 5.14 Structural response of 4-storey zipper braced frame under ground motion N3: a) Regular ground motion excitation N3; b) Interstorey time-history record under ground motion excitation N3; c) Axial forces in zipper columns at specified times; d) Shear forces distribution along the building height at specified times; e) Storey forces induced into structure at specified times.

As it can be seen in the Figure 5.14 b), the interstorey drifts exceeded 1%hs at 2.71s after all braces at the verge of buckling consumed their strength. The larger peak ground acceleration value drives the structure toward side-way deflection. A maximum interstorey drift of 2.2%hs was recorded at $t=2.94s$ and a residual drift of 1%hs at the end of the ground motion. On the other hand, during the entire ground motion excitation, the interstorey drifts were uniformly distributed along the height of the structure. From Figures 5.14 c) & e) it is noticed that the axial load in zippers was at the compression side at $t=2.62s$, and when the brace of the 2nd floor buckled, the bottom zippers were activated in tension ($t = 2.64s$). This is explained by an increase unbalance brace load due to the

buckling of the bottom braces. As expected, the lateral forces also redistributed and are shown in Figure 5.14e while the shear force is shown in Figure 5.14d.

5.3.3.3 Performance assessment of the 8-story building

The seismic response of the 8-storey braced frame subjected to ground motions with different characteristics is more complex than the behaviours of the 4-storey zipper frame. Due to the higher modes effect, the sequence of buckling braces does not always follow the simplified order considered in the design method: the braces buckle either at the top and buckling is propagated downward or at the bottom and buckling is propagated upward. However, braces located at adjacent floors reach the buckling strength almost simultaneously or successively.

As illustrated in Figure 5.16, the 8-storey building under ground motion excitation R1 is prone to deformed in the shape of the first mode of vibration. Therefore, the buckling of braces is initiating at the first floor and propagates upward.

For the studied 8-storey structure, the time when braces reached the buckling strength under the ground motion R1 is shown in Table II-2 of Appendix II and Figure 5.16. The first brace buckled at the bottom floor at 2.3s, and buckling propagated upward within a fraction of a second.

Figure 5.15 b) shows that under ground motion R1 all floors deflect in the same direction and are driven with almost equal interstorey drift. The maximum base shear of 3800kN was reached at $t = 2.3s$ when the first brace buckled at the bottom floor and activated the zipper column's response. The maximum base shear value is about 30% larger than that computed from the static equivalent method. Meanwhile, the lateral

forces induced in the structure had been redistributed as shown in Figures 5.15c and e. At the time sequence 2.34s, the first zipper column was activated.

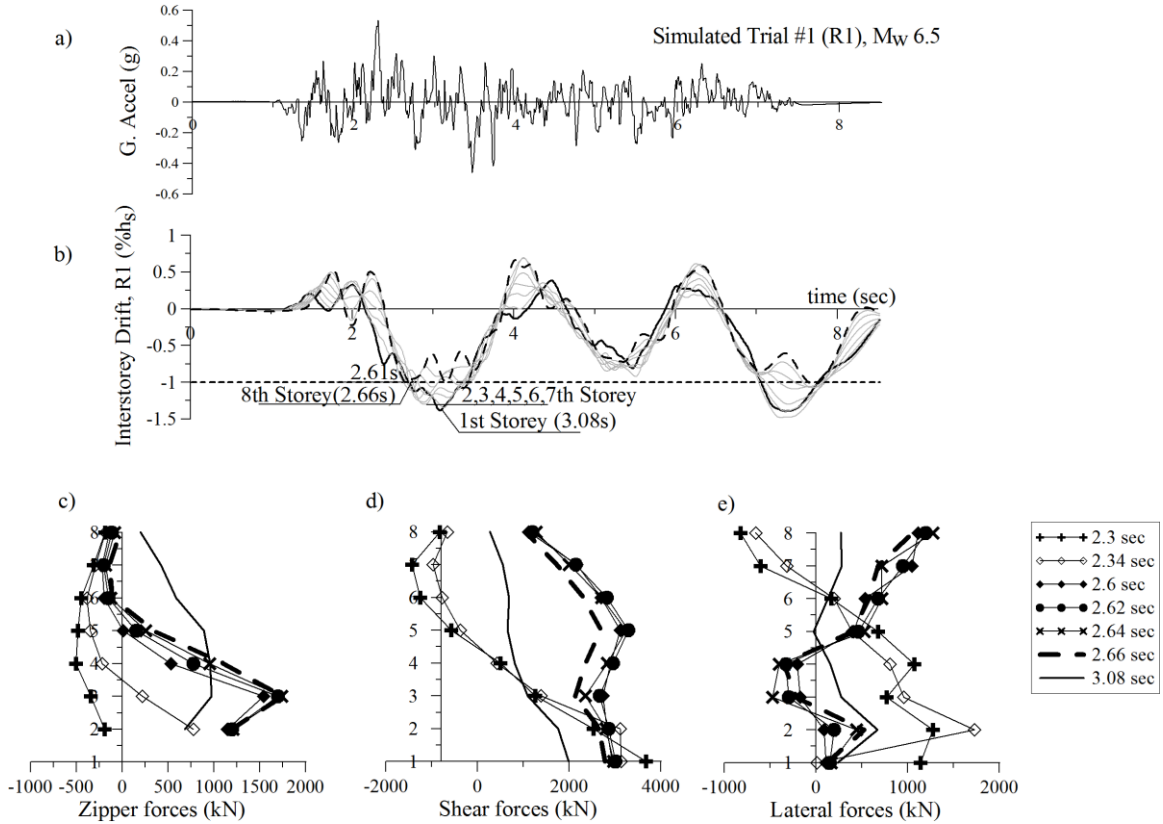


Figure 5.15 Structural response of 8-storey zipper braced frame under ground motion R1: a) Regular ground motion excitation R1; b) Interstorey time-history record under ground motion excitation R1; c) Axial forces in zipper columns at specified time steps; d) Shear forces distribution along the building height at specified time steps; e) Storey forces induced into structure at specified time steps.

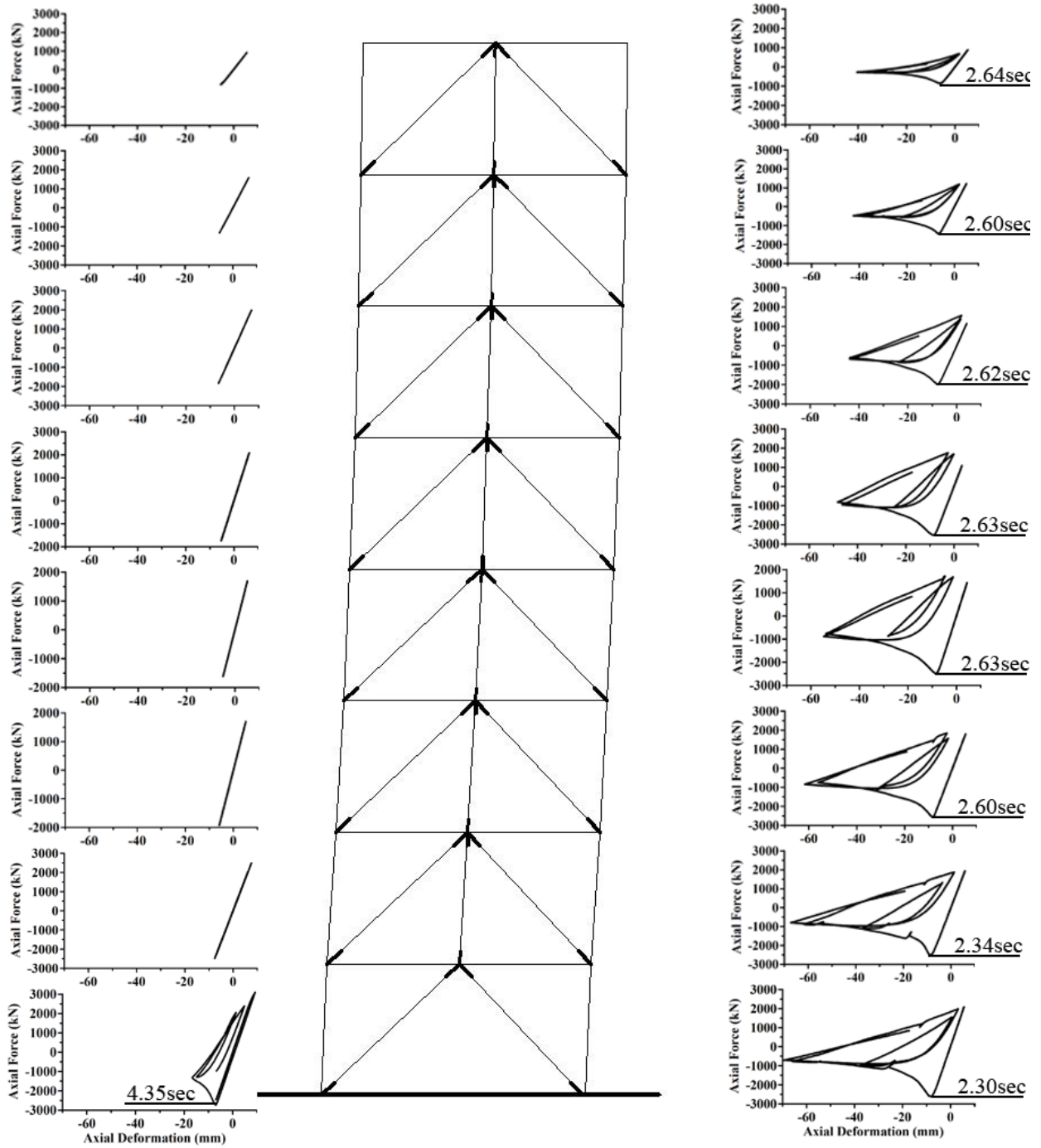


Figure 5.16 Hysteresis loops of braces of 8-storey building under ground motion R1

As shown in Figure 5.16 and Table II-2 of Appendix II, the sequence of braces buckling is within a fraction of a second, from 2.30s to 2.64s. After this time interval,

more specifically at $t = 2.66\text{s}$, the interstorey drifts of all floors reached $1\%h_s$ (Figure 5.15b). Upon $t = 2.66\text{s}$ only the zippers belonging to the lower half of the structure behaved in tension and showed a peak at the 3rd floor. As illustrated in Figure 5.15e, when the first brace buckles, the structure deflects in the 2nd mode shape. When the maximum interstorey drift of $1.3\%h_s$ was reached at $t = 3.08\text{s}$, all zippers acted in tension.

A similar seismic response was found under the Near-field ground motion excitation N2. In this case, the first brace buckled at the top floor of the structure at the time step 3.78s , when a uniform distribution of shear force over the structure height accompanied by a larger storey force at the roof level was observed. All zipper columns behaved in compression. After buckling initiated, the amplitude of the accelerogram had reduced. A few seconds after, a larger ground motion pulse ($t = 5.9\text{s}$) drove braces located at the lower three floors to buckle successively, while zippers behaved in compression. After this time sequence, when the ground motion reversed direction, during the time interval from 6.55s to 6.74s , all braces on the verge of buckling, starting with the bottom brace, consumed their strength. A larger tensile force developed in zippers belonging to the lower floors with a concentrated demand at the 3rd floor. During this time, a uniformly distributed shear force had been observed over the structure height and a larger interstorey drift ($1\%h_s$) initiated at the 1st floor. Under this ground motion excitation, several short waves were induced in the structure with a larger demand at the upper floors, while the structure followed the 3rd mode of vibration. Small residual interstorey drift was observed at the end of the ground motion (Figure 5.17b).

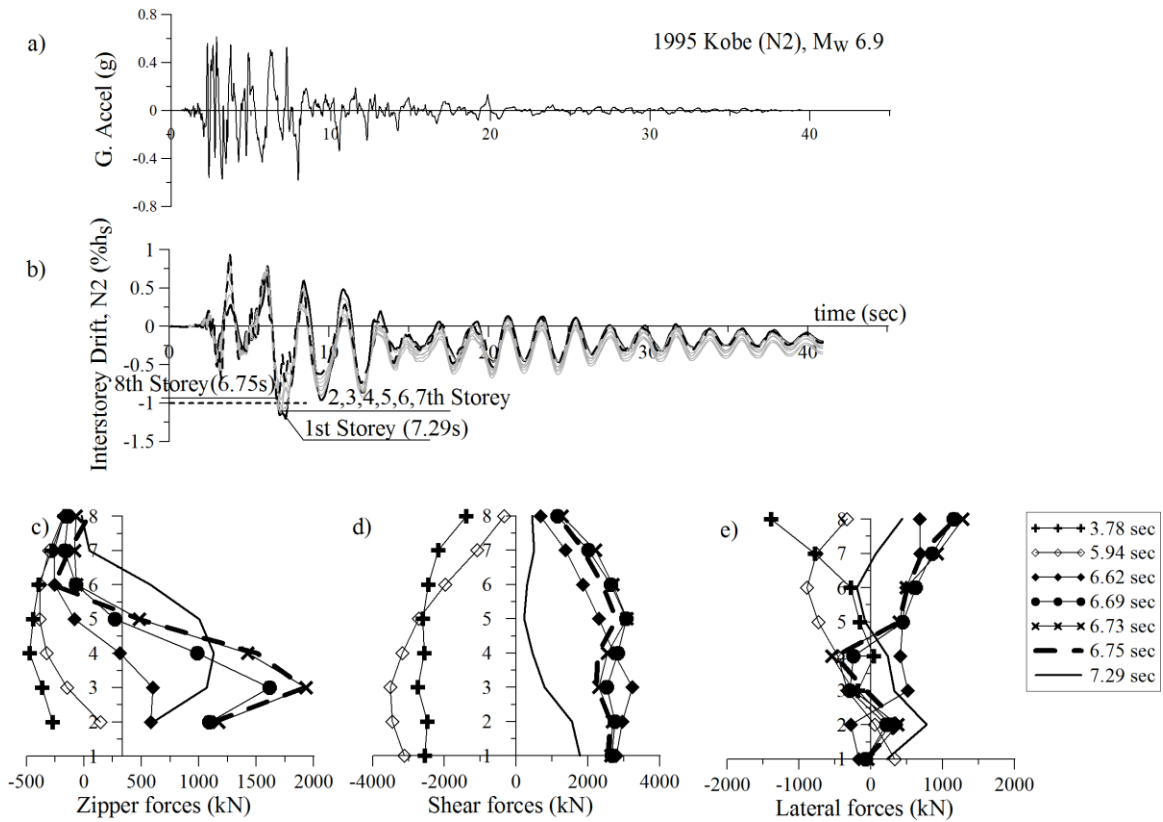


Figure 5.17 Structural response of 8-storey zipper braced frame under ground motion N2: a) Regular ground motion excitation N2; b) Interstorey time-history record under ground motion excitation N2; c) Axial forces in zipper columns at specified times; d) Shear forces distribution along the building height at specified times; e) Storey forces induced into structure at specified times.

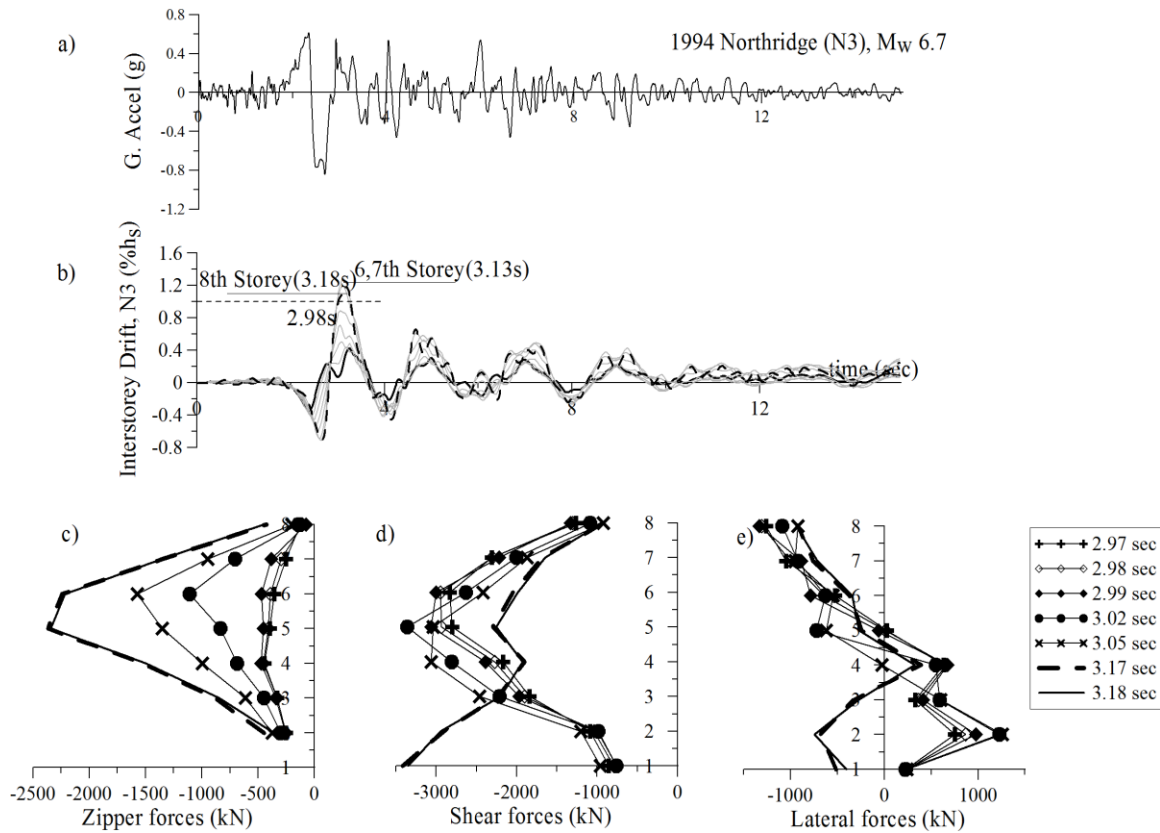


Figure 5.18 Structural response of 8-storey zipper braced frame under ground motion N3: a) Regular ground motion excitation N3; b) Interstorey time-history record under ground motion excitation N3; c) Axial forces in zipper columns at specified times; d) Shear forces distribution along the building height at specified times; e) Storey forces induced into structure at specified times.

Under the ground motion excitation N3, the first buckled brace was located at the top floor (2.97s) and propagated downward within a fraction of a second. The sequences of brace buckling are shown in Table II-2 in Appendix II. Right after the buckling occurred, the interstorey drifts of the top three floors exceed 1% storey height as illustrated in Figure 5.18 b. Accompanied with the progressive buckling of braces, a large increase in compressive forces in zippers was observed and is depicted in Figure 5.18 c.

Large storey forces (Figure 5.18) were developed at the roof level while the general behaviour of the structure was dominated by the second mode of vibration. At the

time of brace buckling zippers were loaded in compression and the proposed design method was validated.

For the 8-storey buildings, from the figures depicted above, the contribution of zipper columns to carry and transfer the unbalance forces due to braces buckling to adjacent stories is clearly illustrated. Uniform distributed storey drift over the structure height is confirmed as well as a maximum interstorey drift value below the code limit (2.5%hs). At the location when large storey force is developed, the brace buckles and zippers are activated in tension or compression depending on the location of the first buckled brace. In general, braces start buckling at a lateral deformation corresponding to 1%hs.

5.3.3.4 Performance assessment of the 12-story building

The structural behaviour of the 12-storey zipper braced frame system is more sensitive to seismic excitations than the 4- and 8-storey buildings. The higher modes effect influences the distribution of storey forces over the building height and in consequence the location of the first brace, which reaches the verge of buckling. Due to higher modes contribution the expectation of full zipper mechanism still applies even if the sequences of brace buckling is more sensitive to ground acceleration. However, the proposed design method is confirmed for all studied cases.

Under the ground motion R1, the first buckled brace ($t = 2.58s$) was located at the first floor as shown in Appendix II and corresponds to the larger value of base shear, which is about 30% larger than that computed from the static equivalent method. Then, the buckling started at the brace of the 7th floor and propagated upwards due to the higher

modes effect. It was noticed that the 10th floor seemed to undergo the largest interstorey drifts at $t = 2.99\text{s}$ when a larger storey force was intercepted. However, the drifts values were always kept under the 2.5% storey height limit.

The behaviour of the building was dominated by the higher mode effects. As illustrated in Figure 5.19 b), the structure underwent two main oscillations in two adjacent cycles. The time-history interstorey drift record shows a peak at 3.14s, right after all upper braces belonging to the upper six floors reached the buckling strength. A second larger interstorey drift was recorded at the roof level at $t = 4.16\text{s}$, but, on the other half-span of the structure after the ground motion reversed direction. During the time interval ($t = 4.13\text{s} - t=4.61\text{s}$), zipper columns were activated mostly in compression. As can be seen from Figure 5.19 c), the zippers at the 6, 7, 8, 9, 10 stories were heavily loaded in compression while transferring the unbalance vertical force downward.

Distinctively, due to the higher modes effect and a longer natural period of vibration of the structure, the braces located at the upper floors of the 12-storey zipper braced frame structure are more likely to buckle prior to the ones at the bottom. For the same reason, the earthquake impulse and acceleration amplitude is not strong enough to buckle all half-span braces of the structure at once. Therefore, the buckling of braces is naturally divided into tiers of buckled braces.

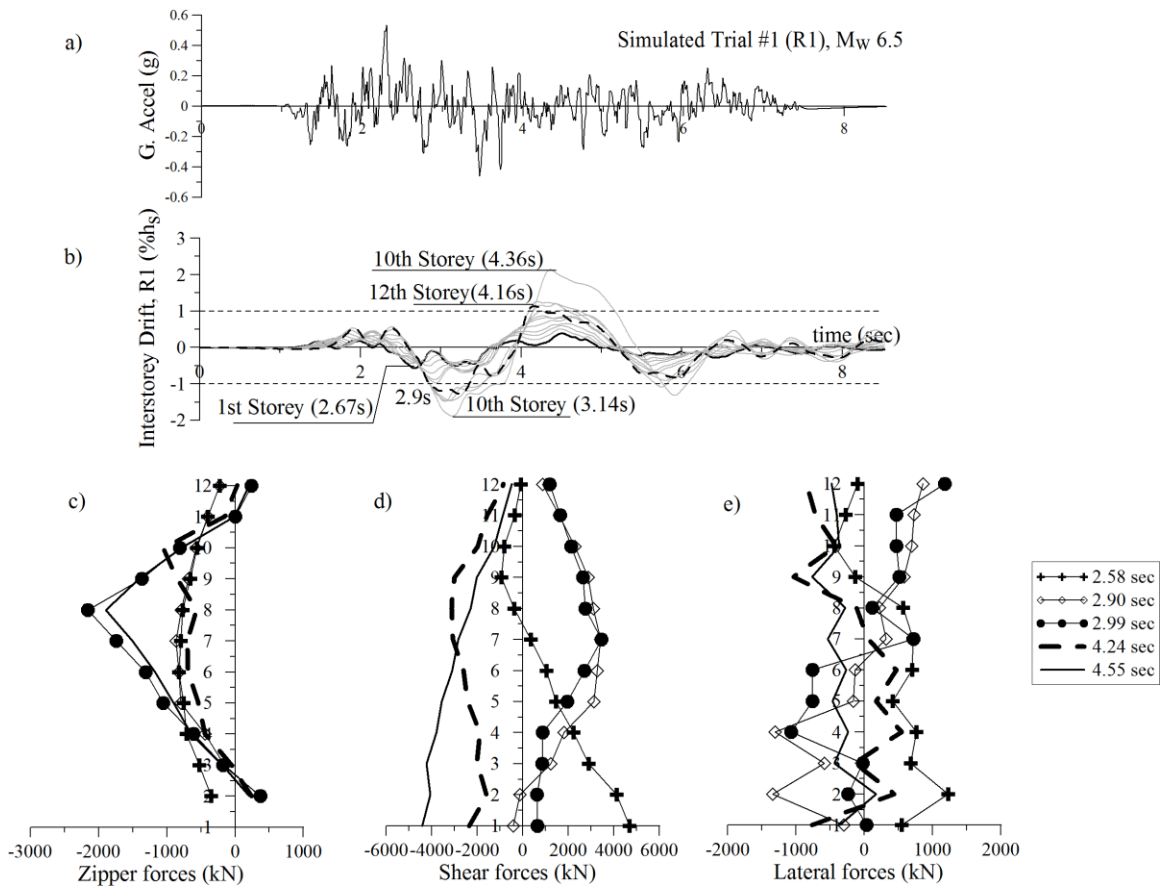


Figure 5.19 Structural response of 12-storey zipper braced frame under ground motion R1: a) Regular ground motion excitation R1; b) Interstorey time-history record under ground motion excitation R1; c) Axial forces in zipper columns at specified times; d) Shear forces distribution along the building height at specified times; e) Storey forces induced into structure at specified times.

Under ground motion excitation R5, the buckling of all the braces can be divided into phases. In the first phase, at 2.99s, only the top left brace buckled. Then, during the next ground motion cycle, the braces located at the left side of the 10th and 11th floor buckled at 4.31s and 4.34s respectively, while the building deflected in the 2nd mode shape. After 4.62s, when the excitation came from the other side, the braces located on the other half-span of the structures started to buckle. The following tier of buckling braces involved the braces of the 10th, 11th and 12th floors and occurred from the time sequence 4.62s to 4.66s. Again, the building deflected in the 2nd mode shape and the

occurrence of whipping effect was observed. After the ground motion reversed sign the group of braces belonging to the lower half of the building (up to the 6th floor) reached the verge of buckling at 5.78s and propagated upward. A larger value of base shear was intercepted at 5.78s which progressed upward and drove the bottom zipper to act in tension. This behaviour, the correlation of the ground motion signature, with the forces developed in zippers and the distribution of lateral forces at each floor, is illustrated in Figure 5.20.

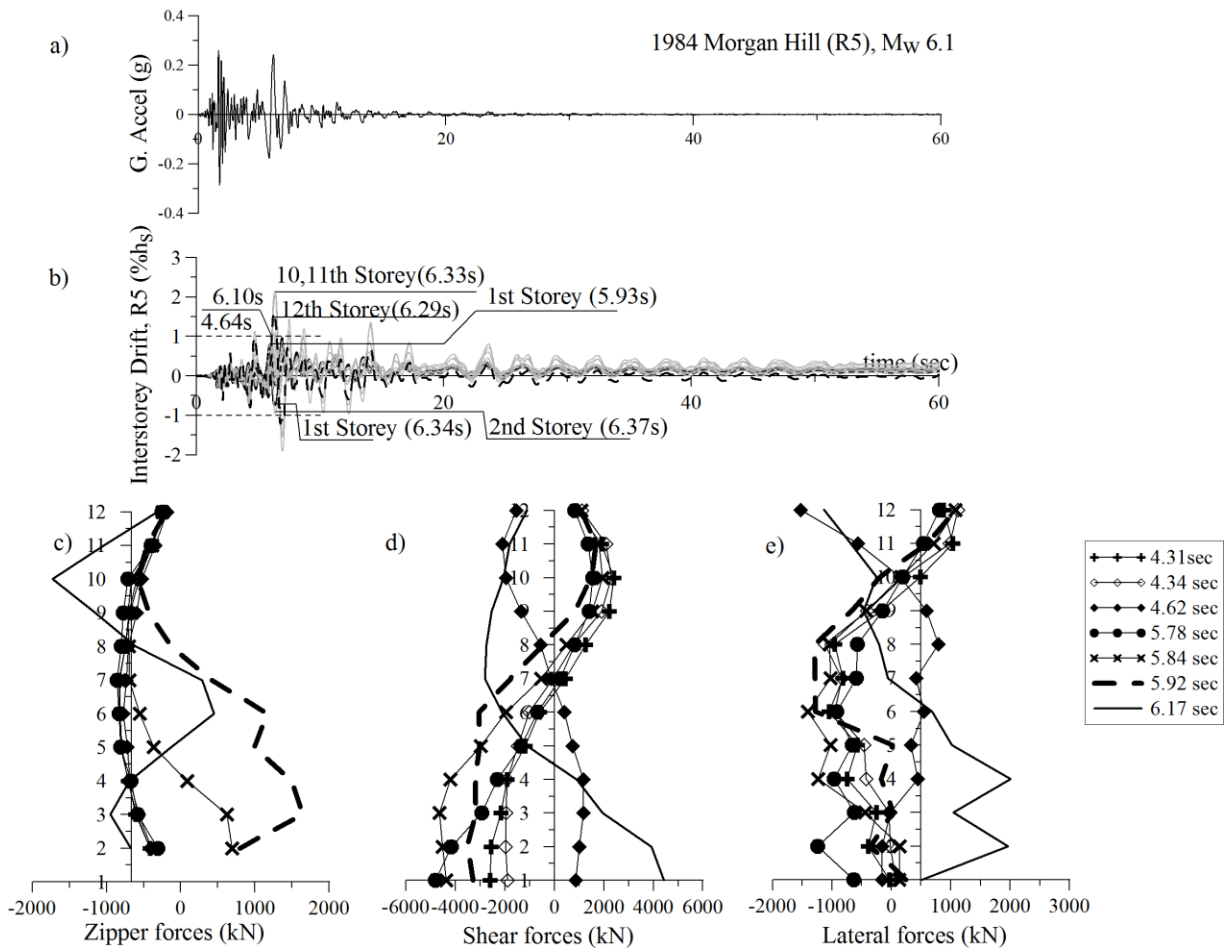


Figure 5.20 Structural response of 12-storey zipper braced frame under ground motion R5: a) Regular ground motion excitation R5; b) Interstorey time-history record under ground motion excitation R5; c) Axial forces in zipper columns at specified times; d) Shear forces distribution along the building height at specified times; e) Storey forces induced into structure at specified times

To further emphasise the behaviour of the zipper columns and the effect of ground motion on the seismic response, the forces developed in zippers, lateral and shear forces over the structure height as well as the time history interstorey drift displacement under the ground motion excitation R7, is shown in Figure 5.21. In this case, the first brace buckled at the top floor at 6.99s and propagated downward as shown in Table II-3 of Appendix II.

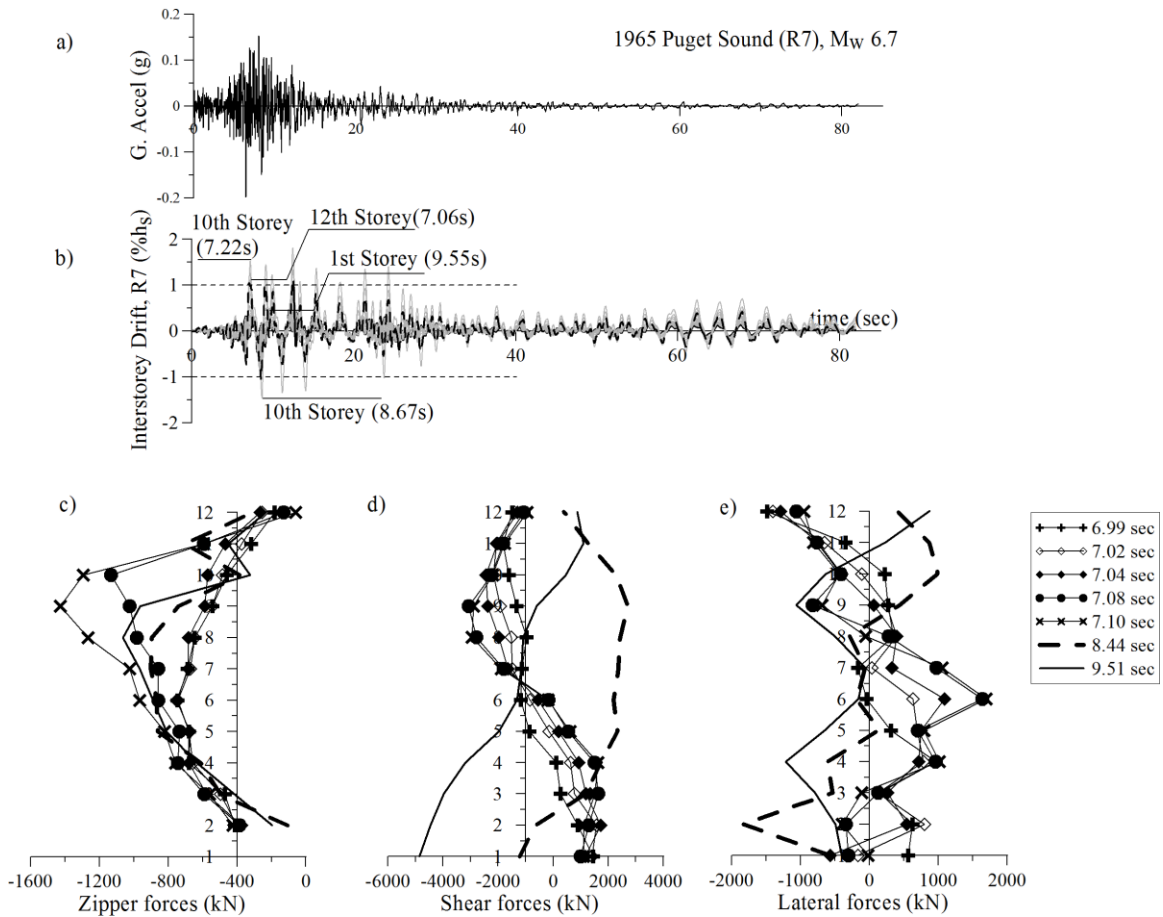


Figure 5.21 Structural response of 12-storey zipper braced frame under ground motion R7: a) Regular ground motion excitation R7; b) Interstorey time-history record under ground motion excitation R7; c) Axial forces in zipper columns at specified times; d) Shear forces distribution along the building height at specified times; e) Storey forces induced into structure at specified times.

The interstorey drifts of the upper part of the structure exceed the 1% storey height limit, right after the buckling of the first brace which occurred at the roof level at $t = 7.87s$. The unbalanced forces due to the buckling of compressive braces load the zippers in compression. While the compressive forces acting on zipper columns increase, the maximum lateral force induced into the top storey decreases and migrates downward.

5.4 Discussion of results

The analyses conducted with ETABS, Drain2DX and OpenSees have shown almost the same fundamental period for the three studied structures in the elastic range (Table 5.3).

Table 5.3 Analytical fundamental periods of vibration of the 4-, 8- and 12-structures

Story	Height	T_a	ETABS			Drain2DX			OpenSEES		
	[m]	[s]	T_1 [s]	T_2 [s]	T_1/T_a	T_1 [s]	T_2 [s]	T_1/T_a	T_1 [s]	T_2 [s]	T_1/T_a
4	15.3	0.76	0.72	0.28	0.95	0.70	0.27	0.92	0.75	0.29	0.99
8	30.4	1.52	1.74	0.59	1.14	1.70	0.56	1.12	1.75	0.59	1.15
12	45.7	2.28	2.74	0.86	1.20	2.71	0.83	1.19	2.76	0.88	1.21

In the given table, T_a is the fundamental period calculated as per the current edition of NBCC times two ($T_a = 2 \times (0.025h)$, where h is the height of the building), which in fact is the allowable upper limit. For the low-rise (4-storey) building, a very good match was found, while for the 12-storey building this difference has slightly increased. By obtaining almost the same dynamic properties with the three computer programs, the accuracy of the computation is validated.

Figure 5.22 shows the time-history roof displacement of the 4-story zipper braced frame obtained from Drain2DX, OpenSees and ETABS.

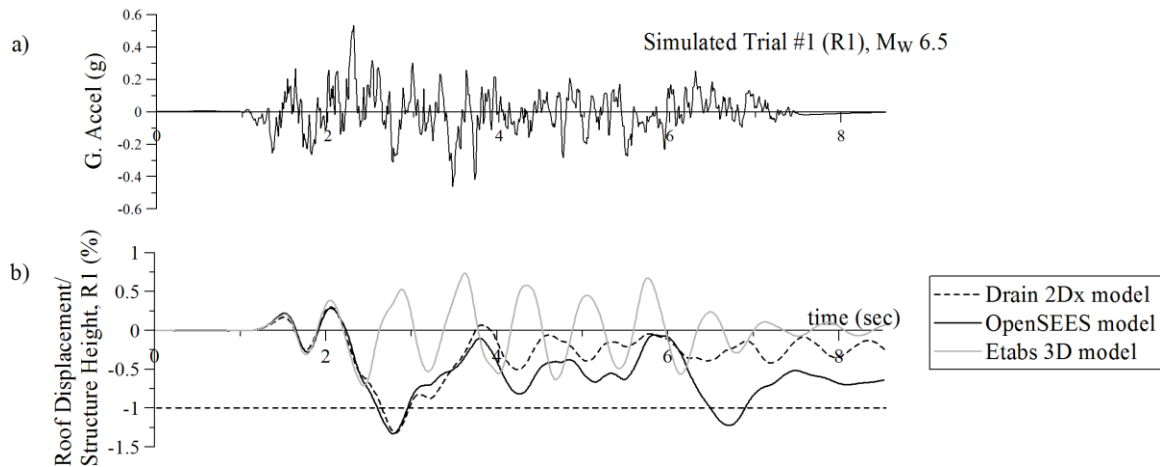


Figure 5.22 Roof displacement time-history record of the 4-storey structure under ground motion excitation R1, obtained from Drain OpenSees and ETABS: a) Ground motion R1; b) Roof displacement time-history record.

As can be observed from the figure, when the structure behaves elastically, the results obtained from Drain and OpenSees well agreed with that from the ETABS. However, after the first brace buckled (at $t = 2.32\text{s}$) and inelasticity initiated, the response of the structure models in OpenSees and Drain2Dx were driven as expected. It is noted that no plastic characteristics were assigned to the ETABS model. The difference between the results obtained in Drain2DX and OpenSees models are explained by the limitation of the Drain2DX brace model which has been discussed in Chapter 3. Another difference consists in the damping formulation in both programs.

Implemented in OpenSees, the Rayleigh damping command allows users to choose from the initial and tangential stiffness matrix, which is used to formulate the damping matrix. The initial stiffness proportional damping is used for simplicity while for a more accurate result the tangential stiffness proportional damping should be considered. The difference between considering initial stiffness proportional damping and tangential proportional damping is very small when specified damping ratio is lower than

2%. However, assigning tangential proportional damping to the model raises considerable difficulties to the convergence process. User discretion is required at this stage.

In Drain2DX, each element has a constant viscous damping matrix equal to βK_{β} , where K_{β} is the damper stiffness matrix of the element, which is set equal to the initial element stiffness, K_0 . Regarding this, at 2% damping, Drain2DX simulation shows a larger hysteresis capacity of braces than OpenSees. Therefore, this damping parameter has an impact on the obtained cumulative energy dissipation in Drain2Dx, which is larger than that resulted in OpenSees (see Chapter 3).

The differences in the hysteresis behaviour of a brace HSS203x203x9.5 in an one storey chevron braced frame when 1% and 2% damping is assigned is shown in Figure 5.23 and 5.24 only for discussion.

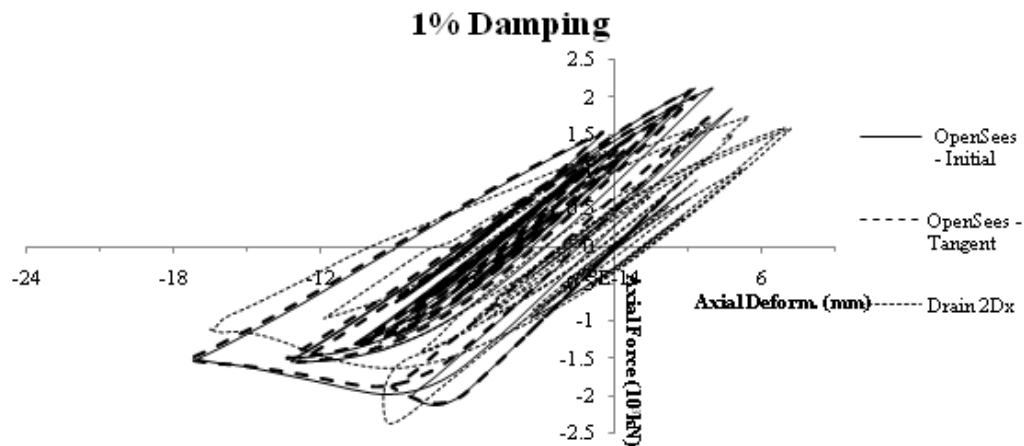


Figure 5.23 Brace hysteresis behaviour at 1% damping

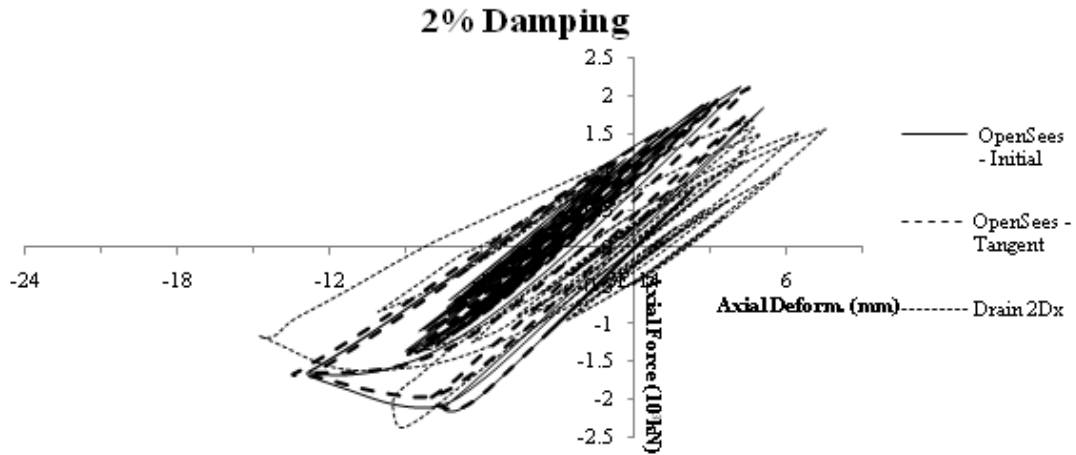


Figure 5.24 Brace hysteresis behaviour at 2% damping

Recalling the magnitude of zipper axial forces obtained in Drain2DX and OpenSees (Figure 5.3 and 5.10), similar envelopes are shown under the regular type of ground motions. Considering the mean+SD values of both interstorey drift envelopes and zipper axial force envelopes, the results obtained from both Drain2DX and OpenSees programs are in agreement. Therefore, the proposed design method has been validated through non-linear time-history dynamic analysis.

By considering the brace buckling sequence under different ground motion excitations as shown in Appendix II, it is shown that it follows closely to the scenarios captured by the design method. In addition, a good estimation of the capacity of zipper columns able to carry the unbalanced brace forces and to transfer them efficiently to adjacent stories until a full zipper mechanism is reached over the structure height has been found.

Future research work is required to validate the design method for structures with more than 12 stories, and for structures located in different seismic hazard zones.

CHAPTER SIX: Conclusions and Future Perspectives

6.1 Conclusions

Chevron braced frames have been widely used in North America as a structural configuration against earthquake excitations. Due its limitation in redistributing the internal brace forces once braces buckle, the structure is exposed to storey mechanism formation and reduced energy dissipation capacity. In light of this, zipper columns are introduced to overcome the CBF limits. In this study, zipper columns are designed to remain in elastic range throughout the entire ground motion excitations while transferring the unbalance brace forces resulted from buckling.

The first objective pursued in this study was to refine the method proposed by Tremblay and Tirca (2003), who have considered only the LP-ST (Sequential triangular) load redistribution pattern for zipper column design. Thus, in this study, in order to capture the maximum compressive and tensile forces in zipper columns, the following force redistribution patterns are considered, such as: LP-T (Triangular), LP-ST, LP-P (Parabolic), LP-SP (Sequential parabolic), LP-U (Uniform) and LP-SU (Sequential uniform).

In the compression side, a small difference exists between the zipper force envelope defined by the LP-ST and LP-SP patterns. The larger values were estimated

when the LP-ST pattern was considered, which was then selected for the zipper column design.

In the tension side, the maximum force envelope was captured by the LP-P pattern, followed by the LP-ST and LP-SP patterns. Accordingly, the LP-P pattern is recommended and adopted in design.

The second objective of this study was to validate the proposed design method under different circumstances, and to evaluate the behaviour of zipper braced frames. To analyze the inelastic behaviour of a zipper braced frame structure, two finite element computer programs: Drain2DX and OpenSees were compared. The accuracy of modeling brace inelastic behaviour with both programs was validated in Chapter 3 against experimental test results. In this validation, the effects of local buckling, residual stress and low-cycle fatigue have been neglected.

A new P-M interaction curve was proposed and implemented in the Drain2DX program to define the yielding surface of a HSS profile, such that a better match between computation and experimental test would be obtained. Better results were identified for stocky and intermediate braces when the cumulative energy dissipation parameter had been employed to measure the modeling accuracy.

Parameter studies of the construction of an OpenSees brace model have been carried out on a general basis, and recommendations for brace modeling in the OpenSees environment have been given. Brace models consisted of a minimum of 4 nonlinear beam-column elements with finely meshed fibre sections, 4 integration points per element, and an initial sinusoidal out-of-straightness with amplitude corresponding to

1/500th brace length was found to give a satisfactory buckling force. An equation for determining the value of the out-of-straightness has also been verified. In terms of cumulative energy dissipation, OpenSees offers a better match than Drain2DX due to its omission of the Bauschinger effect and assumption of concentrated plasticity.

On this basis, numerical models of zipper braced frames of a 4-, 8- and 12-storey buildings were designed according to the proposed method and analyzed with the Drain2DX and OpenSees programs. Three ground motion ensembles (regular, Cascadia and Near-field) consisting of 16 ground motions, were selected and scaled to match the design spectrum of a specified site location.

A two-step ground motion scaling method has been proposed in this study, which requires the match of spectrums over the periods of interest: $0.2T_1 - 1.5T_1$.

The results of the nonlinear dynamic analyses examined in Chapter 5 have shown uniformly distributed interstorey drifts over the structure height and the tendency of expected zipper mechanism formation. The maximum forces induced into the zippers were well-predicted by the proposed design method. Detailed investigation reveals that the presence of zipper columns efficiently transferred the unbalanced brace forces from the floor where brace buckled to adjacent non-damaged floors. Adding zipper columns in chevron braced frame successfully triggered the zipper mechanism which leads to uniformly distributed damage to the structure.

In ETABS, Drain 2Dx and OpenSees similar dynamic characteristics have been obtained.

For the 4-storey building, under a large number of ground motion excitations, the first brace buckles at the bottom floor. Buckling has initiated when the base shear reaches its maximum value simultaneously with a larger storey force. When the first brace buckles, the structure deflects in the first-mode shape. Buckling of brace normally starts when the interstorey drift of corresponding stories is around 1%hs.

For the 8-storey building, buckling initiates either at the first floor and propagates upward, or at the roof level and progresses downward. Different earthquake characteristics lead the building to behave differently. The higher modes effect has been observed, as well as the occurrence of the whipping effect. In general, when the first brace has buckled, the structure deflects either in the 2nd or the 3rd vibration mode shape. It is observed that buckling of braces also initiates when the interstorey drift reaches 1%hs.

The behaviour of the 12-storey building is similar with that of the 8-storey building. However, the subsequent buckling of braces cannot be developed under a singular ground motion cycle and is divided in tiers of braces buckling. The effect of higher mode effect is further emphasized.

Theses analyses were performed at the design level, while the structures still have remaining strength until failure is initiated. To discuss the behaviour of the structure at the near-collapse state, the incremental dynamic analysis method has to be employed in future studies.

6.2 Future Perspectives

Although the design methodology proposed by this study has been proven efficient through numerical simulations, the lateral force load pattern which offers the conservative zipper force envelope cannot be observed in all the analyses. On the other hand, due to the complicity of plastic deformation involved in zipper braced frame behaviour, it is unlikely to find a certain lateral force redistribution path after braces have buckled. In this respect, experimental tests are required to further verify the structure response of zipper braced frames. An 8-storey chevron braced frame with zipper columns samples will be tested on a shake table to demonstrate the effectiveness of zipper braced frame behaviour.

Meanwhile, more accurate brace models can be developed, if local buckling, residual stress and low-cycle fatigue are implemented. Although these models will considerably increase the computation time, by employing a more powerful computer and more accurate models, sophisticated hybrid tests can be carried out with OpenSees.

IDA method has to be considered in order to study the occurrence of collapse through dynamic instability.

REFERENCES

American Society of Civil Engineers (ASCE), (2000). Prestandard and Commentary for the Seismic Rehabilitation of Buildings, prepared for the SAC Joint Venture, published by the Federal Emergency Management Agency, FEMA-356, Washington, D.C.

Aguero, A., Izvernari, C. and Tremblay, R., (2006). Modelling of the Seismic Response of Concentrically Braced Steel Steel Frames using the OpenSees Analysis Environment. *International Journal of Advanced Steel Construction*, 2, 3, pp 242-274.

Aguero, A., Izvernari, C. and Tremblay, R., (2005). Numerical Comparison and Optimization of Force and Displacement Based Elements for the Analysis of the Inelastic Cyclic Response of Steel Bracing Members. *Advances in Steel Structure*, Vol. II, 1235-1240.

Applied Technology Council, (1992). Guidelines for Cyclic Seismic Testing of Components of Steel Structures, ATC-24, Redwood City, CA.

Archambault, M.H., (1995). Etude du comportement seismique des contreventements ductile en X avec profiles tubulaires en acier. Rapport No. EPM/GCS-1995-09 Ecole Polytechnique, Montreal.

Astaneh-Asl, A., Goel, S.C. and Hanson, R.D., (1985). Cyclic Out-ofPlane Buckling of Double-Angle Bracing. *Journal of Structural Engineers*, ASCE, 111, pp. 1135-1153.

Baker, J. W., (2009). The conditional mean spectrum: A tool for ground motion selection, ASCE Journal of Structural Engineering (in press.)

Broderick B.M., Elghazouli, AY, Goggins, J., (2008). Earthquake testing and response analysis of concentrically-braced sub-frames, Journal of Constructional Steel Research, Vol 64, Issus9.

Bruneau, M., Engelhardt, M., Filiatrault, A., Goel, S. C., Itani, A., Hajjar, J., Leon, R., Ricles, J., Stojadinovic, B. and Uang, C.-M., (2005). Review of selected recent research on US seismic design and retrofit strategies for steel structures. Progress in Structural Engineering and Materials, 7:103–114. doi:10.1002/pse.192.

Canadian Standard Association. (2009), CAN/CSA-S16-09 Limit States Design of Steel Structures. Canadian Standard Association, Toronto, ON.

De Sousa, R. M., (2000). Force-Based Finite Element for Large Displacement Inelastic Analysis of Frames PhD Thesis, University of California, Berkeley.

Dicleli, M. and Mehta, A., (2007). Simulation of Inelastic Cyclic Buckling Behaviour of Steel Box Sections. Computer & Structures Journal pp. 446-457.

Federal Emergency Management Agency (FEMA), (2000). Prestandard and Commentary for the Seismic Rehabilitation of Buildings, FEMA-356, Washington, D.C.

Gioncu, V. and Tirca, L., (1996). Rotation Capacity of Rectangular Hollow Section Beams. 7th International Symposium on Tubular Structures, Miskolc, Hungary.

International Code Council, (2000). International Building Code, Falls Church, Virginia.

Ikeda, K. and Mahin, S., (1984). A Refined Physical Theory Model for Predicting the Seismic Behaviour of Braced Steel Frames. Report no. UCB/EERC-84/12, Earthquake Engineering Research Center, Univ. of California, Berkeley, Ca.

International Conference of Building Officials (ICBO). (2001). California Building Code, Whittier, California.

Izvernari, C. (2007). The seismic behaviour of steel braces with large sections, Master Thesis. Génie Civil. Département des Génies Civil, Géologique et des Mines. École Polytechnique de Montréal, Canada. Avril.

Lacerte, M and Tremblay, R., (2007). Making Use of Brace Overstrength to Improve the Seismic Response of Multi-Storey Split-X Concentrically Braced Steel Frames. Canadian Journal of Civil Engineering.

Leon R.T., Yang C. S., (2003). Special Inverted-V-braced Frames with Suspended Zipper Struts. International Workshop on Steel and Concrete Composite Construction, IWSCCC, National Center for Research on Earthquake, Taipei, Taiwan.

Leowardi, S. and Walpole, W., (1996). Performance of Steel Brace Members. Report no. ISSN 0110-3326, Univ. of Cantenbury, New Zealand.

Mazzoni, S., McKenna, F., Scott, M., Fenves, G. et al., (2007). OpenSees User Manual, <http://opensees.berkeley.edu/OpenSees/manuals/usermanual/OpenSeesCommandLanguageManual.pdf>.

Menegotto, M. and Pinto, P.E., (1973). Method of analysis for Cyclic Loaded R.C. Plane Frame Including Changes in Geometry and Non-elastic Behaviour of Elements under Combined Normal Force and Bending. Proc. IABSE Symposium on Resistance and

Ultimate Deformability of Structures Acted On by Well Defined Repeated Loads, pp. 15-22.

McKenna, F., (1997). Object Oriented Finite Element Analysis: Frameworks for Analysis Algorithms and Parallel Computing. Ph.D. Thesis, Department of Civil Engineering, University of California, Berkeley, CA.

McKenna, F. and Fenves, G.L., (2004). Open System for Earthquake Engineering Simulation (OpenSees). Pacific Earthquake Engineering Research Center (PEER), University of California, Berkeley, CA. (<http://opensees.berkeley.edu/index.html>)

Nouri G.R, H. Imani Kalesar, Zahra Ameli, (2009). The Applicability of the Zipper Strut to Seismic Rehabilitation of Steel Structures. World Academy of Science, Engineering and Technology.

Prakash, V., G.A. Powell, and S. Campbell, (1993). DRAIN-2DX Base Program Description and User Guide. Department of Civil Engineering. University of California. Berkeley, California.

Shaback, B., and Brown, T., (2003). Behaviour of Square Hollow Structural Steel Braces with End Connections under Reversed Cyclic Axial Loading. Canadian Journal of Civil Engineering, 30 (4) pp. 745-753.

Tremblay, R., Archambault, M.-H., and Filiatrault. A., (2003). Seismic Response of Concentrically Braced Steel Frames Made with Rectangular Hollow Bracing Members. ASCE Journal of Structural Engineering 129 (12), pp. 1626-1636.

Tremblay, R., (2002). Inelastic Seismic Response of Steel Bracing Members. Journal of Constructional Steel Research, 58, pp. 665-701

Tremblay, R., Tirca L.. (2003). Behaviour and design of multi-story zipper concentrically braced steel frames for the mitigation of soft-story response. In: Proceedings of the conference on behaviour of steel structures in seismic areas. 2003. p. 471-7.

Tirca L., Tremblay R., (2004). Influence of building height and ground motion type on the seismic behaviour of zipper concentrically braced steel frames. 13th World Conference on Earthquake Engineering. 2004. Paper No. 2894.

Uriz, P., Filippou, F.C., and Mahin, S., (2008). Model for Cyclic Inelastic Buckling of Steel Braces, *Journal of Structural Engineering*, ASCE, pp. 619-628.

Uriz, P. and Mahin, S., (2008). Toward Earthquake Resistant Design of Concentrically Braced Steel Frame Structures. PEER 2008/08 report

Uriz, P. and Mahin, S., (2004). Seismic Performance Assessment of Concentrically Braced Steel Frames. Proc. 13th World Conference on Earthquake Eng., Vancouver, BC., Paper No. 1639.

Uriz, P., and Mahin, S. A., (2004). Seismic Vulnerability Assessment of Concentrically Braced Steel Frames. *International Journal of Steel Structures*, 4(4), 239-248.

Walpole, W. and Leowardi, S., (1995). The behaviour of brace members under cycling loading. *Structural Stability and Design*, Kitipornchai, Hancock & Brandford (eds), 1995 Balkema, ISBN 90 5410 582 8.

Yang, C. S., (2006). Analytical and Experimental Study of Concentrically Braced Frames with Zipper Struts. PhD thesis, Georgia Institute of Technology.

Yang, C.-S., Leon, R.T., and DesRoches, R., 2008. Pushover Test and Analysis of a Braced Frame with Suspended Zipper Struts, ASCE Journal of Structural Engineering.

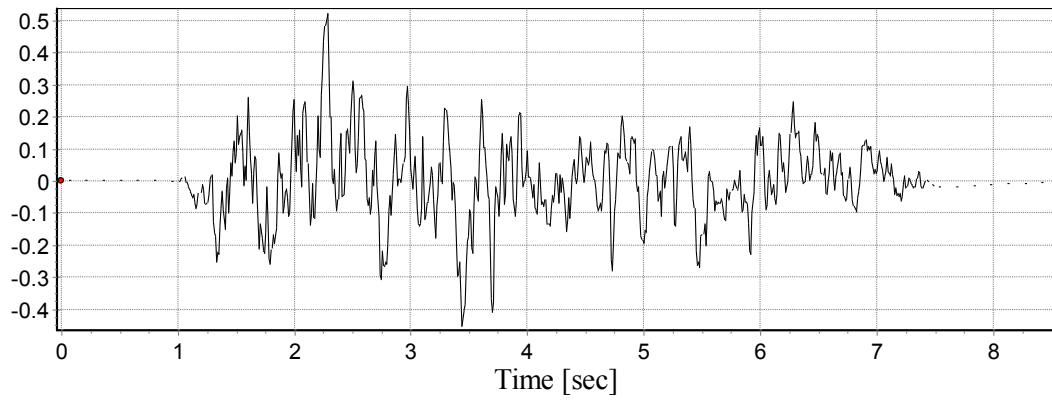
Yang, T. Y., Moehle, J. P., and Stojadinovic B., (2009). Performance Evaluation of Innovative Steel Braced Frames. Pacific Earthquake Engineering Research Center.

Denaya Hinds, K., Walsh, K., Hill, M., Abdullah, M., (2007). Analytical Studies of The Suspended Zipper Frame & Control Devices. Proceedings of the 2007 earthquake Engineering Symposium for Young Researchers.

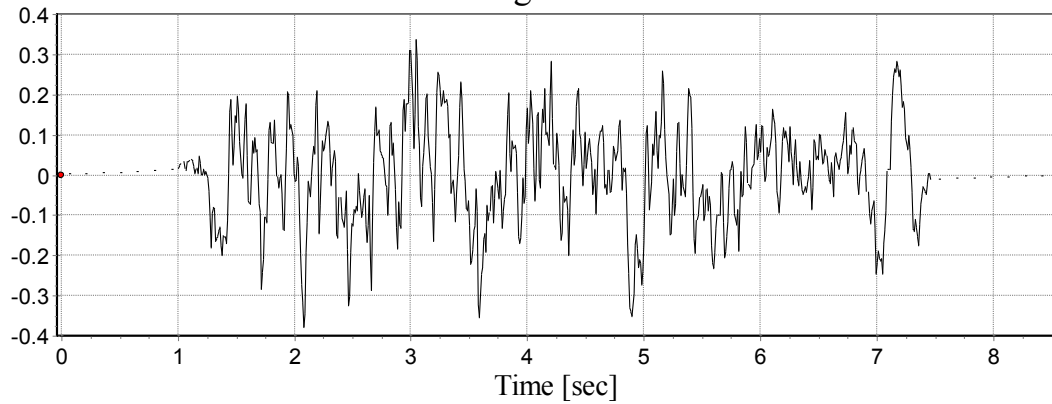
Ziemia, R.D., (2010). Guide to Stability Design Criteria for Metal Structure, sixth edition, Wiley-Interscience, New York.

APPENDIX I: Selected Ground Motion Time-History Records

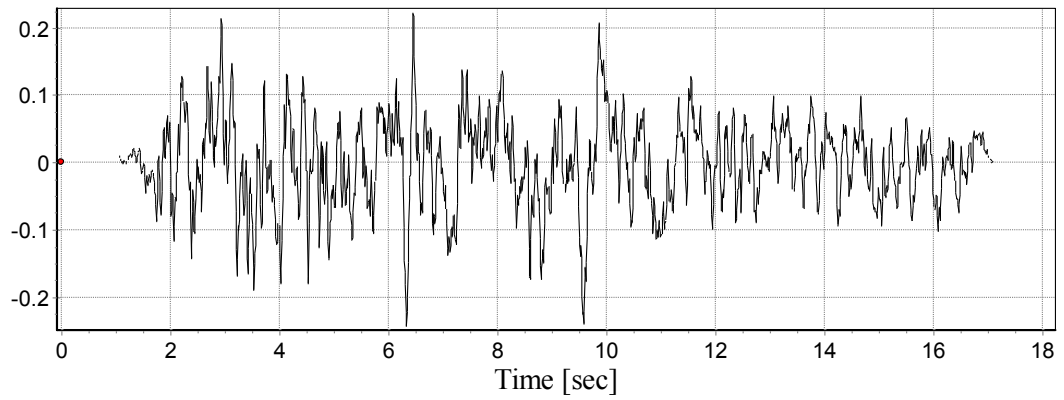
Accelerogram R1



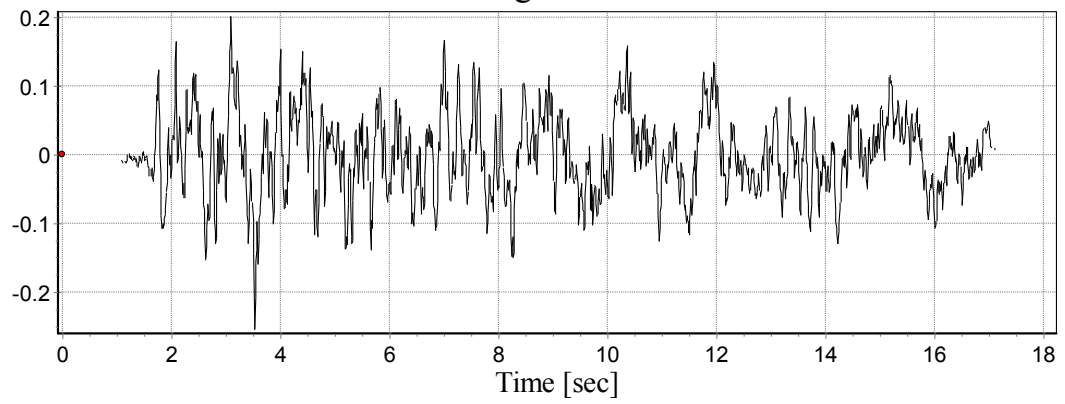
Accelerogram R2



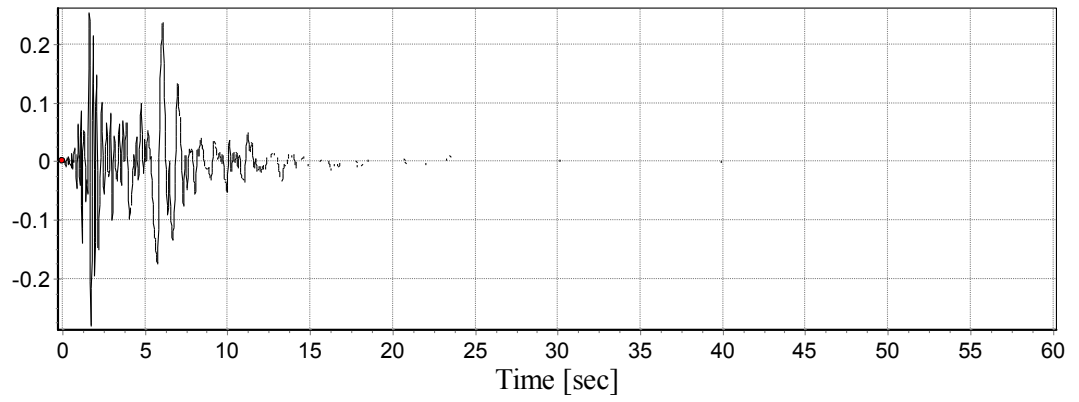
Accelerogram R3



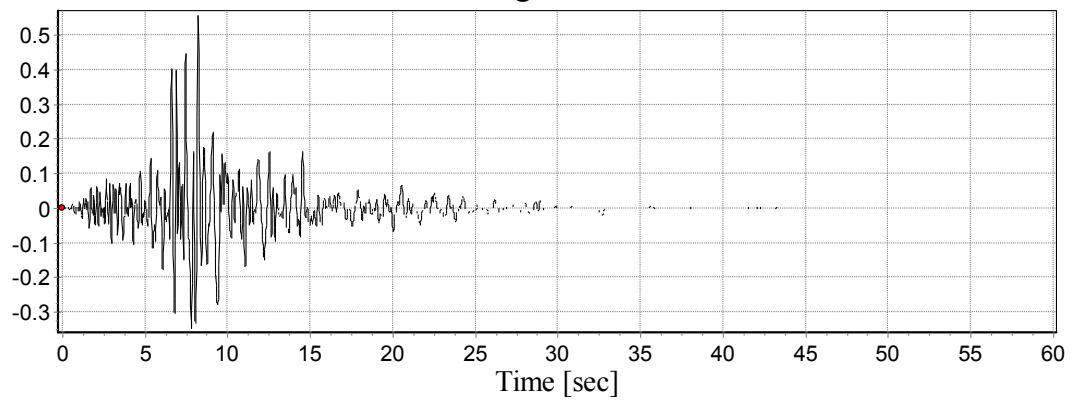
Accelerogram R4



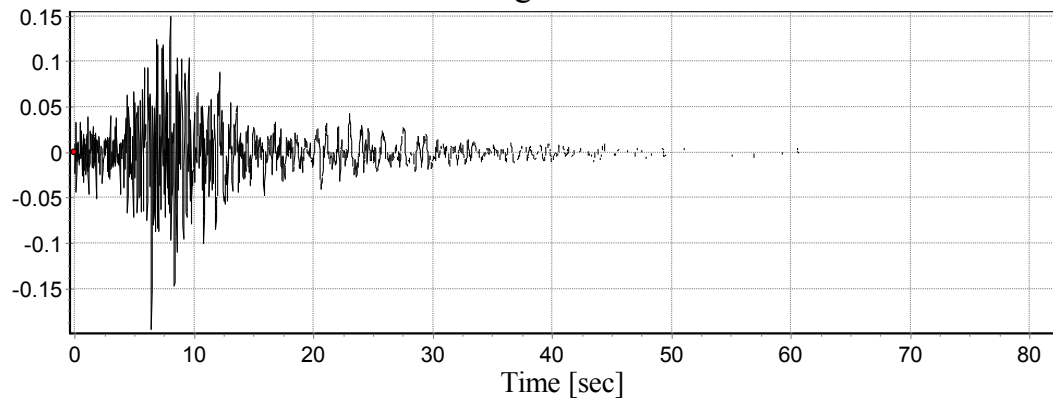
Accelerogram R5



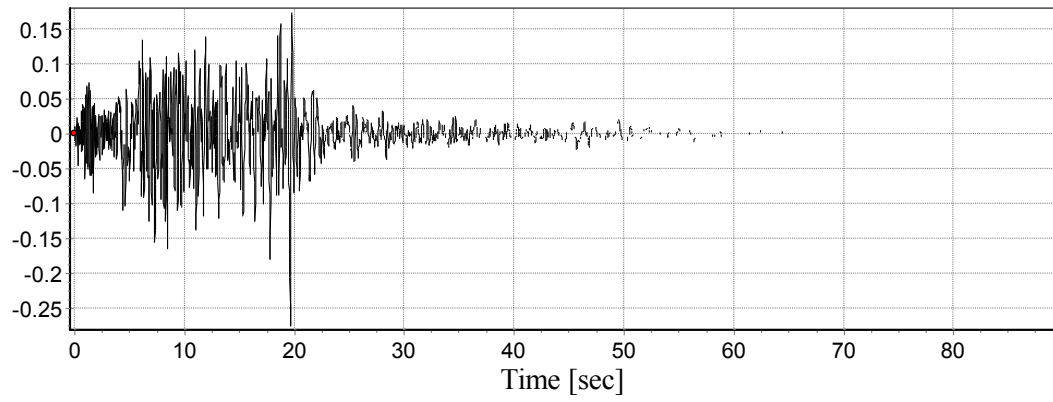
Accelerogram R6



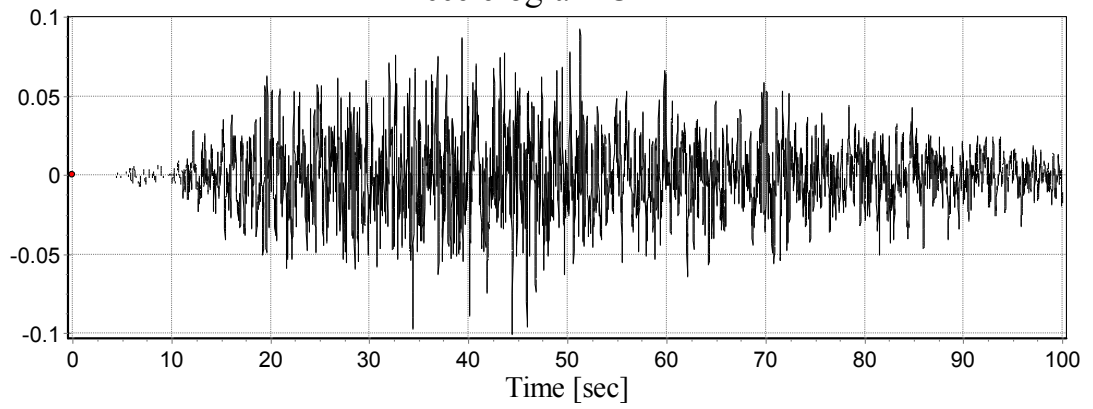
Accelerogram R7



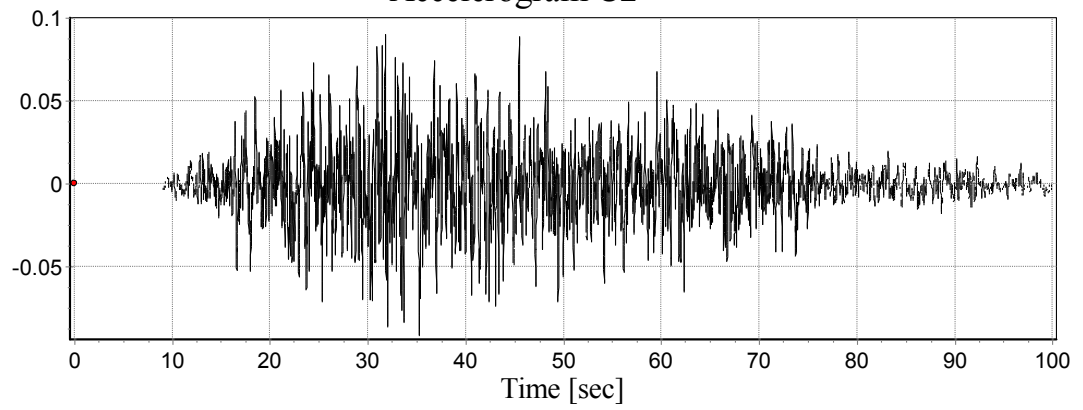
Accelerogram R8



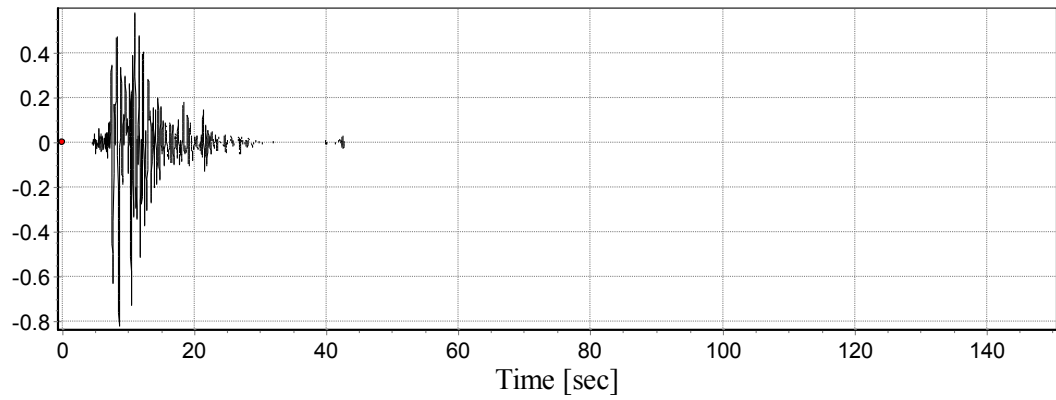
Accelerogram C1



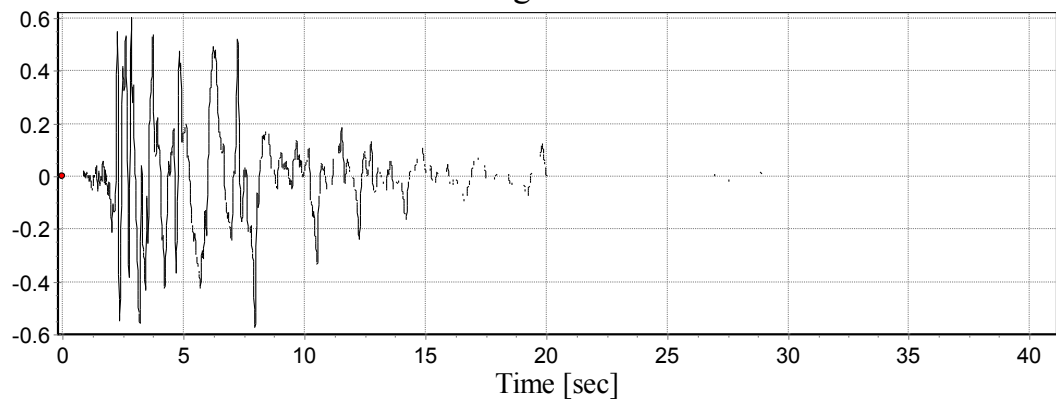
Accelerogram C2



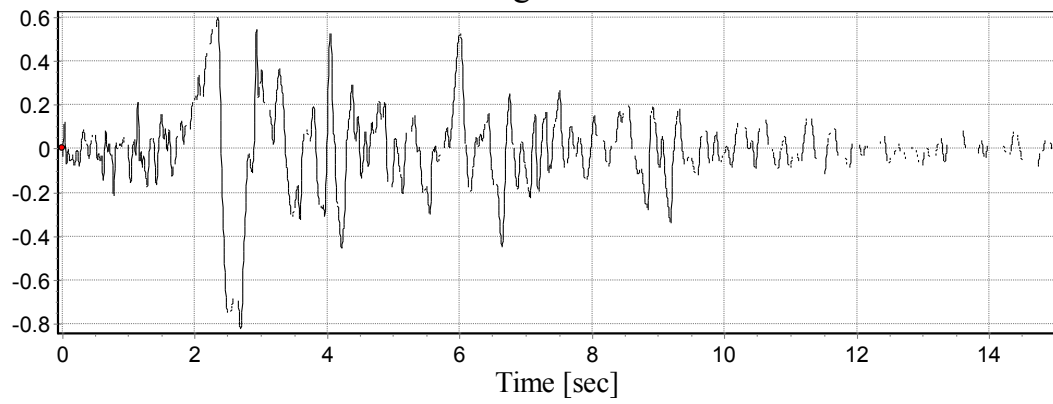
Accelerogram N1



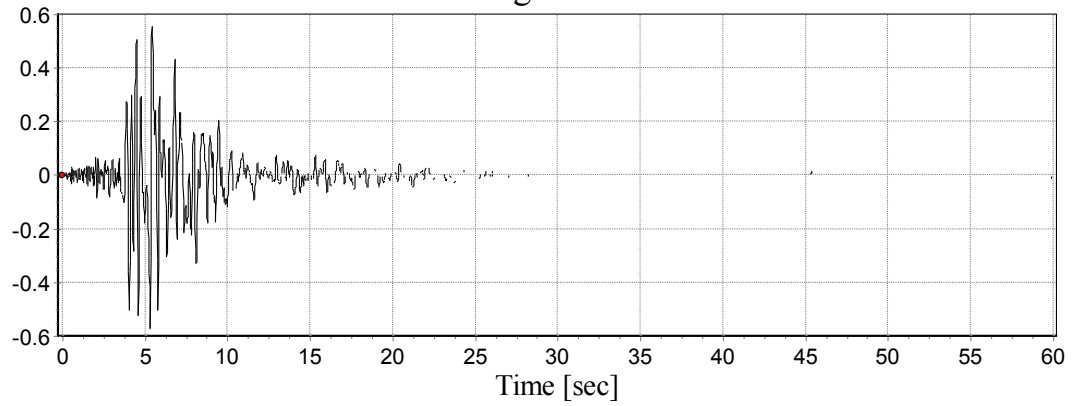
Accelerogram N2



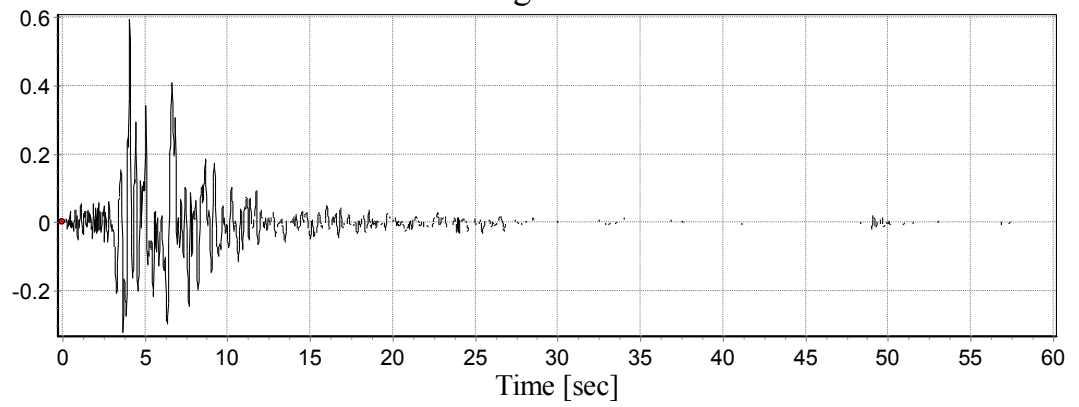
Accelerogram N3



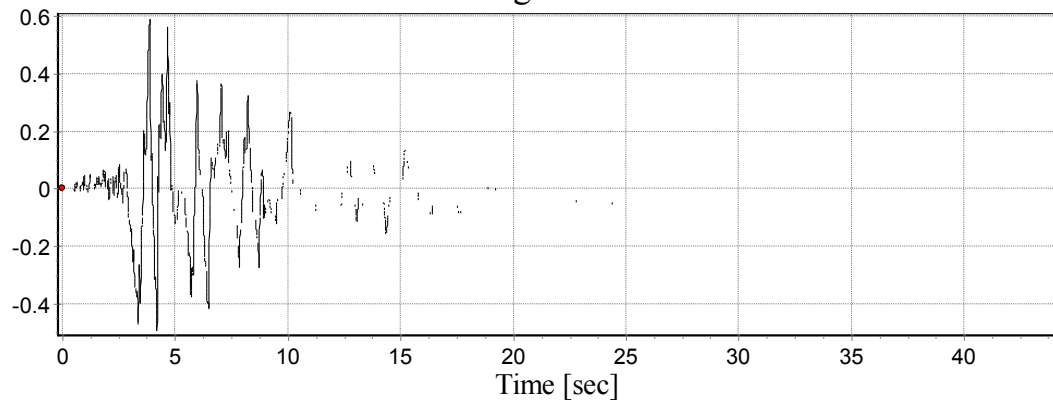
Accelerogram N4



Accelerogram N5



Accelerogram N6



APPENDIX II: Buckling Sequences of Zipper Braced Frame under Ground Motion

Excitations as obtained in OpenSees

Table II.1 Buckling sequences of braces of the 4-storey structure under different ground motion excitations (in seconds)

Level	Left Brace	Right Brace	Left Brace	Right Brace	Left Brace	Right Brace	Left Brace	Right Brace
	R1		R2		R3		R4	
4	2.41	N/A	7.45	3.75	3.04	6.56	3.28	N/A
3	2.37	N/A	N/A	3.74	3.02	9.79	3.26	3.8
2	2.35	N/A	N/A	3.74	3	3.66	3.24	N/A
1	2.32	N/A	3.12	3.68	2.95	3.61	3.22	2.86
	R5		R6		R7		R8	
4	6.18	N/A	8.48	7.96	7.06	N/A	N/A	9.89
3	6.17	5.8	N/A	7.95	12.25	N/A	15.85	19.78
2	6.15	5.77	N/A	7.94	8.98	N/A	15.83	N/A
1	6.1	5.73	7.54	7.93	8.95	6.46	N/A	N/A
	C1		C2		N1		N2	
4	21.04	N/A	N/A	23.83	N/A	8.66	3.88	N/A
3	21.01	N/A	N/A	23.81	N/A	7.76	3.84	4.38
2	20.98	N/A	N/A	23.8	8.12	8.66	3.87	3.32
1	17.96	17.57	N/A	23.78	8.09	7.78	2.63	3.3
	N3		N4		N5		N6	
4	N/A	2.67	4.66	N/A	4.26	N/A	3.91	4.42
3	N/A	2.65	4.67	N/A	4.25	N/A	3.89	N/A
2	N/A	2.64	5.63	N/A	4.27	N/A	3.88	N/A
1	2.36	2.62	4.55	5.3	4.29	6.47	3.85	3.3

Table II.2 Buckling sequences of braces of the 8-storey structure under different ground motion excitations (in seconds)

Level	Left Brace	Right Brace						
	R1		R2		R3		R4	
8	2.64	N/A	N/A	N/A	N/A	N/A	N/A	3.94
7	2.6	N/A	N/A	N/A	N/A	N/A	N/A	N/A
6	2.62	N/A	3.55	N/A	N/A	N/A	N/A	N/A
5	2.63	N/A	3.52	N/A	N/A	N/A	N/A	N/A
4	2.63	N/A	3.49	N/A	N/A	4.03	4.9	N/A
3	2.6	N/A	3.46	N/A	N/A	3.99	4.85	10.17
2	2.34	N/A	3.48	5.72	8.2	3.98	4.51	10.05
1	2.3	4.35	3.46	5.68	2.96	3.94	4.47	N/A
	R5		R6		R7		R8	
8	6.49	6.02	7	8.19	N/A	N/A	N/A	N/A
7	6.52	6	N/A	8.19	N/A	6.92	N/A	N/A
6	N/A	6	N/A	8.23	N/A	6.95	N/A	N/A
5	N/A	6	N/A	8.28	N/A	6.98	N/A	N/A
4	N/A	5.97	N/A	8.27	N/A	8.83	N/A	N/A
3	N/A	5.92	N/A	8.22	8.08	8.8	5.99	N/A
2	N/A	5.91	7.21	8.01	8.04	7.13	5.97	5.05
1	N/A	5.86	7.18	7.96	7.62	6.73	5.94	5.02
	C1		C2		N1		N2	
8	25.28	N/A	41.57	35.67	9.84	10.73	6.74	3.78
6	25.22	N/A	N/A	35.71	N/A	10.78	6.71	N/A
6	25.22	N/A	N/A	35.71	N/A	10.78	6.71	N/A
5	25.21	N/A	N/A	35.74	N/A	10.89	6.73	N/A
4	N/A	N/A	N/A	35.74	N/A	10.85	6.69	N/A
3	N/A	N/A	N/A	35.69	N/A	10.83	6.62	5.94
2	20.25	19.32	17.69	32.69	N/A	9.2	6.58	5.94
1	20.21	19.28	17.66	N/A	10.12	9.17	6.55	5.9
	N3		N4		N5		N6	
8	N/A	2.99	4.84	5.66	4.46	N/A	N/A	N/A
7	N/A	2.97	4.86	5.68	4.46	N/A	N/A	N/A
6	N/A	2.99	N/A	N/A	4.52	N/A	N/A	N/A
5	N/A	3.02	N/A	N/A	7.09	N/A	N/A	N/A
4	N/A	3.05	N/A	10.27	7.06	N/A	N/A	N/A
3	N/A	N/A	N/A	8.28	6.9	N/A	4.9	3.62
2	N/A	N/A	6.3	5.4	N/A	N/A	4.5	3.51
1	N/A	3.17	4.57	5.38	4.22	3.93	4.46	3.38

Table II.3 Buckling sequences of braces of the 12-storey structure under different ground motion excitations (in seconds)

Level	Left Brace	Right Brace						
	R1		R2		R3		R4	
12	2.99	N/A	3.79	N/A	N/A	7.74	N/A	4.13
11	2.95	4.17	3.76	N/A	N/A	7.71	3.78	4.13
10	2.92	4.13	3.7	N/A	3.56	7.72	3.78	4.16
9	2.93	4.24	3.72	N/A	N/A	N/A	N/A	4.2
8	2.9	4.23	3.73	N/A	N/A	N/A	N/A	N/A
7	2.97	N/A	7.11	N/A	N/A	10.13	N/A	N/A
6	N/A	4.61	7.07	N/A	N/A	9.79	N/A	N/A
5	N/A	4.55	7.09	5.83	N/A	9.75	15.77	17.04
4	N/A	N/A	N/A	N/A	N/A	9.76	N/A	N/A
3	N/A	N/A	N/A	5.85	N/A	9.73	N/A	N/A
2	N/A	N/A	N/A	5.83	N/A	N/A	15.82	N/A
1	2.58	4.48	7.28	5.75	N/A	4.44	15.68	N/A
	R5		R6		R7		R8	
12	2.99	4.62	7.18	8.53	N/A	6.99	N/A	7.78
11	4.34	4.63	N/A	8.5	N/A	7.02	N/A	7.76
10	4.31	4.66	N/A	8.47	8.44	7.04	6.36	7.72
9	N/A	6.16	N/A	8.48	N/A	7.08	N/A	7.71
8	N/A	6.17	N/A	8.47	N/A	7.1	6.53	7.7
7	N/A	6.2	N/A	N/A	N/A	N/A	N/A	7.81
6	N/A	5.92	N/A	N/A	N/A	N/A	N/A	7.82
5	N/A	5.87	N/A	N/A	N/A	N/A	6.73	7.83
4	N/A	5.86	N/A	N/A	N/A	N/A	N/A	8.07
3	N/A	5.84	7.61	N/A	N/A	N/A	N/A	N/A
2	6.20	5.81	7.58	N/A	N/A	N/A	N/A	N/A
1	6.17	5.78	7.56	N/A	8.06	9.51	6.66	7.96
	C1		C2		N1		N2	
12	N/A	42.45	N/A	35.98	7.89	8.13	N/A	8.43
11	N/A	42.42	N/A	30.83	7.87	8.13	N/A	6.46
10	N/A	42.37	N/A	30.8	8.71	8.17	N/A	6.39
9	N/A	42.47	N/A	35.93	8.73	N/A	N/A	8.39
8	N/A	42.27	N/A	35.93	N/A	N/A	N/A	11.15
7	N/A	42.28	N/A	35.96	N/A	N/A	N/A	11.36
6	N/A	42.21	N/A	35.96	N/A	N/A	N/A	N/A
5	N/A	42.16	N/A	35.93	N/A	N/A	N/A	N/A
4	N/A	42.22	N/A	36.02	N/A	N/A	N/A	N/A
3	N/A	42.18	31.84	36.03	N/A	8.68	7.35	N/A
2	N/A	42.19	24.35	36.01	8.27	8.64	7.31	N/A
1	40.94	42.13	24.3	22.53	8.24	8.62	7.29	4.3

	N3		N4		N5		N6	
12	2.77	3.2	6.09	5.78	N/A	N/A	8.04	N/A
11	2.75	3.21	6.12	5.74	N/A	N/A	7.79	3.91
10	2.71	3.19	6.13	5.7	N/A	N/A	7.74	3.87
9	2.73	N/A	N/A	5.7	N/A	N/A	5.2	N/A
8	2.68	N/A	N/A	N/A	N/A	N/A	5.15	N/A
7	N/A	N/A	N/A	N/A	N/A	N/A	5.15	N/A
6	N/A	N/A	9.82	N/A	N/A	6.48	4.81	N/A
5	N/A	N/A	9.78	N/A	5.22	6.45	4.74	6.75
4	N/A	N/A	N/A	N/A	N/A	6.48	4.76	N/A
3	N/A	N/A	N/A	N/A	5.27	6.46	4.74	N/A
2	N/A	N/A	N/A	N/A	5.11	6.45	4.73	N/A
1	2.38	N/A	N/A	N/A	5.07	6.41	4.71	N/A